MIDLANDS STATE UNIVERSITY

DETECTION OF LIMESTONE DEPOSITS IN THE NYANDA MOUNTAIN RANGE, MASVINGO, USING GROUND MAGNETIC GEOPHYSICAL SURVEY

A Dissertation By

Simbarashe Chipokore

(R104593N - HPHY)

May 2014

This dissertation was prepared by Simbarashe Chipokore (R104593N) during his fourth year of study period which ran from August 2013 to May 2014 and submitted as a pre-requisite in partial-fulfillment of the Bachelors of Science Honors Degree in Physics as required by the Midlands State University.

MIDLANDS STATE UNIVERSITY

FACULTY OF SCIENCE AND TECHNOLOGY

DEPARTMENT OF PHYSICS

NAME: SIMBARASHE CHIPOKORE

REG #: R104593N

MODULE: HPH438 DISSERTATION

YEAR: 2014

LEVEL: 4

TITLE:

DETECTION OF LIMESTONE DEPOSITS IN THE NYANDA MOUNTAIN RANGE, MASVINGO, USING GROUND MAGNETIC GEOPHYSICAL SURVEY.

DETECTION OF LIMESTONE DEPOSITS IN THE NYANDA MOUNTAIN RANGE, MASVINGO, USING GROUND MAGNETIC GEOPHYSICAL SURVEY.

By

SIMBARASHE CHIPOKORE

R104593N

Submitted in partial fulfilment of the requirement for the

Bachelor of Science Physics Honours Degree

Department of Physics

In the

Faculty of Science and Technology

At the

Midlands State University,

Gweru

May 2014

Supervisor……..……..

Co-supervisor……..…….

DECLARATION

I, Simbarashe Chipokore, hereby declare that I am the sole author of this thesis. I authorise the Midlands State University to lend this thesis to other institutions or individuals for the purpose of scholarly research

Signature …… Date …….

APPROVAL

This dissertation entitled **"DETECTION OF LIMESTONE DEPOSITS IN THE NYANDA MOUNTAIN RANGE, MASVINGO, USING GROUND MAGNETIC GEOPHYSICAL SURVEY"** by Simbarashe Chipokore (R104593N) meets the regulations governing the awarding of the Bachelors of Science Physics Honours Degree by the Midlands State University, and is approved for its contribution to knowledge and literal presentation.

Supervisor ……..

Date ……

ABSTRACT

Geophysical survey techniques have successfully been applied to near-surface limestone detection in karstic terrains. A magnetic geophysical survey to delineate the karstic structure of the Nyanda Mountains, Masvingo, was carried out in the interest of mapping out limestone deposits required for cement production. The magnetic-total-field-anomaly maps helped reveal the metamorphic and sedimentary units in the study area. Although only part of the mountain range was surveyed for this project, the results suggested that the buried limestone units had an undulating karstic topography including a probable pinnacle structure. A synthetic modelling study was carried out, and it validated the reliability of the results. Finally, the findings indicated that the geophysical survey techniques used here were successful in detecting limestone deposits through the rather vertical terrain difficult to traverse carrying ground penetrating radar or resistivity instruments, which are usually employed to explore limestone deposits. The magnetic survey was also cost effective with respect to the cost demands of the other possible geophysical techniques. The study results were digitised from GEM-systems magnetic data loggers by Oasis Montaj and was exported to mapping software, MapInfo. To access the geodatabase the user needs to have ArcGIS 8.3 or later and basic EXCELL software.

KEYWORDS: limestone; geophysics; geomagnetic field; non-magnetic; anomaly map

ACKNOWLEDGEMENTS

All the praises are for the Almighty, God, and unto Jesus Christ, who bestowed me with the ability and potential to complete this thesis. I also pay my gratitude to the Almighty for enabling me to complete this degree program within due course of time.

I would like to acknowledge all individuals and organizations that supported me during my BSc study at the Midlands State University. I am grateful to the Zimbabwean Government for giving me the opportunity to study and to Knowledge Factory Limited for assisting me with study techniques, equipment, software and guidance and SINO Zimbabwe who allowed me to use their project for educational purposes.

My principal supervisor Mr B. Siachingoma for introducing and inspiring me in the application of ground magnetics, for his guidance, scientific criticism and helpful suggestions without which this thesis would not have been viable. I am also grateful to my second supervisor Mr A Nechibvute for his critical review and scientific discussions.

I would like to express my sincere gratitude to Mr T Gumede for his invaluable guidance in all respects of geophysics, data acquisition and processing and for solving the problems I encountered during the processing of the data with no time from wherever he was. I am indebted also to the Physics Department staff, Mr Mazheke, Mr Mazunga, Mr Gora and Mrs Mugabe for providing me requisite information and knowledge for compilation of my complete thesis.

Words are very few to express enormous humble obligations to my affectionate siblings, Nomsa and Tinashe for their prayers and strong determination to enabling me to achieve. And I can never find words to express my gratitude to Juliet Mavengere and Tracy Chipokore.

DEDICATION

To my wife, Sharmil, my daughter, Matipamufaro Sandra, and my sister, Nomsa.

To my brother Tinashe, the great architect who has never lived to grace his designs.

CONTENTS

TITLE: i
DECLARATION iii
APPROVAL iv
ABSTRACT v
ACKNOWLEDGEMENTS vi
DEDICATION vii
CONTENTS viii
LIST OF FIGURES xi
CHAPTER 1: INTRODUCTION AND LITERATURE REVIEW 1
Introduction 1
Background and literature review 2
Study area 5
Limestone in the area 6
Access and Infrastructure 7
Topography and Climate 7
Limestone 8
Magnetic properties of limestone 8
Problem definition 8
Objective of the research 9
General objective of the research 9
Specific objectives of the research 9
Research questions 9
Justification of study 9
Limitations to study 10
CHAPTER 2: THEORETICAL ASPECTS 11

Introduction 11
The geomagnetic field 12
Basic concepts 16
Temporal variations 21
Diurnal variations 21
Micro pulsations 22
Magnetic storms 22
Secular variation. 23
International Geomagnetic Reference Field (IGRF) 24
Rock magnetism 24
Magnetic anomalies 25
Instrumentation 28
The proton precession magnetometer 28
CHAPTER 3: METHODOLOGY 31
Methodology 31
Reviewing previous geological and geophysical studies 31
Reconnaissance and geological mapping 33
The Magnetic survey 33
Data correction and reduction 36
Data visualisation and enhancement 38
Map construction 38
Data interpretation 44
Conclusion 45
CHAPTER 4: RESULTS AND DISCUSSIONS 46
Introduction 46
Data download 46
Data manipulation 47

Data reduction and correction 48
Image processing and discussions 53
Interpretations and geological integration 62
Qualitative interpretation 62
Quantitative interpretation 65
The principle of non-uniqueness 65
Economy of hypothesis - simplification of sources in modelling. 65
Integration with the geology 66
CHAPTER 5: CONCLUSIONS 68
Recommendations 69
REFERENCES 70

LIST OF FIGURES

Fig 1 the Masvingo Greenstone Belt and surrounding geologies *3*
Fig 2 the Masvingo Greenstone Belt gravity map *3*
Fig 3 the magnetic anomaly maps of the Masvingo Greenstone Belt and surrounding geologies. *4*
Fig 4 the global location of Masvingo province in which the survey area is situated (maphill, 2014). *5*
Fig 5 the Nyanda range bounded by the green diamond shape on the physical 3D map of the area. *5*
Fig 6 the satellite image of the Nyanda Mountains (googlemaps, 2014). *6*
Fig 7 shows one of the karstic caves right on the surveyed area. *6*
Fig 8 the main divisions of the Earth's volume, the Earth's dipolar magnetic field and the inclination of the field at varying latitudes respectively. *12*
Fig 9 The vector total magnetic field may be defined either as (a) three orthogonal components (horizontal north, horizontal east and vertical) or (b) as the scalar magnitude of the total field, ***F*** *and two angles, the inclination from the horizontal, I and the declination from true (geographic) north, D.* *13*
Fig 10 Geocentric axial dipole. *14*
Fig 11 compass needle portraying magnetic declination *15*
Fig 12 the magnetic flux surrounding a bar magnet and schematic representation of an element of material in which elementary dipoles align in the direction of an external field ***B*** *to produce an overall induced magnetization.* *16*
Fig 13 Variations in ***F*** *at a fixed point recorded over a number of weeks. Each tick-mark on the time axis is one day.* *21*
Fig 14 the solar wind distorts the outer reaches of the earth's magnetic field causing current loops in the ionosphere on the day-side of the rotating planet. *21*
Fig 15 Variations in ***F*** *recorded at stations a few tens of kilometres apart showing the nature of micro pulsations and their variation from place to place on the Earth's surface.* *22*
Fig 16 a typical magnetic storm, as observed at a time of high solar activity. The onset of the storm is sudden and violent variations in ***F*** *may be seen over several tens of hours. Return to 'normal field conditions may take several days.* *22*

Fig 17 the variations in F from a series of observations at repeat station (dots) in 1970 and 1975. The variations of F with position are shown as heavy lines, while thinner lines show the expected change in F with time in the years ahead. 23
Fig 18 Histogram showing mean values and ranges in susceptibility of common rock types. (USGS, 2014) 25
Fig 19 Vector representation of the geomagnetic field with and without a superimposed magnetic anomaly. 26
*Fig 20 the horizontal (**ΔH**), vertical (Δ**Z**) and total field (Δ**B**) anomalies due to an isolated positive pole. 27*
Fig 21 at a given location, the magnetometer records the vector sum of the ambient geomagnetic field and the anomalous contribution from (one or more) local sources. 27
Fig 22 GSM19T proton precession magnetometer 28
Fig 23 the magnetometer computer box unit and the sensor being used to collect readings during the Nyanda mountains survey. 29
Fig 24 principles of proton magnetometer 30
Fig 25 showing the conceptual framework of the research project 32
Fig 26 tie lines between bases in a magnetic survey with a 1 nT instrument. 35
Fig 27 the GARMIN GPS receiver used for the magnetic survey 36
Fig 28 the removal of a regional gradient from a magnetic field by trend analysis. The regional field is approximated by a linear trend. 37
Fig 29 A graph showing a typical magnetic field strength variation which can be measured along a profile. 38
Fig 30 The HSV colour model. 41
Fig 31 a pixel made up of a 3 x 3 dot pattern may be used to create ten grey levels. 42
Fig 32 9-point two-dimensional smoothing operator. 42
Fig 33 First horizontal derivative filtering on gridded data. 43
Fig 34 Second vertical derivative operators for gridded data 44
Fig 35 text file from the GEMlink 5.0 download for the project. 47
Fig 36 the text import wizard 48
Fig 37 sorting data using MS Excel so as to perform data quality check. 49
Fig 38 Oasis montaj IGRF calculator 50
Fig 39 Overview of the IGRF correction process 51
Fig 40 full window showing how excel was used to create profiles for the data 51
Fig 41 the profile plots for all the surveyed lines 52

Fig 42 profile plot for the first line of the survey *52*
Fig 43 profile plot of the middle most surveyed line *52*
Fig 44 profile plot of the last surveyed line *53*
Fig 45 Geosoft window showing the database for the magnetic data for this survey *54*
Fig 46 survey line path and tie line positions *55*
Fig 47 grey scale raster image from the magnetic survey data *55*
Fig 48 minimum curvature grid *56*
Fig 49 normal distribution colour (a) and linear distribution colour method (b) *57*
Fig 50 log linear colour method (a) and histogram equalisation colour method with wet look shading (b) *57*
Fig 51 bi-directional line gridding (a) and kriging gridding (b) *58*
Fig 52 direct gridding (a) and inverse distance weighted gridding (b) *58*
Fig 53 horizontal gradient filter (a) and vertical derivative filter (b) *60*
Fig 54 colour shaded grid (a) and showing trend lines removed (b) *61*
Fig 55 showing contour lines on the colour shaded grid (a) and showing the line path on the colour shaded grid (b) *62*
Fig 56 filtered grid showing the interpreted survey area (a) and showing interpreted colour shaded grid (b) *64*
Fig 57 showing interpreted minimum curvature grid *64*
Fig 58 source modelling *66*
Fig 59 depth modelling *67*

CHAPTER 1: INTRODUCTION AND LITERATURE REVIEW

Introduction

Exploration geophysics is the applied branch of geophysics which uses surface methods to measure the physical properties of the subsurface earth, along with the anomalies in these properties, in order to detect or infer the presence and position of ore minerals, hydrocarbons, geothermal reservoirs, groundwater reservoirs, and other geological structures (Kearey, 2002). It is the practical application of physical methods (such as seismic, gravitational, magnetic, electrical and electromagnetic) to measure the physical properties of rocks, and in particular, to detect the measurable physical differences between rocks that contain ore deposits or hydrocarbons and those without.

Magneto-metric surveys are useful in defining magnetic anomalies which represent ore (direct detection), or in some cases gangue minerals associated with ore deposits (indirect or inferential detection). The most direct method of detection of ore via magnetism involves detecting iron ore mineralisation via mapping magnetic anomalies associated with banded iron formations which usually contain magnetite in some proportion.

The aim of this magnetic survey was to detect limestone deposits by investigating subsurface geology on the basis of anomalies in the Earth's magnetic field resulting from the magnetic properties of the underlying rocks. Limestone is effectively non-magnetic while certain rock types contain sufficient magnetic minerals to produce significant magnetic anomalies.

Magnetic anomalies caused by rocks are localized effects superimposed on the normal magnetic field of the Earth (geomagnetic field). All magnetic anomalies caused by rocks are superimposed on the geomagnetic field in the same way that gravity anomalies are superimposed on the Earth's gravitational field (Clark, 1991). The magnetic case is more complex, however, as the geomagnetic field varies not only in amplitude, but also in direction, whereas the gravitational field is everywhere, by definition, vertical. Consequently, knowledge of the behaviour of the geomagnetic field was necessary both in the reduction of magnetic data to a suitable datum and in the interpretation of the resulting anomalies. In this study, the magnetic survey data of the Nyanda Mountains in Masvingo was analysed.

Background and literature review

Nyanda Mountains are located within the Masvingo Greenstone Belt (MGB) (Fig 1). The structure and subsurface configuration of the Belt (MGB) in the Zimbabwe Craton (ZC), were previously investigated using aeromagnetic and gravity data (Ranganai, 2009). The greenstone belt and ultramafic complexes have been shown to be characterized by Bouguer gravity highs, whereas the granitic terrain are lows, with the lowest values over the post-volcanic plutons. (Fig 2).

Magnetic maps compiled from the Zimbabwe Geological Survey national aeromagnetic data set shows that the bulk of the MGB have magnetic low anomaly values associated with limestone. A magnetic high anomaly arises along its northern and western margins over ultramafic units and banded iron formations. The younger granites generally show higher magnetic anomaly values compared to both the greenstone belt and the older gneisses. A pronounced east-northeast-trending broad magnetic high is observed over the Charumbira pluton, and its edges mark the boundaries with the greenstone belt to the north, and the Limpopo belt to the south; with the latter characterized by low magnetic values. Several linear, small amplitude magnetic lows, which are mostly due to faults, trend northwest to southeast and north to south, with some revealing an apparent dextral movement. Derivative maps for both gravity and magnetic data bring out some of the linear features and the edges of the greenstone belt and granite plutons (Ranganai, 2009).

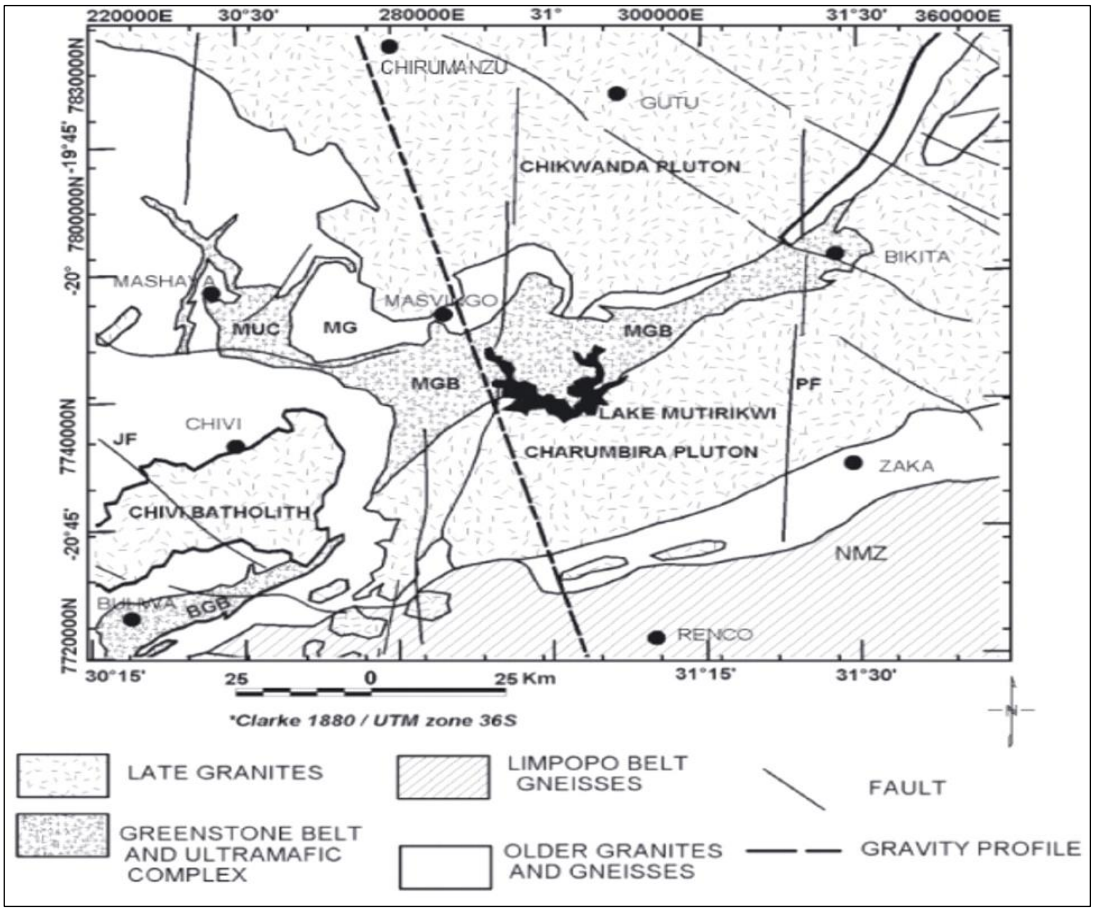

Fig 1 the Masvingo Greenstone Belt and surrounding geologies

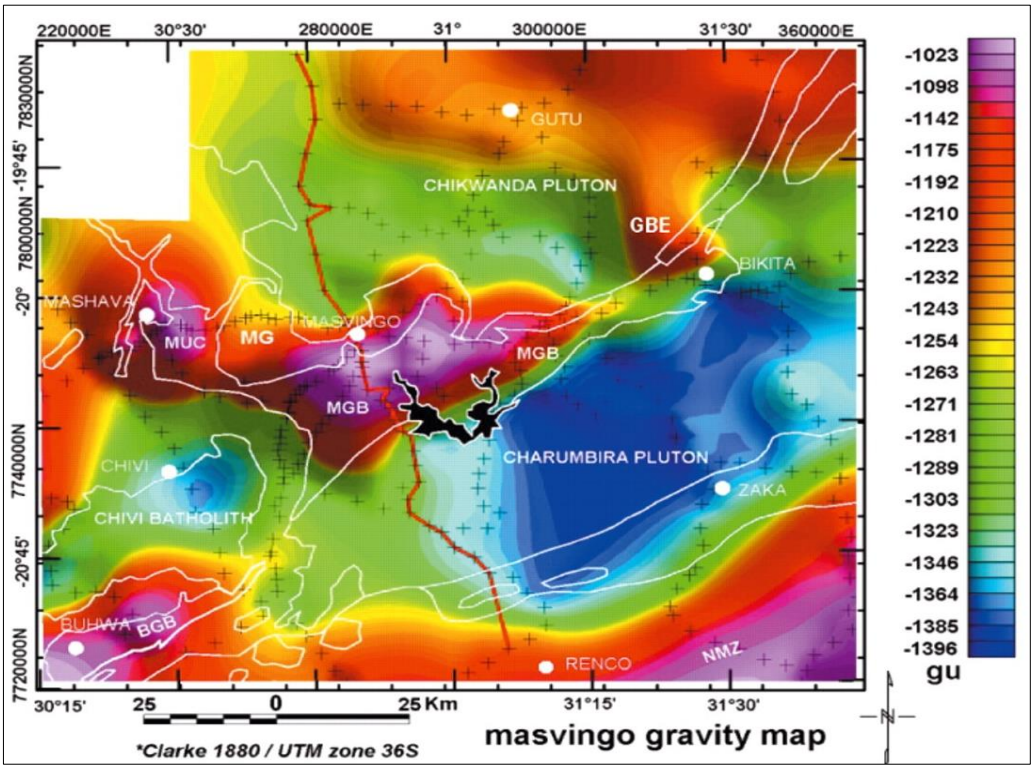

Fig 2 the Masvingo Greenstone Belt gravity map

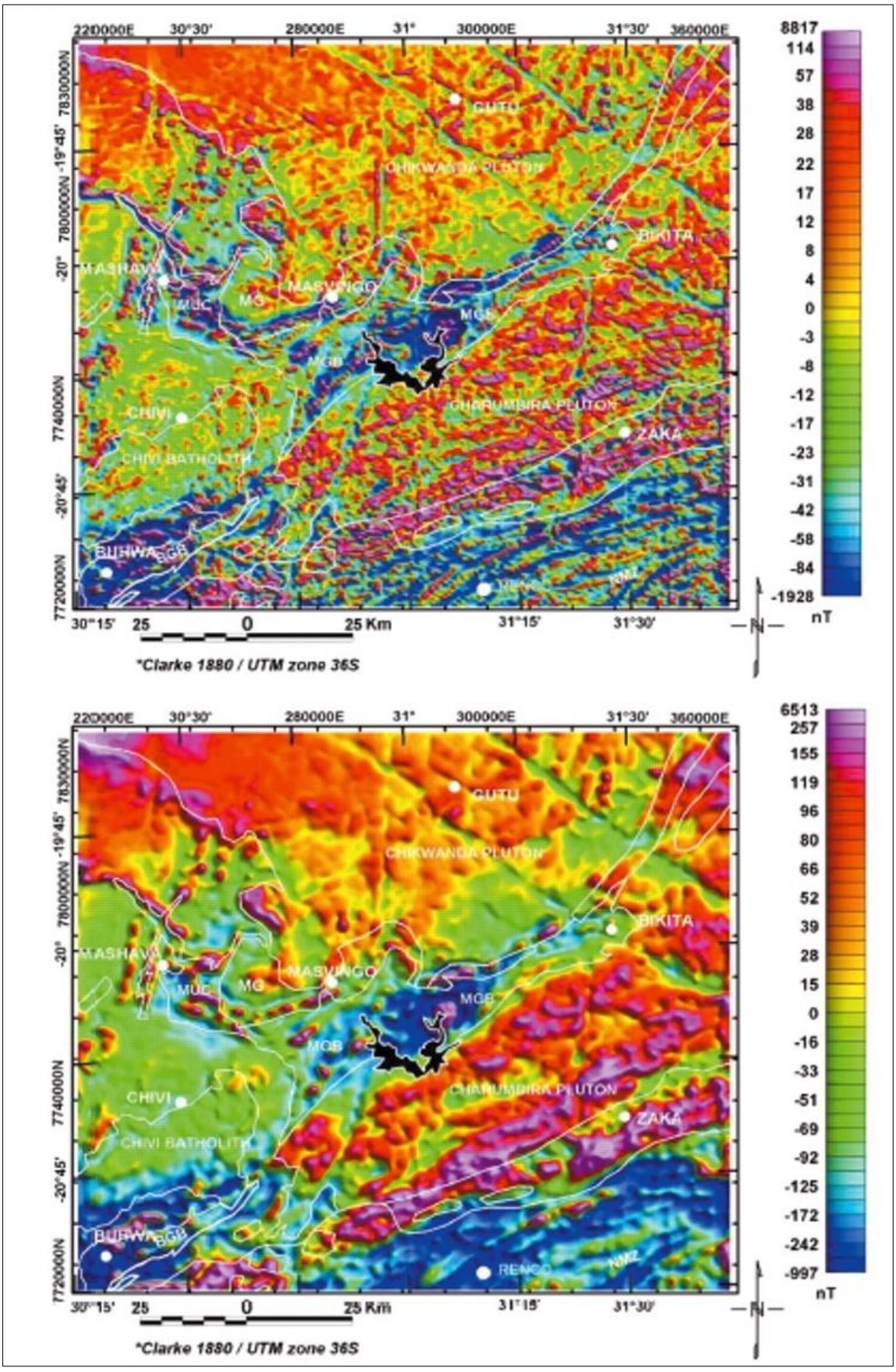

Fig 3 the magnetic anomaly maps of the Masvingo Greenstone Belt and surrounding geologies.

Study area

Nyanda mountain range is about 15km south east of Masvingo town, along the Masvingo-Beitbridge Highway. The survey site is bounded by 7772600N 260800E; 7772600N 262200E; 7772000N 262200E; 7772000N 260800E in local coordinates, ARC1960 UTM zone36S.

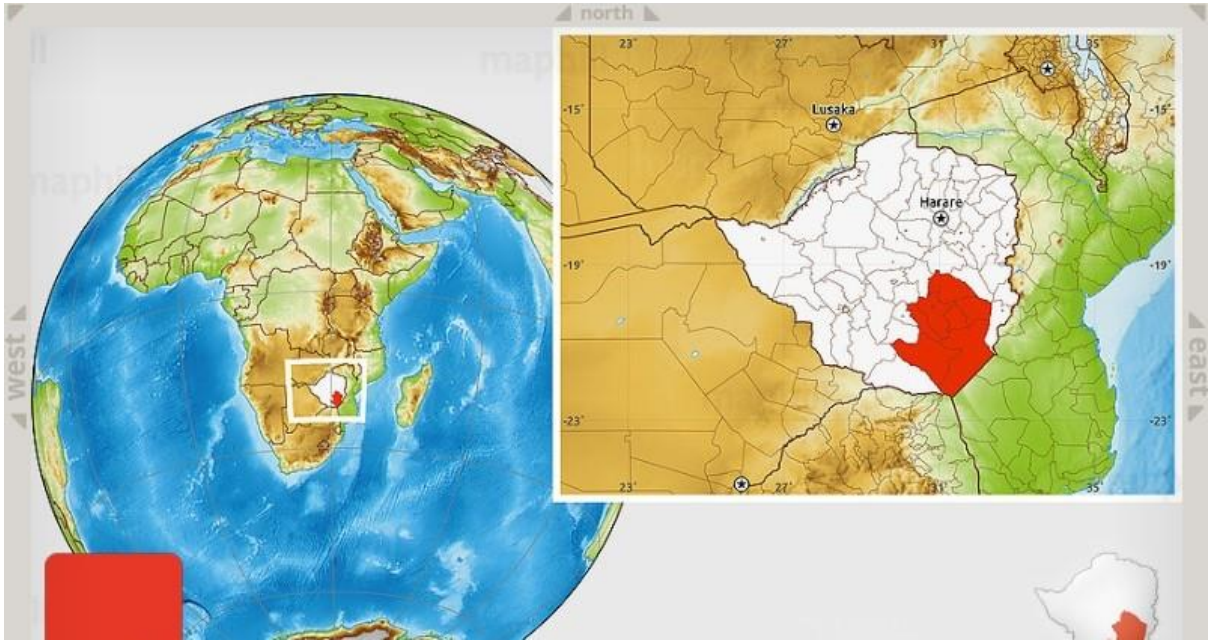

Fig 4 the global location of Masvingo province in which the survey area is situated (maphill, 2014).

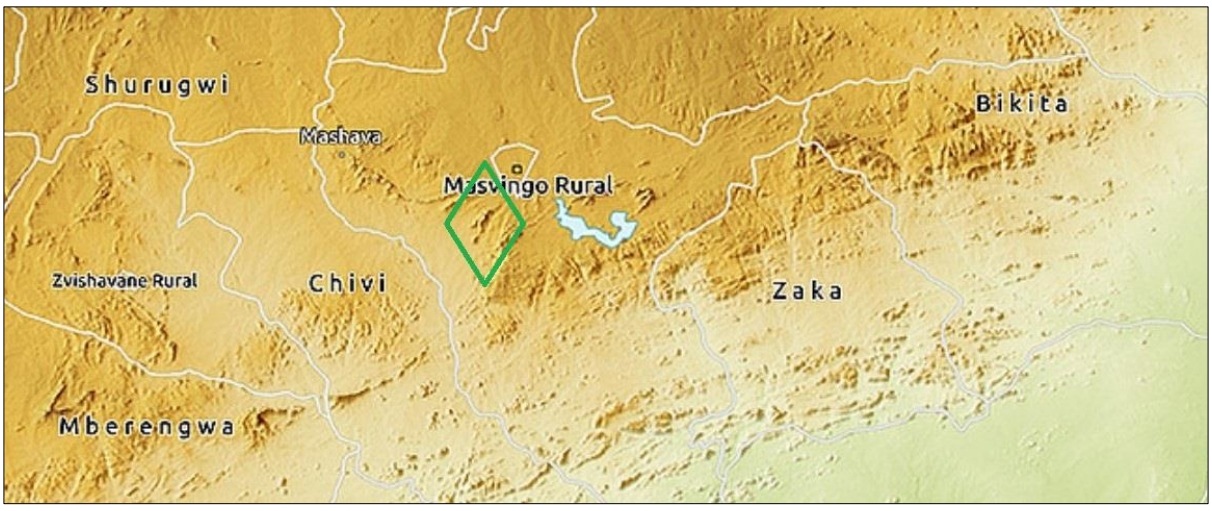

Fig 5 the Nyanda range bounded by the green diamond shape on the physical 3D map of the area.

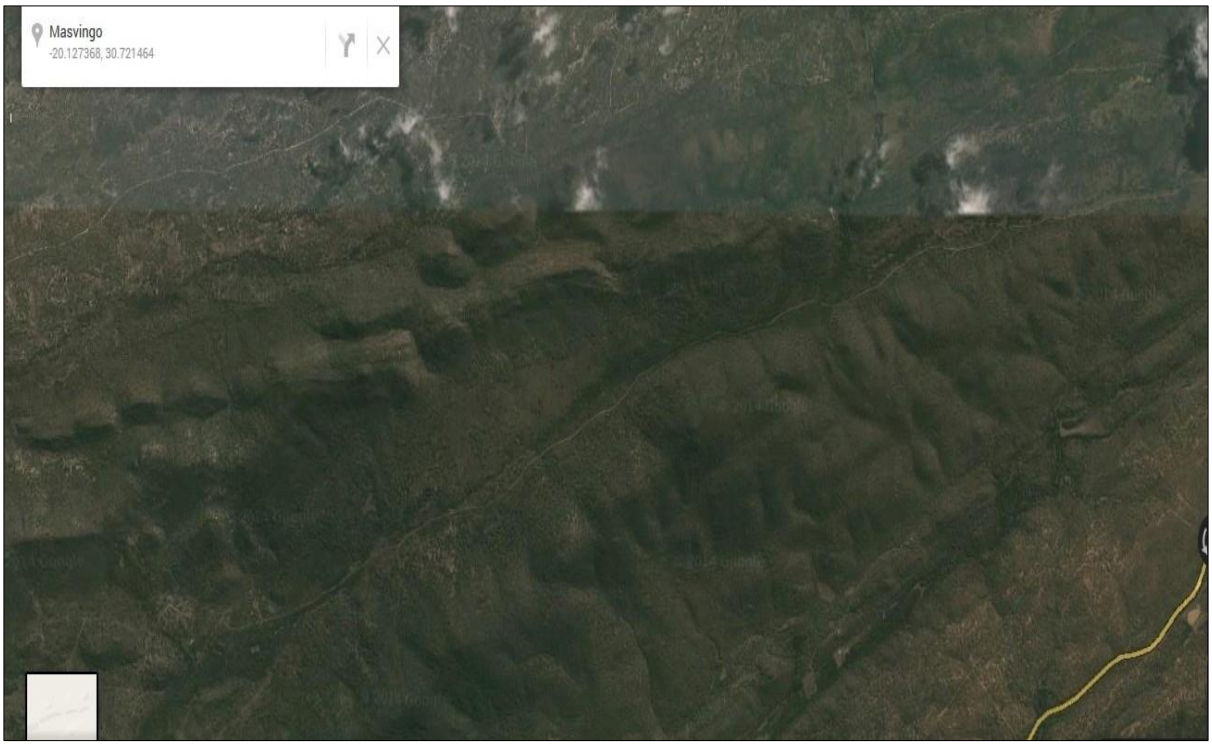

Fig 6 the satellite image of the Nyanda Mountains (googlemaps, 2014).

Limestone in the area.

The MGB has always shown considerable low magnetic values even in the aeromagnetic surveys that were done prior (Ranganai, 2009). Ground geological surveys also revealed vast karstic landscapes and caves all over the area.

Fig 7 shows one of the karstic caves right on the surveyed area.

Access and Infrastructure

- **Roads**

Accessibility to the Nyanda mountain range is fairly easy since the range is very close to a well serviced main road which connects Masvingo and Beitbridge from which an all-weather gravel road link up with the claims areas.

- **Railway Lines**

No railway line passes through the immediate vicinity of the survey area grid. The nearest railway line to the survey area plies the Masvingo-Gweru route.

- **Electricity**

Electric poles and cables are available at the farmhouse within 500m from the survey area although the facilities appear to have been poorly maintained. However, since both poles and power cables are still in place, and electricity supply is already available, connecting power in the survey claims area for any large scale operations will not be difficult.

- **Water**

A water augmentation program is being set up at Bushemead waterworks near Lake Mutirikwi, and also a massive water tank is being built at the Hillside Mountains to cater for the project (Maponga, 2011).

Topography and Climate

The terrain in which the survey area lie very steep. The area is mountainous, and the claims run from the foot of one branch up the peak to the foot and up again towards the peak of the second mountain branch. Outcrop is very abundant especially on the peaks of the two mountain branches and towards the feet of the branches. Weathering is fairly thick in the study area, often exceeding 3m in some places. The thicker weathered zones are generally associated with areas where streams have played a major role in the weathering and erosional processes. Soil colour is dominantly white and pale brown. As regards vegetation, the survey area falls into the Open forest-Tree veld group at the peaks and is slightly dense mountain vegetation near the foot of the main mountain branch. Climate is generally warm, with temperatures exceeding 30^{o}C in summer, and as low as 15^{o}C or less in winter. Rainfall is more marked between November and March. The numerous mountain streams which run from the peaks to the small rivers on the feet of the mountain branches provide with drainage for the survey area.

Limestone

Limestone is a sedimentary rock composed largely of the minerals calcite and aragonite, which are different crystal forms of calcium carbonate ($CaCO_3$). Limestone often contains variable amounts of silica in the form of chert (chalcedony, flint, jasper, etc.) or siliceous skeletal fragment (sponge spicules, diatoms, radiolarians), and varying amounts of clay, silt and sand (terrestrial detritus) carried in by rivers (Bakhtiar, 1986). The karst landscapes are due to the solubility of limestone in water and weak acid solutions. Most cave systems are through limestone bedrock (Hruska, 2000). Limestone has numerous uses: as a building material, as aggregate for the base of roads, as white pigment or filler in products such as toothpaste or paints, and as a chemical feedstock, hence the need to locate limestone reserves so as to guide in its extraction.

Magnetic properties of limestone

Properties of natural remnant magnetism are dependent on grain size of the magnetic carrier such as grain size of magnetite mineral, (multi-domain or single domain). Because the grain size of the magnetic carrier in the limestone is usually below the limit of optional resolution, and its abundance is very low, it is difficult to identify its magnetic minerals. This property is responsible for the low magnetic properties of limestone and the low magnetism is echoed in the low magnetic values exhibited by limestone during a magnetic survey (Parry, 1973).

Problem definition

The main problem at hand was the need to detect limestone deposits sitting on the survey area, Nyanda Mountains in Masvingo. The geology of the survey area suggested limestone deposits but there was need to conduct a geophysical survey which would further enhance and support the discovery of limestone on the range. Ground penetrating radar (GPR) followed by a resistivity survey were suggested. However GPR proved to be quite expensive to conduct, regarding the machinery required and the expertise needed to operate the survey. A resistivity survey, on the other hand, though quite affordable, it again proved to be impossible regarding the terrain to be surveyed which is mountainous and very steep, making the moving of resistivity equipment up and down and up again very strenuous and time consuming. A magnetic survey stood out to be the readily feasible option for the study because it was easier to traverse the terrain with the magnetometer and only a couple of people could undertake the survey in the shortest possible time. It was then envisaged that by conduction a ground

magnetic survey and incorporating the geological studies done prior, the limestone deposits would further be highlighted.

Objective of the research

The study seeks to identify areas where limestone deposits are likely to be concentrated by conducting a subsurface magnetic investigation of the bodies and mapping the prominent reflections of the voids in the caves and other underground carbonate features.

General objective of the research

The overall objective of the study is to obtain and interpret the magnetic survey data and then use the resulting anomaly maps to identify and delineate the limestone rich areas along the mountain range.

Specific objectives of the research

To identify and delineate limestone bodies from relatively high resolution magnetic data using various enhancement filters and grid algorithms so as to come up with the low magnetic areas on the map which will directly relate to the limestone rich areas.

Research questions

General

Based on the work of R.T. Ranganai and O. Gwavava, (Ranganai, 2009), in which they interpreted aeromagnetic data and gravity data for the MGB, can more be done to understand the distribution of limestone deposits around the Nyanda Mountains and their relation to magnetic low values with respect to the geomagnetic field?

Specific

Can a relationship between magnetic low value anomalies to limestone deposits distribution in the study area be established?

What are the criteria for creating a user-friendly mapping system of the study area using the magnetic survey data and previous works?

Justification of study

The motivation behind this study lies in the planned extraction of limestone in the survey area for cement production by SINO Zimbabwe. A cement making plant has been proposed right near the survey area (Maponga, 2011). Limestone and carbonic bodies and other geologic

anomalies should thus be studied attentively and mapped, and all data about them should be recorded carefully.

Limitations to study

- Time limit. It took longer to agree with SINO to allow the author carry out a research project on their behalf.
- Indirect detection of a physical body is always met by ambiguity in interpretation.
- Because of the steep plain, there was need for winding routes from station to station hence stalling the pace
- The main data processing software, Oasis Montaj, and MAPINFO could only be acquired from Knowledge Factory Limited due to unavailability at the university hence this limited the data processing time while awaiting acquisition of the software.
- The raw aeromagnetic and gravity data of the Masvingo greenstone belt could not be retrieved from the Geological Survey of Zimbabwe hence reliance was only on pre-processed anomaly images from the same organisation.

CHAPTER 2: THEORETICAL ASPECTS

Introduction

The science of geophysics applies the principles of physics to the study of the Earth. Geophysical investigations of the interior of the Earth involve measuring at or near the Earth's surface, taking measurements that are influenced by the internal distribution of earth's physical properties. Analysing these measurements reveals how the physical properties of the Earth's interior vary vertically and laterally. By working at different scales, geophysical methods may be applied to a wide range of investigations from studies of the entire Earth (Kearey & Vine, 1996) to exploration of a localized region of the upper crust for engineering or other purposes (McCann, 1997) (Vogelsang, 1995). An alternative method of investigating subsurface geology is, of course, by drilling boreholes, but these are expensive and provide information only at discrete locations.

Measurements in geophysical surveys are made in the field and many are also of fields. Field theory is fundamental to gravity, magnetic and electromagnetic work, and even particle fluxes and seismic wave fronts can be described in terms of radiation fields. The fields used in geophysical surveys may be natural ones (e.g. the Earth's magnetic or gravity fields) but may be created artificially, as when alternating currents are used to generate electromagnetic fields. This leads to the broad classification of geophysical methods into passive and active types, respectively (Kearey, 2002).

Geomagnetism suggests the earth may be made up of three parts: core, mantle and crust. Convection processes in the liquid part of the iron core give rise to a dipolar geomagnetic field that resembles that of a large bar-magnet aligned approximately along the earth's axis of rotation. The mantle plays little part in the earth's magnetism, while interaction of the geomagnetic field with the rocks of the Earth's crust produces the magnetic anomalies recorded in detailed magnetic surveys carried out close to the earth's surface (Reeves C, 2005).

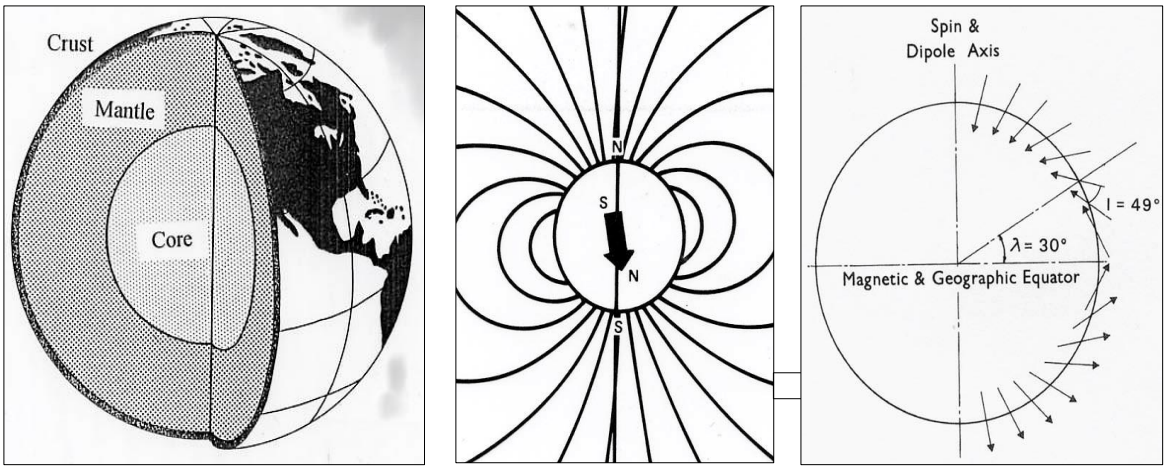

Fig 8 the main divisions of the Earth's volume, the Earth's dipolar magnetic field and the inclination of the field at varying latitudes respectively.

The geomagnetic field

The geomagnetic field is dipolar in nature hence the need for taking some care in specifying the field's direction during a magnetic survey. The field is oriented vertically downward at the north magnetic pole, is horizontal (and pointing north) at the magnetic equator and points vertically upwards at the south magnetic pole. The magnetic poles have moved considerably over historical times and detectable movement occurs even from year to year. Presently, the virtual magnetic poles may differ from the geographic poles by as much as 10 to 20 degrees (Milsom, 2002).

Three scalar values are required in the definition of the geomagnetic field, and are normally expressed either as three orthogonal components (vertical, horizontal-north and horizontal-east components) or the scalar magnitude of the total field vector and its orientation in dip and azimuth. Magnetic surveys have always measured only the scalar magnitude of **F**, hence the latter system is more convenient for present purposes. The angle the total field vector makes above or below the horizontal plane is known as the magnetic inclination, I, which is conventionally positive north of the magnetic equator and negative to the south of it. ($-90° \leq I \leq +90°$). The angle between the vertical plane containing **F** and true (geographic) north is known as the magnetic declination, D, which is reckoned positive to the east and negative to the west. Magnetic declination is less than 15° in most places on the Earth, but may reach 180° along lines joining the magnetic and geographic poles.

Simple dipole theory predicts that the magnetic inclination, I, will be related to geographic latitude, λ, as

$$\text{Tan } I = 2 \tan \lambda \quad \text{..... [1]}$$

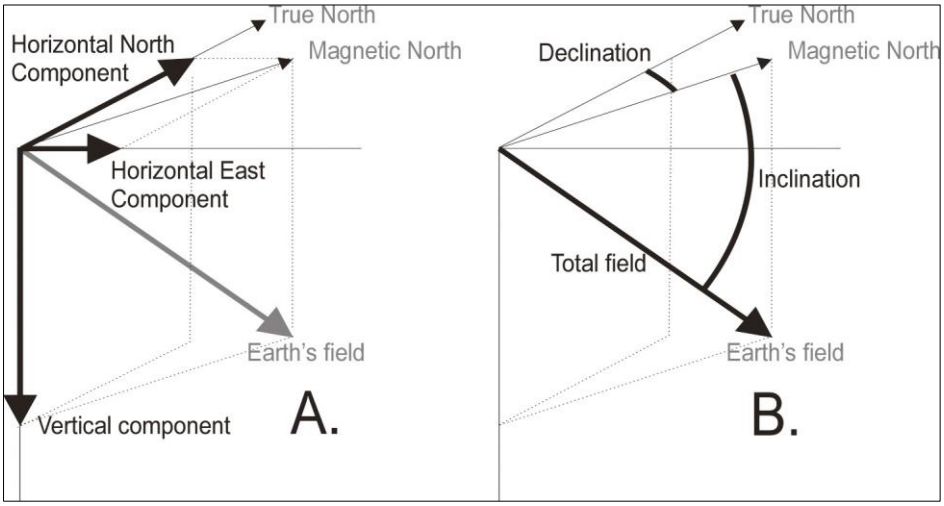

*Fig 9 The vector total magnetic field may be defined either as (a) three orthogonal components (horizontal north, horizontal east and vertical) or (b) as the scalar magnitude of the total field, **F** and two angles, the inclination from the horizontal, I and the declination from true (geographic) north, D.*

The magnetic inclination equation is derived from the diagram (Fig 10), the geometry is for a geocentric axial dipole. The derivation is developed by using spherical coordinates: r, θ, and φ, an additional polar angle, p, is the colatitude and is defined as $\pi - \theta$. After each quantity is derived in spherical coordinates, the resulting equation is altered to provide the results in the convenient forms such as horizontal and vertical components. The large arrow is the magnetic dipole moment, **M**; θ is the polar angle from the positive pole of the magnetic dipole; p is the magnetic colatitude; λ is the geographic latitude; r is the radial distance from the magnetic dipole; **H** is the magnetic field produced by the magnetic dipole; r^ is the unit vector in the direction of r. The inset figure on Fig. 10 in the upper right corner is a magnified version of the stippled region. Inclination, I, is the vertical angle (dip) between the horizontal and **H**. The magnetic field vector **H** can be broken into (1) vertical component, $\mathbf{H}_v = -\mathbf{H}_r$, and (2) horizontal component, $\mathbf{H}_h = \mathbf{H}_\theta . \frac{\partial y}{\partial x}$

From Fig 10, the scalar magnetic potential of a magnetic dipole is

$$V = \frac{\boldsymbol{M}.\hat{r}}{r^2} = \frac{M\cos\theta}{r^2} \quad \text{..... [2]}$$

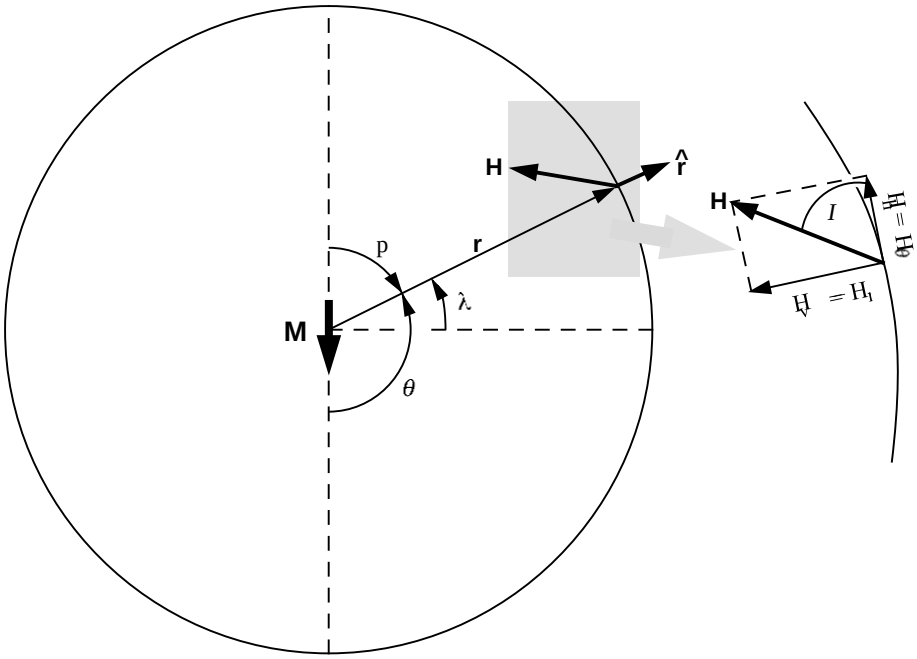

Fig 10 Geocentric axial dipole.

The magnetic field, **H**, is derived from the scalar magnetic potential by taking the gradient of the potential

$$\mathbf{H} = -\nabla V = -\frac{\partial}{\partial r}\hat{r} + \frac{1}{r}\frac{\partial}{\partial \theta}\hat{\theta}\,\frac{M\cos\theta}{r^2} \quad \text{[3]}$$

Separating the differentials yields

$$\mathbf{H} = \frac{\partial}{\partial r}\frac{M\cos\theta}{r^2}\hat{r} - \frac{1}{r}\frac{\partial}{\partial \theta}\hat{\theta}\,\frac{M\cos\theta}{r^2} \quad \text{[4]}$$

Performing the required differentiations leads to

$$\mathbf{H} = \frac{2M\cos\theta}{r^3}\hat{r} + \frac{M\sin\theta}{r^3}\,\hat{\theta} = \mathbf{H}_v\,\hat{r} + \mathbf{H}_\theta\,\hat{\theta} \quad \text{[5]}$$

The horizontal component, $\mathbf{H}_h$, of **H** is then given by

$$\mathbf{H}_h = \mathbf{H}_\theta = \frac{M\cos\theta}{r^3} = \frac{M\sin(\pi-\theta)}{r^3} = \frac{M\sin p}{r^3} \quad \text{[6]}$$

To get this expression in terms of geographic latitude, λ, substitute

$$P = \frac{\pi}{2} - \lambda \quad \text{[7]}$$

To yield

$$\mathbf{H}_h = \frac{M\cos\lambda}{r^3} \quad \text{[8]}$$

The vertical component, $\mathbf{H}_v$, of **H** is

$$\mathbf{H}_v = -\mathbf{H}_r = \frac{2M\cos\theta}{r^3} = \frac{2M\cos p}{r^3} \quad \text{..... [9]}$$

$$\mathbf{H}_v = \frac{2M\sin\lambda}{r^3} \quad \text{..... [10]}$$

The inclination, I, can be determined by

$$\text{Tan I} = \frac{\boldsymbol{H_v}}{H_h} = \frac{2M\cos p}{r^3} \frac{r^3}{M\sin p} = 2\cot p \quad \text{..... [11]}$$

Using $P = \frac{\pi}{2} - \lambda$, the inclination is given as a function of geographic latitude by

$$\text{Tan I} = 2\tan\lambda \quad \text{..... [12] = [1]}$$

Magnetic declination is the angle on the horizontal plane between magnetic north (the direction in which the north end of a compass needle points, corresponding to the direction of the Earth's magnetic field lines) and true north (the direction along a meridian towards the geographic North Pole) (Van Blaricom, 1992). This angle varies depending on one's position on the Earth's surface, and over time. By convention the declination is positive when magnetic north is east of true north, and negative when it is to the west. Isogonic lines are lines on the Earth's surface along which the declination has the same constant value, and lines along which the declination is zero are called agonic lines. The magnetic declination at any particular place can be measured directly by reference to the celestial poles – the points in the heavens around which the stars appear to revolve, and which mark the direction of true north and true south. The instrument used to perform this measurement is known as a declinometer.

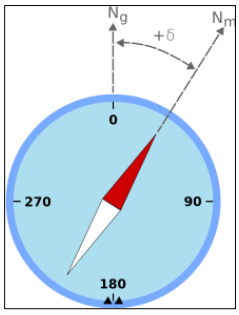

Fig 11 compass needle portraying magnetic declination

Example of magnetic declination (Fig 11) is showing a compass needle with a "positive" (or "easterly") variation from geographic north. N_g is geographic or true north, N_m is magnetic north, and δ is magnetic declination.

Since mapping of local variations in **F** attributable to crustal geology is the purpose of magnetic surveys, it is the definition of the 'normal' or global variation in **F** that must be subtracted from observed **F** to leave the (time invariable) magnetic anomaly that is of concerns. As often in geophysics, the need to define the normal before being able to isolate the 'anomaly' is clear.

Basic concepts

Magnetic flux flows from one end of a magnet to the other, within the vicinity of a bar magnet. A small compass needle assumes directions when suspended within the flux, and hence the flux is mapped. The points within the magnet where the flux converges are known as the poles of the magnet. A freely-suspended bar magnet aligns in the flux of the Earth's magnetic field in the same way. The pole of the magnet which tends to point in the direction of the Earth's North Pole is the north-seeking or positive pole, and this is balanced by a south-seeking or negative pole of identical strength at the opposite end of the magnet.

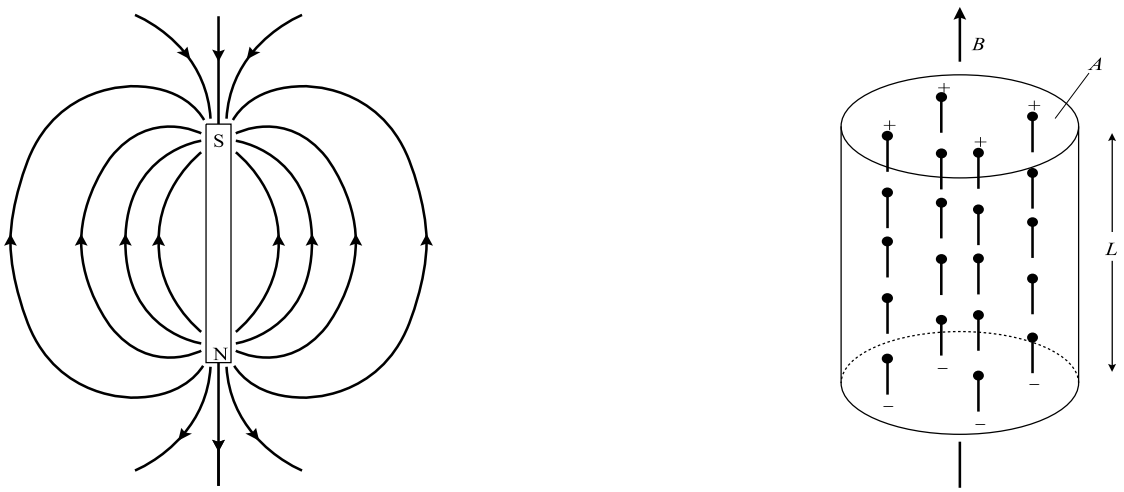

*Fig 12 the magnetic flux surrounding a bar magnet and schematic representation of an element of material in which elementary dipoles align in the direction of an external field **B** to produce an overall induced magnetization.*

The force **F** between two magnetic poles of strengths m_1 and m_2 separated by a distance r is given by

$$\mathbf{F} = \frac{\mu_o m_1 m_2}{4\pi\mu_R r^2} \quad \text{[13]}$$

where μ_o and μ_R are constants corresponding to the magnetic permeability of vacuum and the relative magnetic permeability of the medium separating the poles. The force is attractive if the poles are of different sign and repulsive if they are of like sign. The magnetic field **B** due to a

pole of strength m at a distance r from the pole is defined as the force exerted on a unit positive pole at that point

$$\mathbf{B} = \frac{\mu_o m}{4\pi\mu_R r^2} \quad \text{[14]}$$

Magnetic fields can be defined in terms of magnetic potentials just as with gravitational fields. For a single pole of strength m, the magnetic potential **V** at a distance r from the pole is given by

$$\mathbf{V} = \frac{\mu_o m}{4\pi\,\mu_R\, r} \quad \text{[15]}$$

The magnetic field component in any direction is then given by the partial derivative of the potential in that direction (Parasnis, 1996).

When a current passes through a coil consisting of several turns of wire, a magnetic flux flows through and around the coil annulus which arises from a magnetizing force **H**. The magnitude of **H** is proportional to the number of turns in the coil and the strength of the current, and inversely proportional to the length of the wire, so that **H** is expressed in Am^{-1}. Magnetic induction, or magnetic field, **B,** is the density of the magnetic flux, measured over an area perpendicular to the direction of flow. **B** is proportional to **H** and the constant of proportionality μ is known as the magnetic permeability. Lenz's law of induction relates the rate of change of magnetic flux in a circuit to the voltage developed within it, so that **B** is expressed in Vsm^{-2} (Weber (Wb) m^{-2}). The unit of the Wbm^{-2} is designated the tesla (T). Permeability is consequently expressed in $WbA^{-1}m^{-1}$ or Henry (H) m^{-1}. (Kearey, 2002)

Tesla is too large a unit in which to express the small magnetic anomalies caused by rocks, and a subunit, the nanotesla (nT), is employed ($1nT = 10^{-9}T$).

Magnets are dipoles. The magnetic moment M of a dipole with poles of strength m a distance l apart is given by

$$M = ml \quad \text{[16]}$$

The magnetic moment of a current-carrying coil is proportional to the number of turns in the coil, its cross-sectional area and the magnitude of the current, so that magnetic moment is expressed in Am^2.

Some materials acquire magnetism in the direction of field, which is then lost when the material is removed from the field. This phenomenon is referred to as induced magnetization or

magnetic polarization, and results from the alignment of elementary dipoles within the material in the direction of the field. As a result of this alignment the material has magnetic poles distributed over its surface which correspond to the ends of the dipoles. The intensity of induced magnetization J_i of a material is defined as the dipole moment per unit volume of material such that

$$J_i = \frac{M}{LA} \quad \text{[17]}$$

where M is the magnetic moment of a sample of length L and cross-sectional area A. J_i is consequently expressed in Am^{-1}.

Induced intensity of magnetization is directly proportional to the strength of the magnetizing force H of the inducing field such that

$$J_i = k\mathbf{H} \quad \text{[18]}$$

where k is the magnetic susceptibility of the material. Since J_i and **H** are both measured in Am^{-1}, susceptibility is dimensionless in the SI system.

Magnetic field strength **B** and magnetizing force **H** are related, in a vacuum, as

$$\mathbf{B} = \mu_o\mathbf{H} \quad \text{[19]}$$

where μ_o is the permeability of vacuum (4π X $10^{-7}Hm^{-1}$). Air and water have their permeability almost equal to μ_o and so this relationship can be taken to represent the Earth's magnetic field when it is undisturbed by magnetic materials. Placing a magnetic material in this field will result in a magnetization which gives rise to an additional magnetic field in the region occupied by the material, whose strength is given by $\mu_o J_i$.

Within the body the total magnetic field, or magnetic induction, **B** is given by

$$\mathbf{B} = \mu_o\mathbf{H} + \mu_o Ji \quad \text{[20]}$$

Hence,

$$\mathbf{B} = \mu_o\mathbf{H} + \mu_o k\mathbf{H} = (1+ k)\ \mu_o\mathbf{H} = \mu_R\mu_o\mathbf{H} \quad \text{[21]}$$

where μ_R is a dimensionless constant, called the relative magnetic permeability. The magnetic permeability μ is hence equal to the product of the relative permeability and the permeability of vacuum, and has the same dimensions as μ_R. For air and water μ_R is thus close to unity.

All substances are magnetic at an atomic scale. The spin of its electrons and the orbital path of the electrons around the nucleus gives the atom its dipole behaviour. By quantum theory, two electrons can exist in the same state or electron shell as long as spins are in opposite directions. They become paired electrons and their spin magnetic moments cancel. All electron shells are full and no unpaired electrons exist in diamagnetic materials. When placed in a magnetic field the orbital paths of the electrons rotate so as to produce a magnetic field in opposition to the applied field. Consequently, the susceptibility of diamagnetic substances is weak and negative. In paramagnetic substances, the electron shells are incomplete so that a magnetic field results from the spin of their unpaired electrons. Placed in an external magnetic field, the dipoles corresponding to the unpaired electron spins rotate to produce a field in the same sense as the applied field so that the susceptibility is positive (Telford, 1990). This is still, however, a relatively weak effect.

In some paramagnetic substances whose atoms contain several unpaired electrons, the dipoles associated with the spins of the unpaired electrons are magnetically coupled between adjacent atoms. Such a material constitute a single magnetic domain. This coupling may be either parallel or antiparallel depending on the degree of overlap of the electron orbits. The dipoles are parallel in ferromagnetic materials, giving rise to a very strong spontaneous magnetization which can exist even in the absence of an external magnetic field, and a very high susceptibility. Ferromagnetic substances include iron, cobalt and nickel, and rarely occur naturally in the Earth's crust. In antiferromagnetic materials such as haematite, the dipole coupling is antiparallel with equal numbers of dipoles in each direction. The magnetic fields of the dipoles are self-cancelling so that there is no external magnetic effect. However, defects in the crystal lattice structure of an antiferromagnetic material may give rise to a small net magnetization, called parasitic anti-ferromagnetism. In ferromagnetic materials such as magnetite, the dipole coupling is similarly antiparallel, but the strength of dipoles in each direction are unequal. Consequently ferromagnetic materials can exhibit a strong spontaneous magnetization and a high susceptibility. Virtually all the minerals responsible for the magnetic properties of common rock types fall into this category (Milsom, 2002).

The strength of the magnetization of ferromagnetic and ferrimagnetic substances decreases with temperature and disappears at the Curie temperature. Above this temperature interatomic distances are increased to separations which preclude electron coupling, and the material behaves as an ordinary paramagnetic substance.

In larger materials, the total magnetic energy decreases when the magnetization of each grain subdivides into individual volume elements (magnetic domains) with diameters of the order of a micrometre, within which there is parallel coupling of dipoles. In the absence of any external magnetic field the domains become oriented in such a way as to reduce the magnetic forces between adjacent domains. The boundary between two domains, the Bloch wall, is a narrow zone in which the dipoles cant over from one domain direction to the other.

Placing a multi domain grain in a weak external magnetic field causes the Bloch wall to unroll and causes a growth of those domains magnetized in the direction of the field at the expense of domains magnetized in other directions (Kearey, 1984). This induced magnetization is lost when the applied field is removed as the domain walls rotate back to their original configuration. Applying stronger fields, domain walls unroll irreversibly across small imperfections in the grain so that those domains magnetized in the direction of the field are permanently enlarged. The inherited magnetization remaining after removal of the applied field is known as remnant, or permanent, magnetization J_r. The application of even stronger magnetic fields causes all possible domain wall movements to occur and the material is then said to be magnetically saturated.

Primary remanent magnetization may be acquired either as an igneous rock solidifies and cools through the Curie temperature of its magnetic minerals (thermoremanent magnetization, TRM) or as the magnetic particles of a sediment align within the Earth's field during sedimentation (detrital remanent magnetization, DRM). Secondary remanent magnetizations may be impressed later in the history of a rock as magnetic minerals recrystallize or grow during diagenesis or metamorphism (chemical remanent magnetization, CRM). Remanent magnetization may develop slowly in a rock standing in an ambient magnetic field as the domain magnetizations relax into the direction of the field (viscous remanent magnetization, VRM) (Hoover, 1992).

Any rock containing magnetic minerals may possess both induced and remanent magnetizations J_i and J_r. The relative intensities of induced and remanent magnetizations are commonly expressed in terms of the Königsberger ratio, J_r: J_i. These may be in different directions and may differ significantly in magnitude. The magnetic effects of such a rock arise from the resultant J of the two magnetization vectors. The magnitude of J controls the amplitude of the magnetic anomaly and the orientation of J influences its shape (Kearey, 2002).

Temporal variations

These are the variations in **F** with time over time-scales ranging from seconds to millions of years and they have a profound effect on how magnetic surveys are carried out, on the subtraction of the main field from the measured field to leave the anomaly, and in the interpretation of the resulting anomalies.

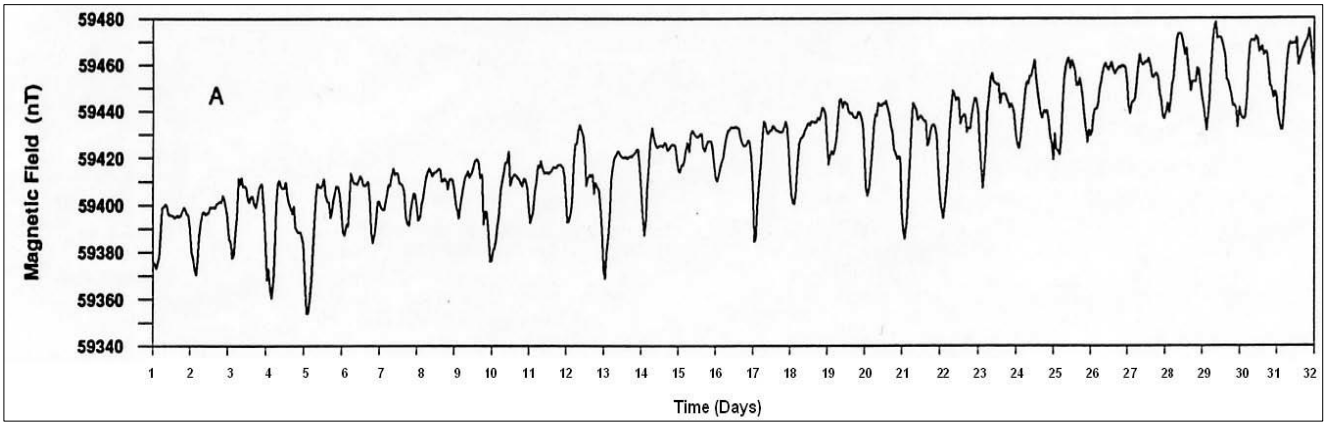

*Fig 13 Variations in **F** at a fixed point recorded over a number of weeks. Each tick-mark on the time axis is one day.*

Diurnal variations

The variations follow a daily cycle associated with the rotation of the earth and they arise from the rotation of the earth with respect to the sun. The 'solar wind' of charged particles emanating from the sun, even under normal or 'quiet sun' conditions, tends to distort the outer regions of the earth's magnetic field. The daily rotation of the earth within this sun-referenced distortion leads to ionospheric currents on the ’day’ side of the planet and a consequential daily cycle of variation in **F** that usually has an amplitude of less than about 50 nT.

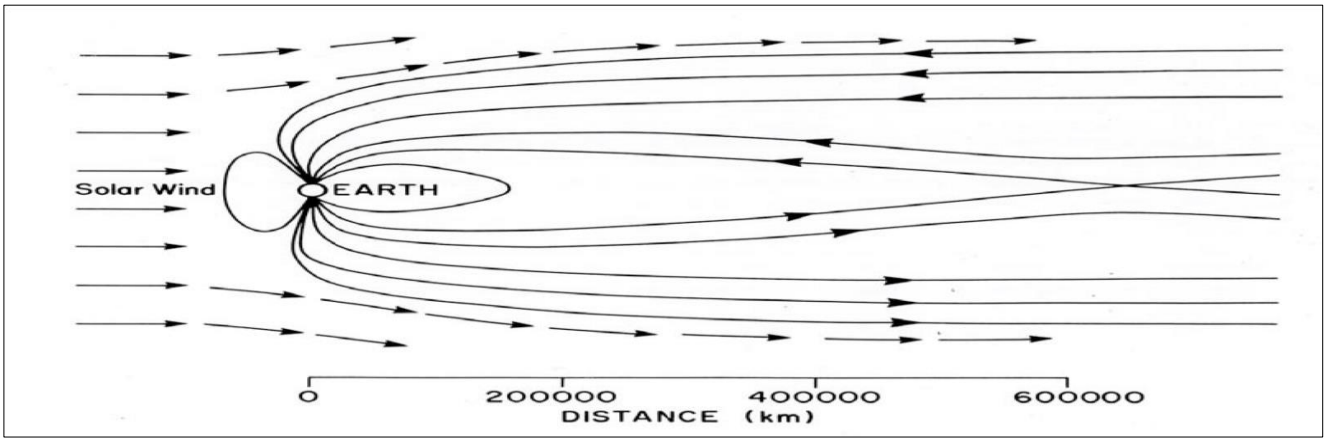

Fig 14 the solar wind distorts the outer reaches of the earth’s magnetic field causing current loops in the ionosphere on the day-side of the rotating planet.

Micro pulsations

These occur on a much shorter time scale, commonly over a few minutes. Although their amplitudes may be only a few nT, their effect on magnetic records made in an aircraft or at a base station on the ground is significant. Unfortunately, the exact shape of a recorded sequence of micro pulsations may change from place to place over a few tens of kilometres, so even subtraction of time variations observed at a fixed location from the anomalies recorded in an aircraft is not without its limitations and effective elimination of such short-term geomagnetic variations is one of the limits presently set to the accuracy with which spatially-related variations in magnetic field may be mapped without distortions attributable to temporal effects.

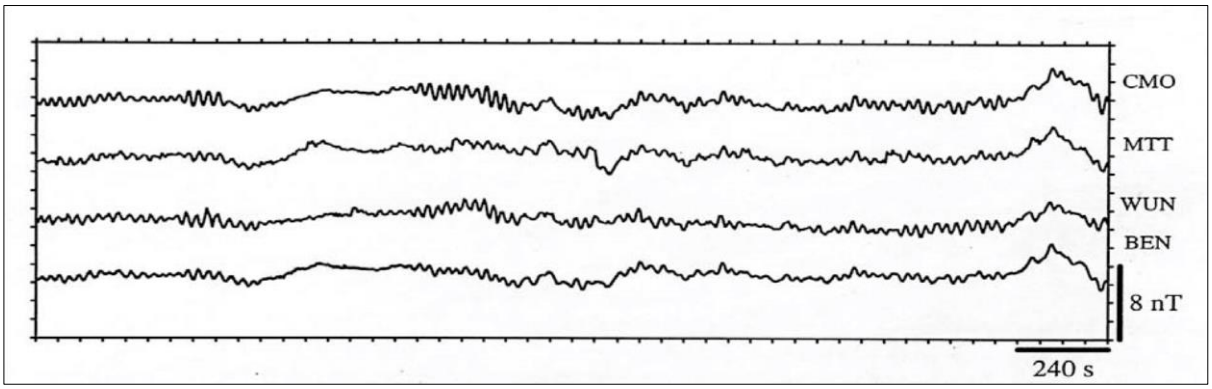

*Fig 15 Variations in **F** recorded at stations a few tens of kilometres apart showing the nature of micro pulsations and their variation from place to place on the Earth's surface.*

Magnetic storms

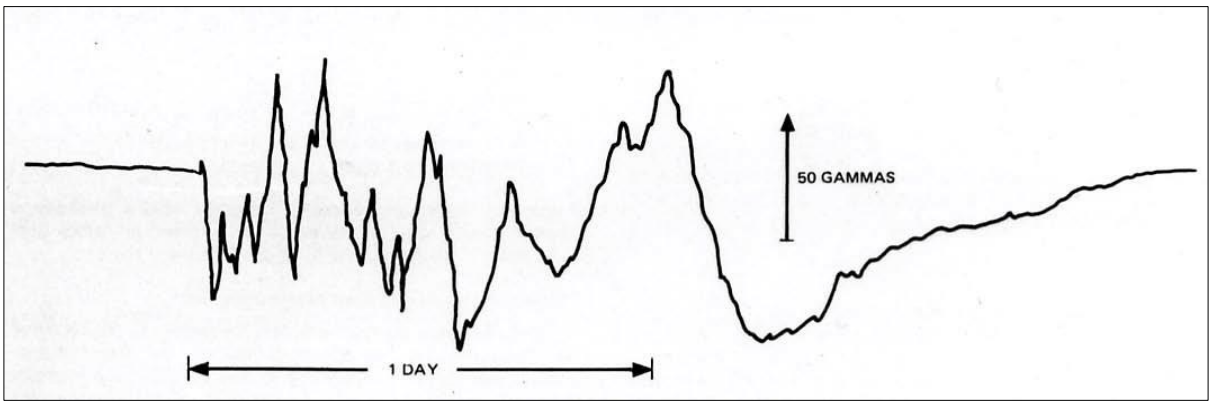

*Fig 16 a typical magnetic storm, as observed at a time of high solar activity. The onset of the storm is sudden and violent variations in **F** may be seen over several tens of hours. Return to 'normal field conditions may take several days.*

These are isolated periods of much higher levels of magnetic variation which are related to sunspot activities. Violent variations of several hundred nT may start quite suddenly and continue for periods in excess of 24 hours. The shape of the curve observed in a storm varies

from place to place and there is no prospect of acquiring information on spatial variations in **F** of the quality required in a magnetic survey while a magnetic storm is in progress.

All three of the above variations operate on time-scales that are short in comparison with the time taken to carry out a magnetic survey, which is usually weeks or months. They therefore require careful monitoring if good data are to be acquired from which reliable spatial, time-invariant magnetic anomalies can be reliably mapped.

Secular variation.

Secular variations occur on a much longer time-scale - hundreds of years – are well documented from historical data and the accurate magnetic observatory records of more recent decades (CSIR, 1975). Their main manifestation globally is changes in size and position of the departures from a simple dipolar field over years and decades. The effects of these changes at a given locality are predictable with a fair degree of accuracy for periods of five to ten years into the future, but such predictions need to be updated as more recent magnetic observatory and earth satellite recordings become available. In magnetic anomaly mapping, secular variations become important when surveys of adjacent or overlapping areas carried out several years apart are to be compared or merged together.

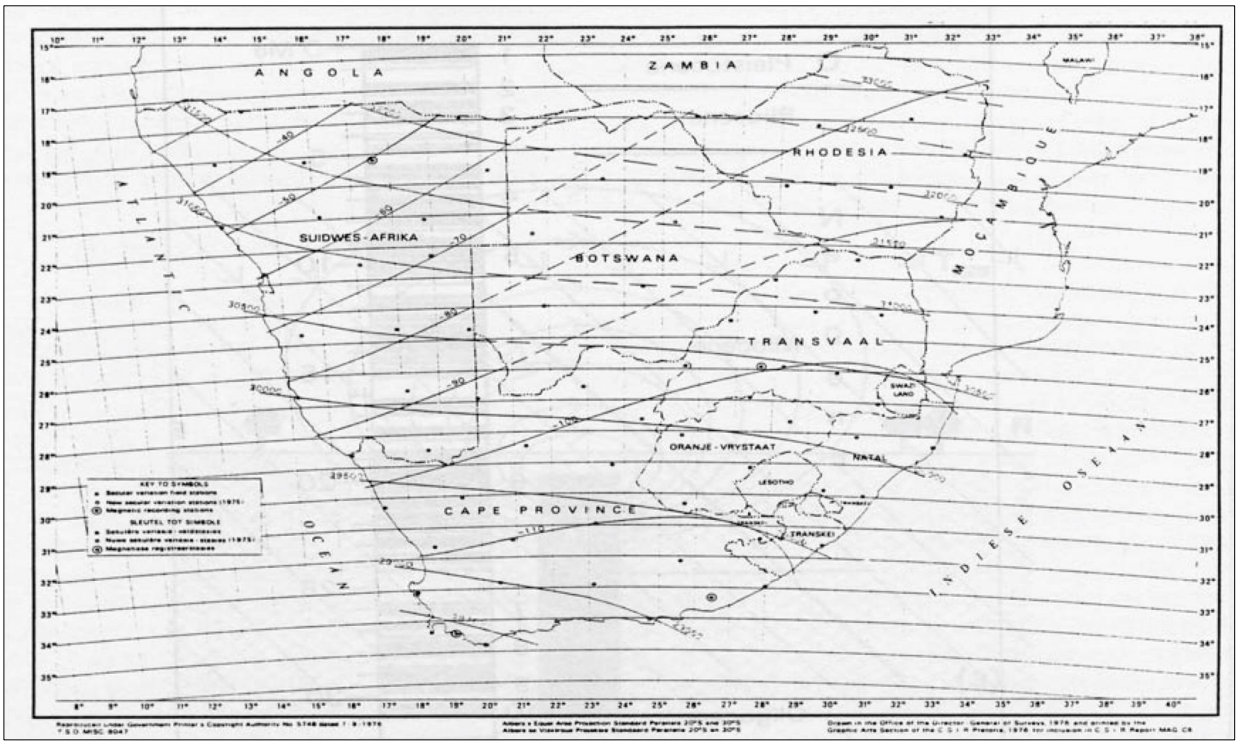

Fig 17 the variations in F from a series of observations at repeat station (dots) in 1970 and 1975. The variations of F with position are shown as heavy lines, while thinner lines show the expected change in F with time in the years ahead.

International Geomagnetic Reference Field (IGRF)

Magnetic surveys records the variations in F with x and y over a survey area while eliminating all time-based variations. The magnitude of **F** will fall be between 20 000 and 70 000 nT everywhere on earth and it can be expected to have local variations of several hundred nT imposed upon it by the effects of the magnetisation of the crustal geology. The 'anomalies' are usually at least two orders of magnitude smaller than the value of the total field. The IGRF provides the means of subtracting on a rational basis the expected variation in the main field to leave anomalies that may be compared from one survey to another, even when surveys are conducted several decades apart and when, as a consequence, the main field may have been subject to considerable secular variation (MacMillan, 2003). IGRF removal involves the subtraction of about 99% of the measured value, hence the IGRF needs to be defined with precision if the remainder is to retain accuracy and credibility.

The International Association of Geomagnetism and Aeronomy (IAGA) publishes the IGRF on a five-yearly basis. A mathematical model is advanced which best fits all actual observational data from geomagnetic observatories, satellites and other approved sources for a given epoch. Software is available which permits the use of these coefficients to calculate IGRF values over any chosen survey area.

Rock magnetism

The magnetic materials contained in the rock forming minerals gives the rocks their marked low magnetic susceptibility. Two geochemical groups provide such minerals. The iron–titanium–oxygen group possesses a solid solution series of magnetic minerals from magnetite (Fe_3O_4) to ulvöspinel (Fe_2TiO_4). Haematite (Fe_2O_3), is antiferromagnetic and does not exhibit magnetic anomalies unless a parasitic antiferromagnetism is developed. The iron–sulphur group provides the magnetic mineral pyrrhotite (FeS_{1+x}, $0 < x < 0.15$) whose magnetic susceptibility is dependent upon the actual composition (Kearey, 2002).

Magnetite is the most common magnetic mineral. Igneous rocks are mostly highly magnetic because of their relatively high magnetite content. The magnetite in igneous rocks is inversely proportional to acidity so that acid igneous rocks are usually less magnetic than basic rocks, despite being variable in their magnetic behaviour. Metamorphic rocks are also variable in their magnetic character. When the partial pressure of oxygen is relatively low, magnetite is resorbed and the iron and oxygen become incorporated into other mineral phases, as the grade of metamorphism increases. However, high oxygen partial pressure results in the formation of

magnetite as an accessory mineral in metamorphic reactions. Magnetite content and susceptibility are extremely variable and they do overlap between different lithologies. Sedimentary rocks are mostly non-magnetic unless they possess a significant amount of magnetite in the heavy mineral fraction. Where magnetic anomalies are observed over sediment covered areas the anomalies are generally caused by an underlying igneous or metamorphic basement, or by intrusions into the sediments.

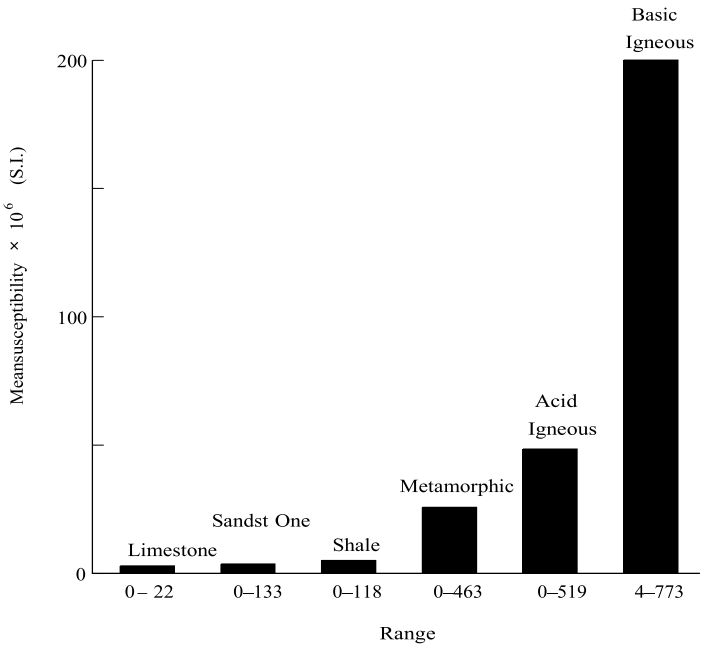

Fig 18 Histogram showing mean values and ranges in susceptibility of common rock types. (USGS, 2014)

Magnetic anomalies

Common causes of magnetic anomalies include dykes, faulted, folded or truncated sills and lava flows, massive basic intrusions, metamorphic basement rocks and magnetite ore bodies. Magnetic anomalies range in amplitude from a few tens of nT over deep metamorphic basement to several hundred nT over basic intrusions and may reach an amplitude of several thousand nT over magnetite ores.

Magnetic anomalies caused by rocks are superimposed on the geomagnetic field. The geomagnetic field varies both in amplitude and direction (William J., 2013). The geomagnetic elements are related as

$$\mathbf{B^2 = H^2 + Z^2} \quad \text{[22]}$$

A magnetic anomaly is hence superimposed on the Earth's field thus causing a change $\Delta\mathbf{B}$ in the strength of the total field vector **B.** If the anomaly gives vertical component $\Delta\mathbf{Z}$ and a

horizontal component $\Delta\mathbf{H}$ at an angle α to **H** then only that part of $\Delta\mathbf{H}$ in the direction of **H**, namely $\Delta\mathbf{H'}$ will contribute to the anomaly such that $\Delta\mathbf{H'} = \Delta\mathbf{H}\ \mathbf{cos}\ \alpha$**.**

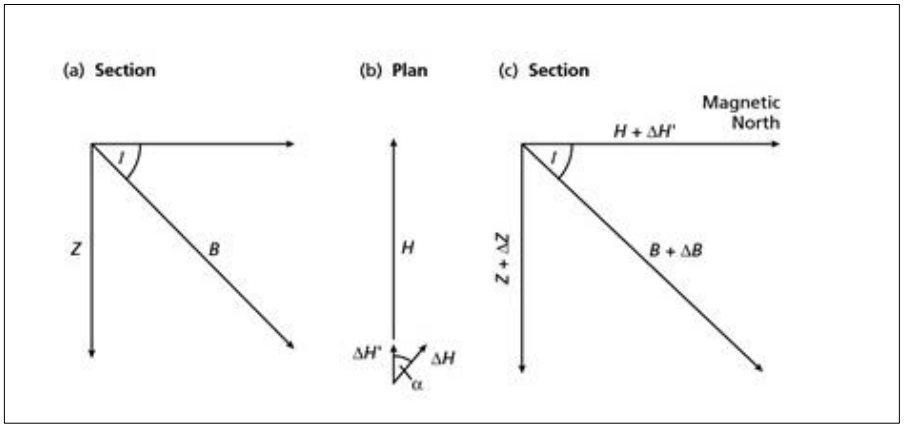

Fig 19 Vector representation of the geomagnetic field with and without a superimposed magnetic anomaly.

Applying to the same vector:

$$(\mathbf{B}+\Delta\mathbf{B})^2 = (\mathbf{H}+\Delta\mathbf{H'})^2 + (\mathbf{Z}+\Delta\mathbf{Z})^2 \quad \text{[23]}$$

By expanding the equality of the above equation and applying to the geomagnetic relation, then the insignificant terms in Δ^2 ignored, the equation reduces to,

$$\Delta\mathbf{B} = \Delta\mathbf{Z}\frac{\boldsymbol{Z}}{\boldsymbol{B}} + \Delta\mathbf{H'}\frac{\boldsymbol{H}}{\boldsymbol{B}} \quad \text{[24]}$$

Further reducible to

$$\Delta\mathbf{B} = \Delta\mathbf{Z}\ \sin\mathbf{I} + \Delta\mathbf{H}\ \cos\mathbf{I}\ \cos\alpha \quad \text{[25]}$$

where I is the inclination of the geomagnetic field. Using this approach, the magnetic anomaly caused by a small isolated magnetic pole of strength m, defined as the effect of this pole on a unit positive pole at the observation point, can be calculated. The pole is situated at depth z, a horizontal distance x and radial distance r from the observation point. The force of repulsion $\Delta\mathbf{B}_r$ on the unit positive pole in the direction r is given by taking $\mu_R = 1$, such that

$$\Delta\mathbf{B}_r = \frac{Cm}{r^2} \quad \text{[26]}$$

And

$$C = \frac{\mu_o}{4\pi}. \quad \text{[27]}$$

Assuming that the profile lies in the direction of magnetic north so that the horizontal component of the anomaly lies in this direction, then the horizontal (**ΔH**) and vertical (Δ**Z**) components of this force can be computed by resolving in the relevant directions

$$\mathbf{\Delta H} = \frac{Cm}{r^2}\cos\theta = \frac{Cmx}{r^2} \quad \text{[28]}$$

$$\mathbf{\Delta Z} = \frac{-Cm}{r^2}\sin\theta = \frac{-Cmz}{r^2} \quad \text{[29]}$$

The vertical field anomaly is negative as, by convention, the z-axis is positive downwards. The horizontal field anomaly is a positive/negative couplet and the vertical field anomaly is centred over the pole.

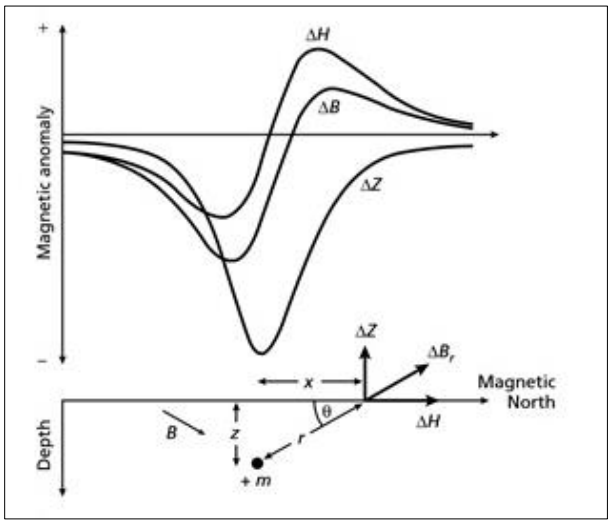

*Fig 20 the horizontal (**ΔH**), vertical (Δ**Z**) and total field (Δ**B**) anomalies due to an isolated positive pole.*

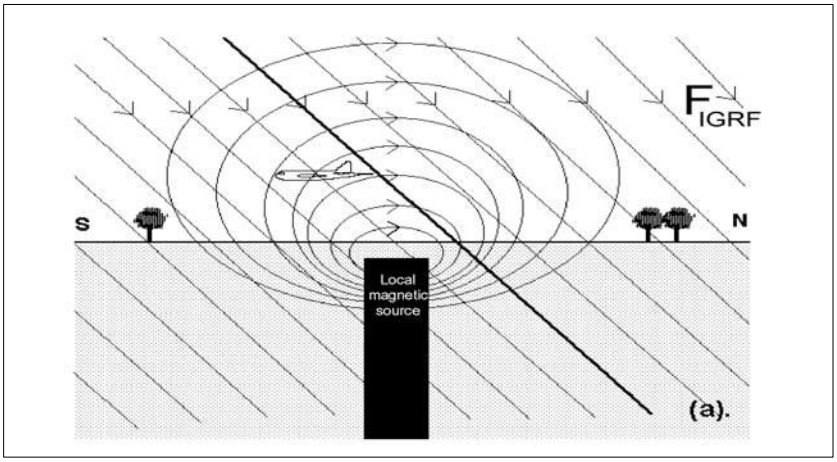

Fig 21 at a given location, the magnetometer records the vector sum of the ambient geomagnetic field and the anomalous contribution from (one or more) local sources.

Instrumentation

Geophysical instruments are used to make physical measurements, such as made in laboratories, at temporal sites and in hostile conditions. They vary in size and complexity. They are made economical to power usage, simple, portable, reliable and rugged. To undertake this magnetic survey, various factors were taken into account for choosing the magnetometer right for the survey. Serviceability of the instrument, comprehensive and comprehensible manual for the instrument, reparability of the instrument, availability of power supplies and batteries, were all considered. The data displays were made clearly legible and the casing waterproof. The keypads were covered so they did not get erased.

The proton precession magnetometer

The GSM 19T proton precession magnetometer was used as a roving field machine in the limestone detection by magnetic anomaly mapping project for Nyanda Mountains, Masvingo, Zimbabwe. The instrument was provided by Knowledge Factory Limited as a full set for the geophysical survey.

Fig 22 GSM19T proton precession magnetometer

The instrument was composed of a data logger, a computer box, external and inbuilt dry batteries, 2+ meters sensor shaft, proton sensor, downloading and connectivity cables, GPS unit, strap back pack. The computer box and the data logger are compacted in one main unit together with the internal battery, while the external battery was connected via a cable when the internal dissipates. The proton sensor was connected to the main unit via a cable also, and it was hoisted by the shaft, adjustable to a desired length. The GPS unit can either be mounted via a cable or used as a separate gadget for position recording. The instrument was strapped on the back as the geophysicist traverses the grid taking readings. The shaft was positioned on the ground on the spot to be recorded on which magnetic readings are to be recorded. The operation of a proton precession magnetometer shall be discussed below.

The proton precession magnetometer makes use of the small magnetic moment of the hydrogen nucleus (proton).

Fig 23 the magnetometer computer box unit and the sensor being used to collect readings during the Nyanda mountains survey.

The sensing element is composed of a container with a low freezing point hydrocarbon fluid about which is wound a coil of copper wire. By passing a polarizing current of the order of an amp through the coil, a strong magnetic field is created, and the moments of the protons in the hydrogen atoms will tend to become aligned along it. Switching off the current makes the protons to realign to the direction of the earth's field (Mussett, 2000). Quantum theory describes this reorientation as occurring as an abrupt 'flip', with the emission of a quantum of electromagnetic energy. In classical mechanics, the protons are described as precessing about the field direction at a frequency proportional to the field strength, emitting an electromagnetic wave as they do so (Milsom, 2002). Both theories relate the electromagnetic frequency to the external field via two of the most accurately known of all physical quantities, Planck's constant and the proton magnetic moment. In the Earth's field of about 50000 nT, the precession frequency is about 2000 Hz. The proton precession magnetometer has sophisticated phase-sensitive circuitry which measure such frequencies to the accuracies of one part in 50000 (i.e. 1 nT) in the half or one second which is all that modern geophysicists will tolerate.

The proton magnetometer tends to erratic readings when in strong field gradients, interference from radio transmitters and power lines and from eddy currents induced in nearby conductors by the termination of the polarizing current. The instrument can only measure total fields, which may cause problems in interpreting large anomalies where the direction of the field changes rapidly from place to place. These are only minor drawbacks. The sensor can be supported on a staff well away from the observer and small magnetic sources on the ground. This is due to the self-orientating property. Readings are obtained as drift-free absolute values in nT, but corrections must still be made for diurnal variations.

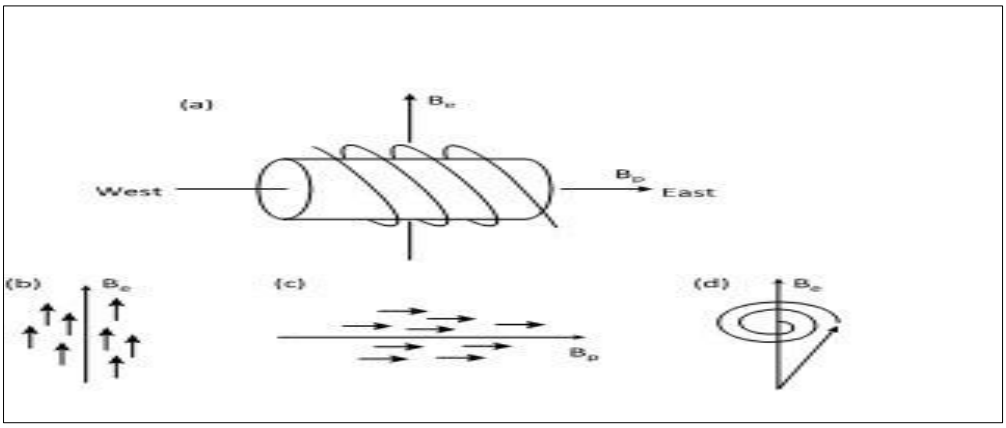

Fig 24 principles of proton magnetometer

From Fig 24, diagram (a) shows a container filled with a liquid rich in hydrogen atoms, such as kerosene or water, surrounded by a coil. Diagram (b) shows the hydrogen nuclei (protons) acting as small dipoles and normally aligning parallel to the ambient geomagnetic field B_e. diagram (c) shows a current being passed through the coil to generate a magnetic field B_p 50–100 times larger than the geomagnetic field, and in a different direction, causing the protons to realign in this new direction and (d) shows the protons returning to their original alignment with B_e by spiralling, or precessing, in phase around this direction. The frequency of the precession is given by

$$f = \frac{\gamma_p B_e}{2\pi} \quad \text{[30]}$$

where γ_p is the gyromagnetic ratio of the proton. At the same time, a measurement of *f*, about 2 kHz, provides a very accurate measurement of the strength of the total geomagnetic field. *f* is determined by measurement of the alternating voltage of the same frequency induced to flow in the coil by the precessing protons. The magnetometer gives absolute readings of the total magnetic field accurate to ±0.1nT. The sensor should ideally lie at an appreciable angle to the total field vector. The proton magnetometer is sensitive to acute magnetic gradients which may cause protons in different parts of the sensor to precess at different rates with a consequent adverse effect on precession signal strength. The GSM 19T proton magnetometers uses the Over Hauser Effect (Kearey, 2002). This is the addition of a liquid containing some free electrons in ‘unpaired’ orbits to the sensor fluid. This effect polarises the protons indirectly using radio frequency energy near 60MHz. The signal generated by the fluid is about 100 times stronger, so there is much lower noise; gradient tolerance is some three times better; sampling rates are faster.

CHAPTER 3: METHODOLOGY

Methodology

The steps taken to complete this research can be generalised into five groups.

1. Reviewing geological and geophysical history and previous studies of the area
2. Reconnaissance and geological mapping of the area
3. Collection and recording of geophysical data and GPS locations of the survey area
4. Data reduction and processing, map construction
5. Data interpretation and anomaly map analysis

Previous geological and geophysical studies have identified and mapped the areas with low magnetic values and karstic landscapes in the area, rich in carbonates and limestone (T. G. Blenkinsop, 1992) (Ranganai, 2009). Most of the studies made use of regional aeromagnetic and gravity surveys to come up with anomaly maps.

The work started by gathering this information and reviewing various literature regarding limestone association with the Masvingo greenstone belt and in particular with Nyanda Mountain range. The review included exploring the regional geology of the area, and a survey preparation for the ground magnetic survey (reconnaissance).

The author went on to carry a geophysical survey over the proposed grid, with the aid of personnel from Knowledge Factory limited since a geophysical survey cannot be carried out by a single person (Van Blaricom, 1992). One was a lines man who guided the author with a GPS unit while he did the data collection with the magnetometer. Data reduction started with data download from the data logger into the desktop computer for manipulation with relative software for anomaly mapping and presentation. This was followed by the map interpretation, discussion of results and conclusion together with further recommendations.

Reviewing previous geological and geophysical studies

The Geological Survey of Zimbabwe and the Ministry of Mines Claims Office assisted much in the background research to the project by providing the geological data and map as well as the gravity and aeromagnetic data of the respective area. Using these maps, the initial visit to the area was guided and the coordinates for the points to be studied were extrapolated. This was done using MAPINFO software and the specific interesting places were pinpointed.

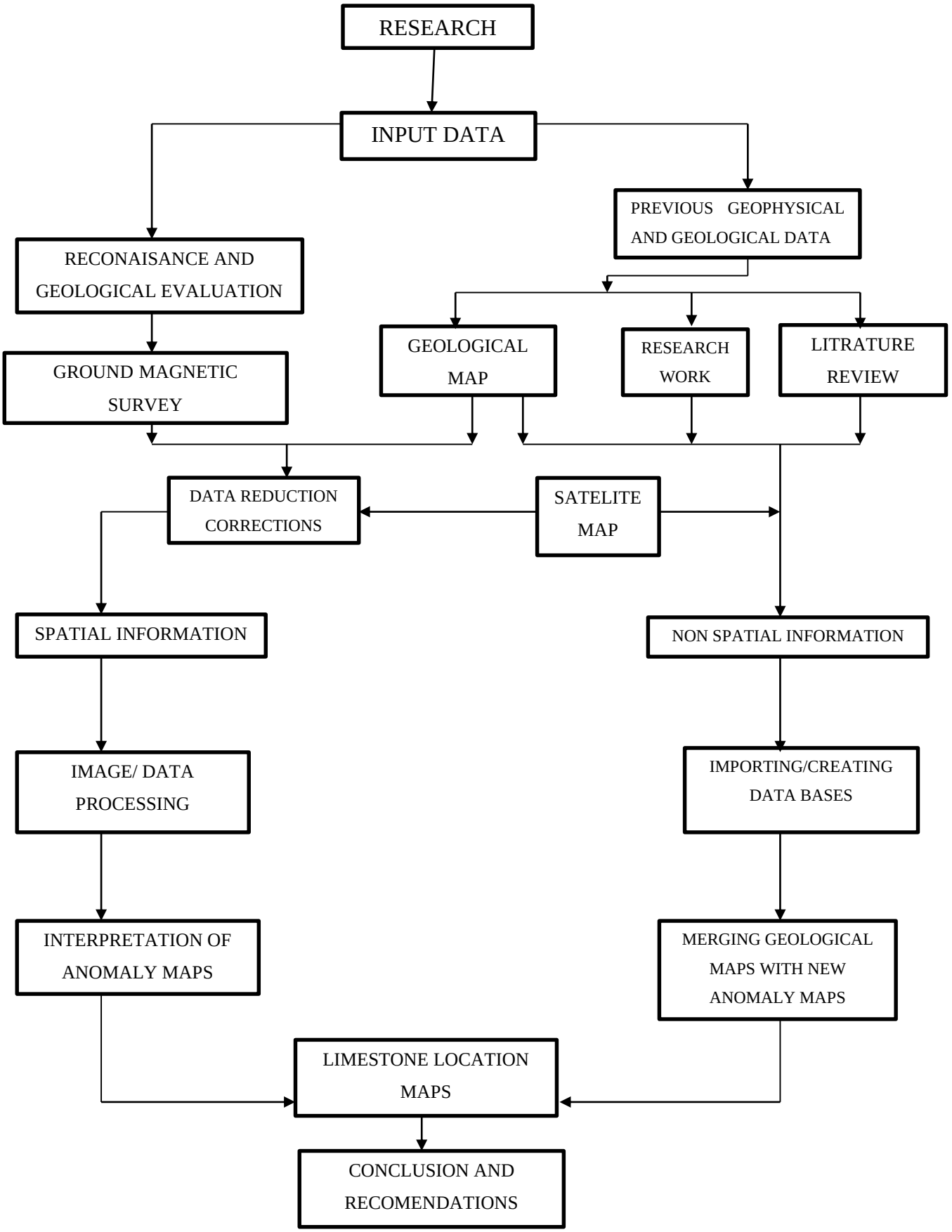

Fig 25 showing the conceptual framework of the research project

Reconnaissance and geological mapping

This included an initial visit to the Nyanda Mountains to establish the site of the survey area on the ground, to make sure that all the lines along which the survey was to be conducted were cut and were easy to move along with the magnetometer without risk of fall. The visit also served to locate the visible karstic landscapes and caves on the mountain range within the survey site. Familiarisation with the area was also done and the community alerted of the pending magnetic survey in the mountains.

The Magnetic survey

Magnetic readings are of true point data. This means that the required and collected values are determined directly at points rather than between points (Milsom, 2002). Precise field notes were always noted since reading points had to be defined and orientations be recorded. All the missed stations and repeated stations were recorded and all points where magnetic noise was likely to affect the readings were noted as well.

Station numbering was made logical and consistent. The UTM zone 36S ARC1960 coordinate system was used (Boyd, 1992). A GPS field book was saved which was later used to crate location points with respective to the magnetic data recorded. The lines were named with respect to the x channels which is also the northing. Stations were numbered sequentially according to their x-y position on the local coordinate system on the ground.

Geophysical results are primarily numerical and must be recorded even more carefully than qualitative observations of field geology. Fortunately the GSM 19T data logger have a memory facility which stores the readings as they are being collected and will hence be downloaded later. This facility is economical considering the fact that geophysical observers are usually in more of a hurry than are geologists, since their work involves instruments that are subject to drift, draw power from batteries at frightening speed or are on hire at high daily rates.

Loss of geophysical data tends to be final. To prevent this, all daily data was downloaded and copies were made just after each field day. Accuracy had be distinguished from sensitivity. The proton magnetometer was sensitive to changes one-tenth of a magnetic variation unit but an equivalent level of accuracy had to be achieved only by carefully making readings and drift and tidal corrections correctly applied. Precision, is concerned only with the numerical presentation of results and the digital data loggers saved the purpose.

The proton magnetometer will not usually record the same results if read repeatedly at the same place. This may be due to changes in background magnetic field but can also be caused by changes in the magnetometer itself, i.e. to drift (Mafirakureva, 2012). Drift correction was made the essential first stage in the magnetic data analysis, and during the survey, repeat readings were collected at base stations. The drift is often related to temperature and unlikely to be linear between two readings taken in the relative cool at the beginning and end of a day if temperatures are 10 or 20 degrees higher at noon. Survey loops were therefore limited to periods of only one or two hours.

During a geophysical survey, signal is the object of the survey and noise is anything else that is measured but is considered to contain no useful information. Extra care was taken to maintain variations in the background field, which were otherwise considered as noise. Magnetic instrument operators could be potent sources of magnetic noise, although the problems were much less acute when the sensor was hoisted on a 2 m pole. Compasses, pocket knives and geological hammers are all detectable at distances below about a metre, and hence had to be eliminated during a survey (Ashwal, 1997).

For a magnetic anomaly to be determined many readings are needed, and regional background levels must be determined, before interpretation can begin. The sensor clearance was 2.5 metres. Readings were taken at 10 metre intervals and lines were spaced at 50 metres. All field readings were taken twice and the two readings were not to differ by no more than 1 nT. Greater differences may indicated high field gradients, which needed further investigation. Large differences between readings at adjacent stations called for an infill at an intermediate point. At each station the location, time and reading were recorded, as well as any relevant topographic or geological information and details of any visible or suspected magnetic sources. The final reading was made at the base first occupied.

Base stations were required for correction purposes. There was need for:

- Drift bases - Repeat stations that mark the starts and ends of sequences of readings and are used to control drift.
- Reference bases – Points where the value of the field being measured has already been established.
- Diurnal bases – Points where regular measurements of background are made whilst field readings are taken elsewhere.

Tie line system was used to fulfil the functions of these bases. The reliability of the survey, and the ease with which later work was tied to it, depends on these tie lines (base stations). In the tie line system used, a reading was taken at base A (Fig 26) and quickly at base B, and repeat readings were then made at A and again at B. the times between the readings were made as short as possible, with maximum acceptable time being thirty minutes, so that drift and diurnal variations could assumed to be linear. Forward looping is the process undertaken where by more bases say C, D etc. were linked in the tie line system (SEG, 2014). Each set of four readings provided two estimates of the difference in field strength between the two bases, and should these fail to agree within the limits of instrument accuracy (±1 nT), further ties had to be made. Differences had to be in the field so that any necessary extra links could be added.

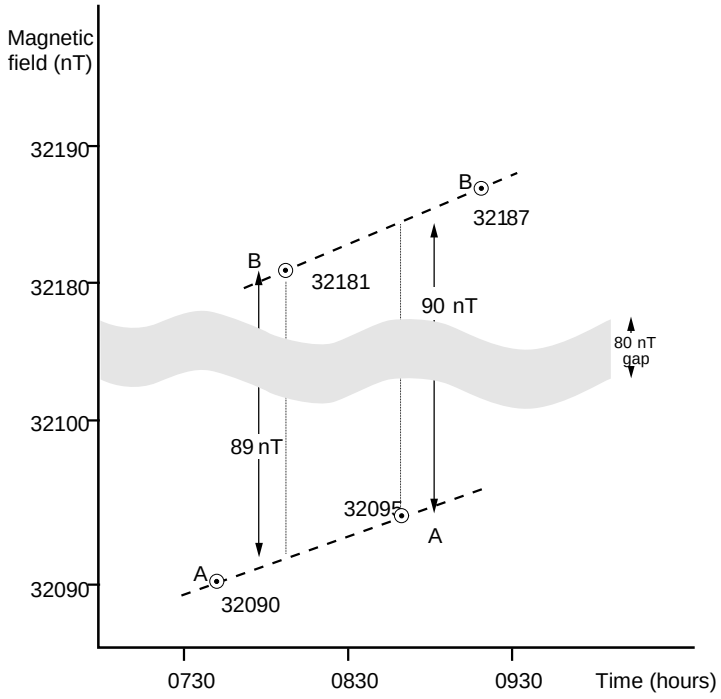

Fig 26 tie lines between bases in a magnetic survey with a 1 nT instrument.

In Fig 26 above, the estimated difference between the two stations would be 89 nT. Note that the plotting scale should be appropriate to instrument sensitivity and that it may be necessary to ‘remove’ some of the range of the graph to allow points to be plotted with sufficient precision.

Although absolute numerical readings are obtained (and can be repeated) at the touch of a button with the proton precession magnetometer, faulty magnetic maps could still be produced if the simple precautions had been ignored. For example, all base locations, used for repeat readings and for continuous diurnal monitoring, had to be checked for field gradients. A point was not used as a base if moving the sensor for a metre produced a significant change.

A small reasonably cheap hand-held GPS receiver, GARMIN GPSmap 78S, was used for the positioning needs of the magnetic survey. The accuracy was a few metres in position and elevation. The accuracies were considerably less, because of multi-path errors (i.e. reflections from topography or tree canopies which provides alternative paths of different lengths) and because of variations in the properties of the atmosphere. Positional fixes were taken from at least 5 satellites at each time.

Fig 27 the GARMIN GPS receiver used for the magnetic survey

Data correction and reduction

Magnetic survey data reduction is necessary so as to remove all causes of magnetic variation from the observations other than those arising from the magnetic effects of the subsurface. For this survey, there was no fixed magnetometer at a base station, so the tie line base system was used to monitor the variations. Differences observed in the tie points were then distributed among the readings at stations occupied during the day according to the time of observation.

The diurnal correction at any time is simply the difference between the standard value at the diurnal station and the actual diurnal reading (QCtools, 2014). The diurnal correction for the data was done by interpolation where necessary, the diurnal value at the time a given field reading was made and to subtract this from the reading. The diurnal station standard value can then be added to give the standard value at the field station (QCtools, 2014).

Geomagnetic correction removes the effect of a geomagnetic reference field from the survey data (GEOMAGMODELS, 2014). For this survey, geomagnetic correction was done using the IGRF which expresses the undisturbed geomagnetic field in terms of a large number of harmonics and includes temporal terms to correct for secular variation. The complexity of the

IGRF requires the calculation of corrections by computer. To remove regional gradients, the single dipole approximations of the earth's field may be used. The equations are given as:

$$\mathbf{Z} = \frac{\mu_o}{4\pi}\frac{2M}{R^3}\cos\theta, \qquad \mathbf{H} = \frac{\mu_o}{4\pi}\frac{M}{R^3}\sin\theta, \quad \text{[31]}$$

$$\frac{\partial Z}{\partial \theta} = -2\mathbf{H}, \qquad \frac{\partial H}{\partial \theta} = \frac{Z}{2} \quad \text{[32]}$$

Z and **H** are vertical and horizontal field components and θ the colatitude in radians, R the radius of the earth, M the magnetic moment of the earth and $\frac{\partial Z}{\partial \theta}$ and $\frac{\partial H}{\partial \theta}$ are rates of change of **Z** and **H** with colatitude respectively.

The trend analysis was however applied to the project data because it is rather easier for application to a relatively small survey area. This involved drawing a trend line and a trend surface for profile data and real data respectively, and fitting these using the least square criterion, and subsequently subtracting from the observed data to leave the local anomalies as positive and negative residuals.

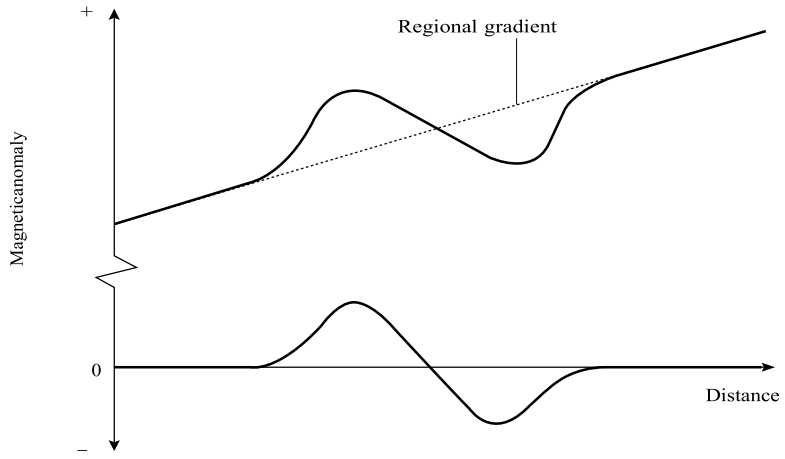

Fig 28 the removal of a regional gradient from a magnetic field by trend analysis. The regional field is approximated by a linear trend.

The elevation corrections were not applied since the vertical gradient of the geomagnetic field is only some $0.03nTm^{-1}$ at the poles and $-0.015nTm^{-1}$ at the equator. Terrain corrections were also omitted since though the influence of topography can be significant in ground magnetic surveys it is not completely predictable as it depends upon the magnetic properties of the topographic features (Jelsma, 1998). Having applied diurnal and geomagnetic corrections, all the remaining magnetic field variations were considered to be caused solely by spatial variations in the magnetic properties of the subsurface and were referred to as magnetic

anomalies. Cultured noise out to be filtered. This was achieved by employing Oasis Montaj filter to the noted data which could possess noisy readings.

Data visualisation and enhancement

As part of data processing, the corrected data (removal of diurnal, geomagnetic, noise etc. variations) have to be reviewed and enhanced before it is put up for map construction and anomaly mapping as well as filtering (Grant, 1965). The magnetic data was visualised in profile lines and waveforms for various aspects, monitoring changes and further reducing noise variations. Waveforms of magnetic interests are generally continuous functions of distance and time. Readings were taken of the magnetic field strength at points along survey lines. These are the sampling precision (dynamic range) and the sampling frequency. Dynamic range is an expression of ratio of largest measurable amplitude A_{max} to the smallest measurable amplitude A_{min} in a sampled function. Sampling frequency is number of sampling points in unit time or distance.

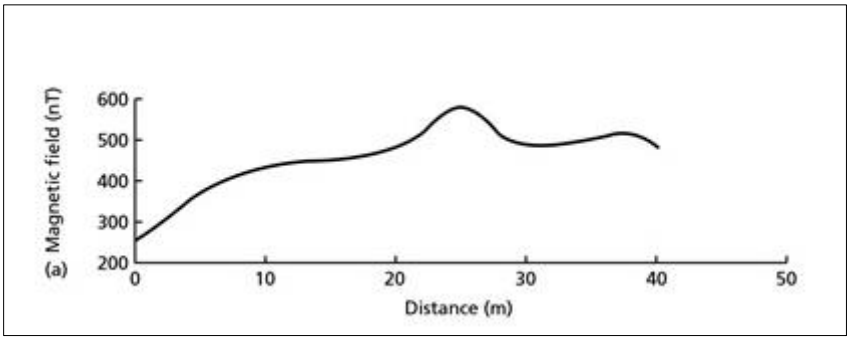

Fig 29 A graph showing a typical magnetic field strength variation which can be measured along a profile.

Map construction

After processing geophysical waveforms, the content is extracted for geological interpretation. Colour shaded contour maps were generated from the magnetic data.

Computer contouring can then be considered logically in three stages:

1. Gridding: Observational data are interpolated onto a grid;
2. Contouring: Gridded data are contoured to produce a 'plot file';
3. Plotting: The plot file is used to drive the physical plotting device.

Computer algorithms were employed to undertake all 3 stages of map processing using the Oasis montaj Geosoft software. Once a reliable grid has been created, several types of visual

presentation were made available, of which contouring was the most prominent. Most of the alternative methods relied on using the grid or raster directly by displaying each grid value as a picture element or pixel on a screen display. The only immediate consequence of using a pixel or image presentation is that, usually, a smaller grid-cell size needs to be used in grid creation; the 2.5 mm grid cell size recommended for the contour map is too coarse for pixel display (Hadipandoyo, 1986).

Interpretative maps were generated in order to facilitate the interpretation exercise and were aimed at improving the spatial mapping resolution of the lithomagnetic units and enhancing subtle features of limited amplitude and continuity. Transforms in frequency and space domain were effected using GEOSOFT and MapInfo mapping packages.

- Reduction-to-the pole:

This transform generates a total field data whose magnetic field anomaly is commensurate with a 90° inclination of the earth's magnetic field for the induced magnetisation of the prospect area (McElhinny, 2000). The effect is to simplify the magnetic map and render anomalies independent of strike direction, and generating symmetrical anomalies over steeply dipping dyke like magnetic sources. Anomalies asymmetric (significant LOs) then reflect flatly dipping sources, or those with a strong remanent magnetization.

- Gradient Data

Gradient data emphasizes shallow source responses at the expense of broader regional features, and allow for the recognition of low amplitude, short wavelength magnetic anomalies (dykes and structures) in areas of significant magnetic relief. Vertical gradients are less complex over steeply dipping magnetic sources and visual inspection of the resulting HI/LO ratios allows for a further check on the dip of the magnetic source.

Second vertical derivative further boost the response of shallow targets but higher noise levels are experienced. Over isolated bodies, second derivative data has the advantage that zero level contours approximate contacts of magnetic body, rendering this data of some significant use in semi quantitatively outlining the plan position of stratigraphic units.

- Image processed data

Relief Shading highlights short wavelength, low amplitude anomalies at shallow depths in total field and other related data sets. Steep features generate sharp, intense shadows. Where the

azimuth is at a large angle to the strike (perpendicular), the process allows for the visual confirmation of strike continuity along sectors where anomalies are poorly developed (Briggs, 1974).

- Grey-scale raster map

In this presentation, each cell of the grid was ascribed a grey pixel, the brightness of which depends on the magnetic value at that grid point. The highest values were white, the lowest black, (or vice versa). Subtle variations in grey-tone over long ranges are not detected by the human eye, but local contrasts are easily seen. For this reason, short-wavelength anomalies tend to stand out and there is an enhancement of anomalies attributable to near-surface geological features. At certain magnetic inclinations, the negative lobe of an anomaly which flanks a positive (or vice versa) often gives an optical '3D' effect, as through the magnetic anomaly field were an undulating white surface, illuminated from the side of anomalies that appear bright.

- Shaded relief raster maps

The human eye can easily be deceived into seeing the magnetic variations as though they were physical topography. Even a simple positive anomaly which appears white (or black) in grey-scale can be made to appear to the eye as a hill by calculating the first horizontal derivative in the direction of a supposed illumination. A positive slope (i.e. a slope facing towards the 'sun' and given a light shade) then appears brighter than a negative slope (i.e. a slope facing away from the 'sun' and shaded dark).

- Colour Raster Maps

The colour raster map simulates the hand colouring of intervals between contour lines with a range of colours from the natural spectrum: red (high) through orange, yellow, green and blue (low). For each grid value, an appropriate colour shade is chosen (most probably again after some judicious contrast stretching across the available colour range) depending on its magnetic value, and plotted on the computer colour screen or on a paper map using an appropriate colour table.

- Combined colour raster and shaded relief maps

Since the shaded relief style of presentation described above tends to emphasise the short wavelength features; it tends to be complementary to the colour raster which tends to emphasise

the long wavelength features. In fact, the two styles were combined by overprinting the grey of the shaded relief onto the colour map. One advantage is to reveal magnetic features that are of low amplitude and so become 'lost' within one colour level on the colour map. Cartesian coordinate space of the red green-blue additive colour system of screen displays (or the subtractive magenta-yellow-cyan colour system on paper) to a cylindrical coordinate space of hue, saturation and value (HSV, Fig 30) which is more attuned to human visual perception (Bhattacharyya, 1965). In the HSV model, hue refers to the repetitive colour sequence of the natural colour wheel (red-yellow-green-cyan-blue magenta-red), value is the intensity of the colour and saturation is the lack of white.

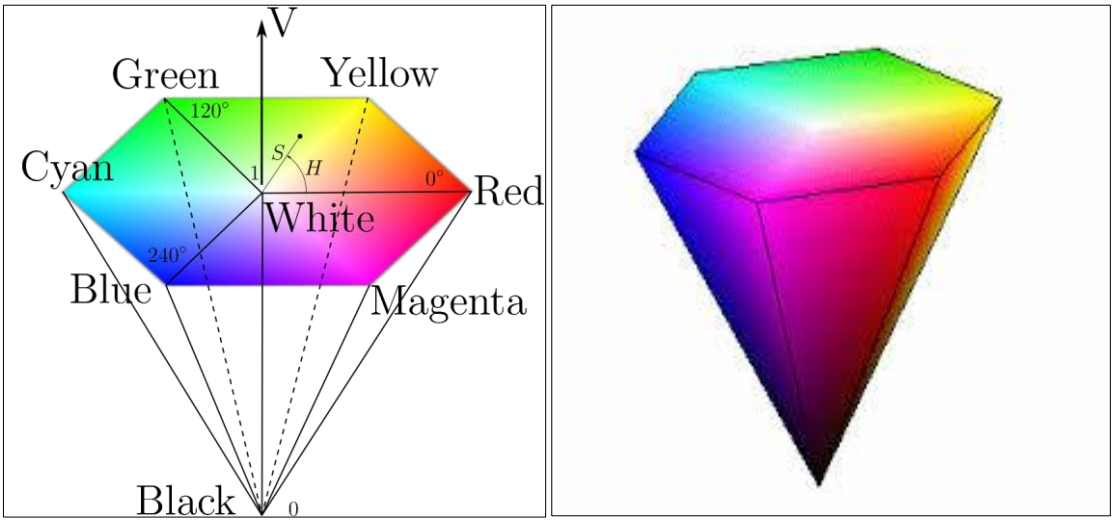

Fig 30 The HSV colour model.

Hue is measured around the vertical axis from 0º to 360°, saturation varies from 0 at the vertical axis radiating out to 1 on the surfaces of the hex-cone and value varies from black (0) through shades of grey along the central axis to white (1) at the top. Thus, for a colour of constant hue and saturation, if its value is decreased it darkens towards black, and for a colour of constant hue and value, if its saturation is increased it becomes whiter. In normal perception of landscapes, the hue remains constant, while areas in direct sunlight are under saturated and appear 'washed out'. At the same time, areas in relative shadow are low in value with less reflected light.

To achieve this on a geophysical image, negative values of the horizontal gradient are used to decrease the colour value towards black and positive values of the gradient are used to reduce saturation towards the axis. Images prepared in this way look very bright and pleasing to the eye.

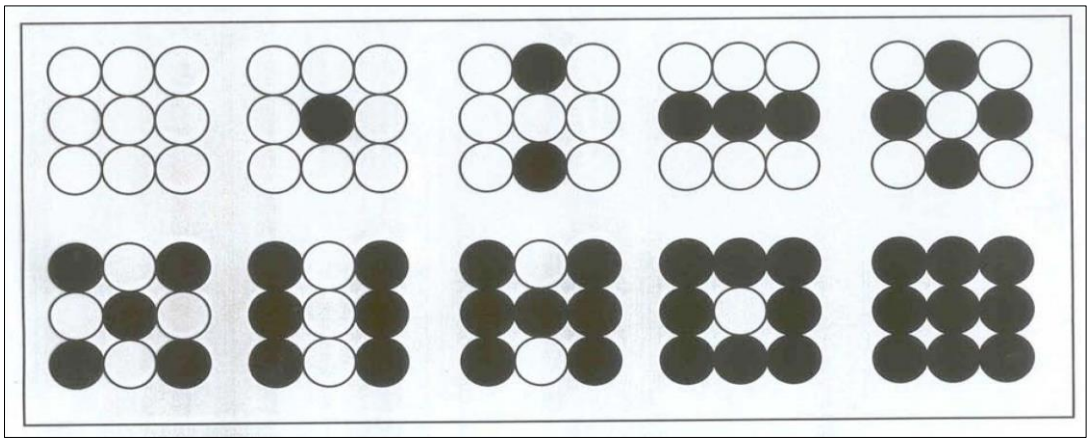

Fig 31 a pixel made up of a 3 x 3 dot pattern may be used to create ten grey levels.

- Smoothing.

The two-dimensional equivalent of the 3-point smoothing operator is a 3 x 3 array of filter values, each having a weight of 1/9. The effect of such a filter is to average the value at a given grid node together with the values at its eight nearest neighbours to give a new value at the centre point. The operator is moved row-by-row over the whole grid to produce a new grid of smoothed values. If necessary, the operator may be used repeatedly (i.e. applied again to the output grid of the first operation) for further smoothing.

1/9	**1/9**	**1/9**
+	+	+
1/9	**1/9**	**1/9**
+	+	+
1/9	**1/9**	**1/9**
+	+	+

Fig 32 9-point two-dimensional smoothing operator.

- First horizontal derivative

On a profile, the first horizontal derivative may be calculated only in the forward (or in the reverse) direction along the profile itself (wikipedia, 2014). With gridded data, the derivative may be computed in any azimuth from 0 to 360°. The distance between the samples being two grid units is taken into account by taking only one half of the actual values in the top and bottom rows (1/8 + 1/4 + 1/8 = 1/2). Operators A or B give the derivatives in the y- and x-directions respectively. The first horizontal derivative in any other azimuth direction may be calculated

as (A cos φ + B sin φ) with appropriate regard to the sign of the cosines and sins as φ goes from 0 to 360°

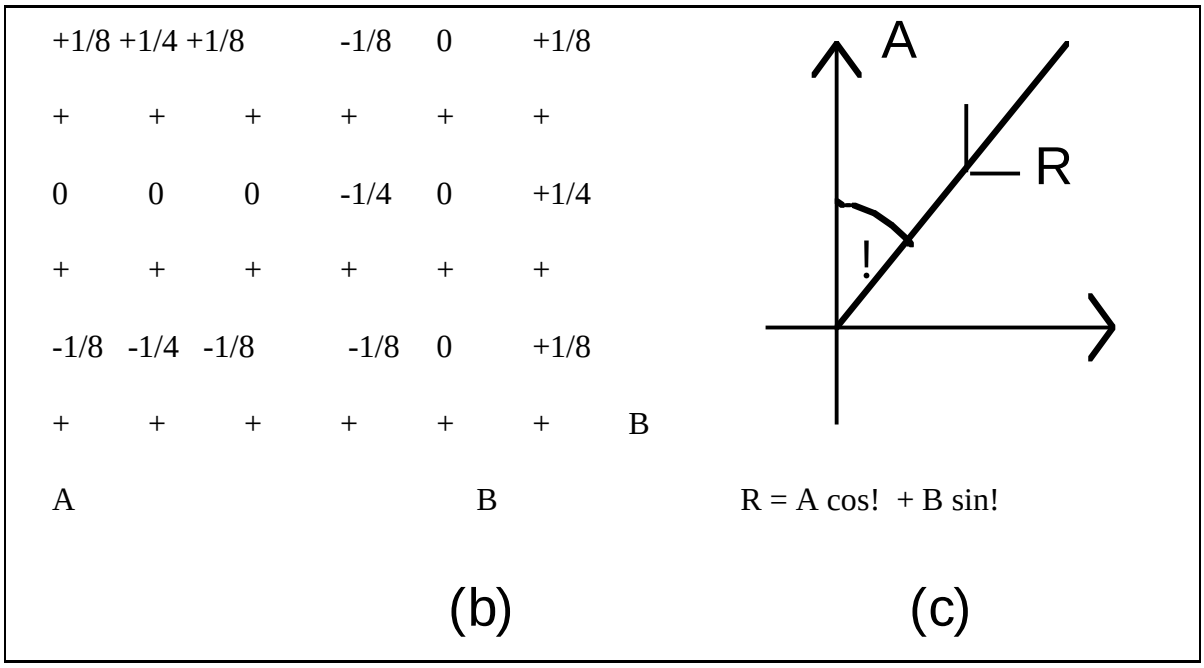

Fig 33 First horizontal derivative filtering on gridded data.

- Second vertical derivative.

The second vertical derivative has the advantage of being non directional. By using the Laplacian potential field property that the sum of the second derivatives in the three orthogonal directions equals zero, then the sum of the estimates of the north-south and east-west second horizontal derivatives will equal (-1) x (the second vertical derivative). By analogy with the second horizontal derivative operator for profile data, an estimate of d^2f/dx^2 is given by the operator and for d^2f/dy^2 by the second operator.

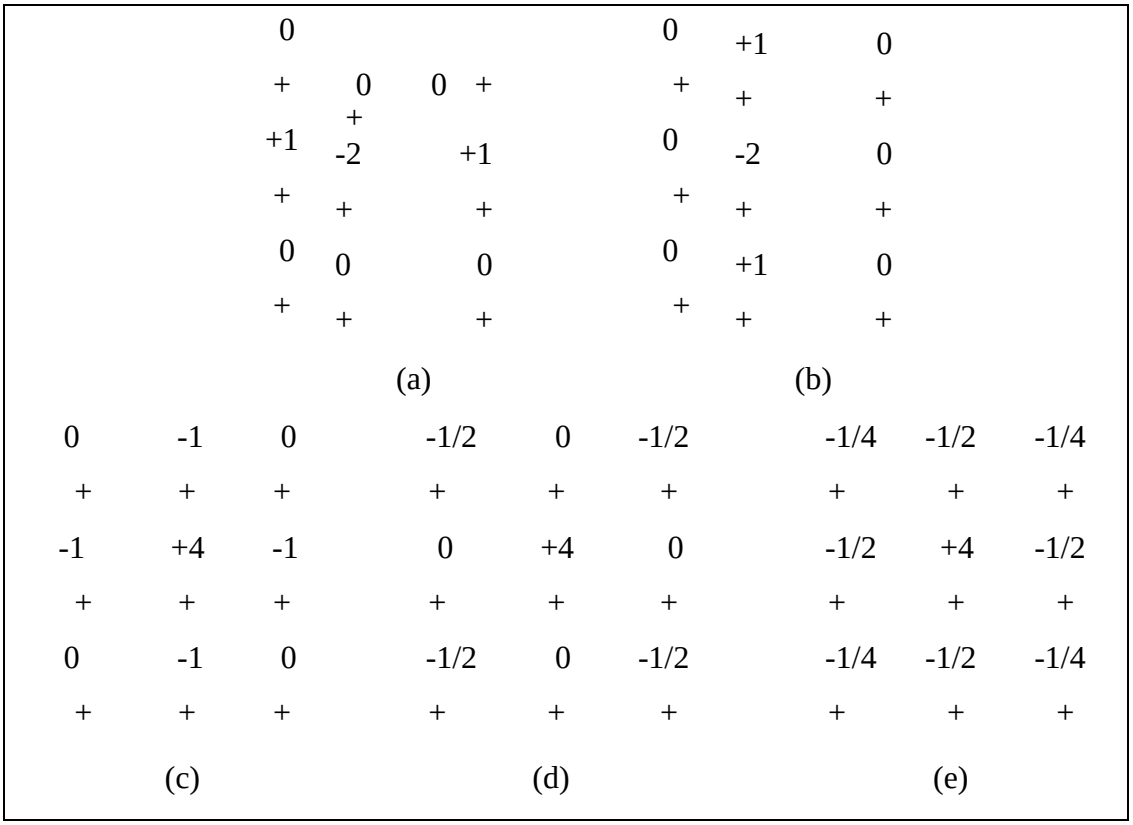

Fig 34 Second vertical derivative operators for gridded data

Data interpretation

Magnetic data interpretation utilises natural potential fields based on inverse square laws of attraction. The magnetic anomaly of a finite body invariably contains positive and negative elements arising from the dipolar nature of magnetism. When the density is a scalar, the intensity of magnetisation is a vector and direction of magnetisation in a body controls the shape of its magnetic anomaly. Bodies of identical shape can thus give rise to different magnetic anomalies. Magnetic anomalies are hence not related to the shape of the anomalies. Intensity of magnetisation of a rock depends thus on amount, size, shape and distribution of its contained ferromagnetic minerals. Anomalies are independent of distance units employed, such that the same magnitude anomaly is produced by a 3m cube on a meter scale as a 3km cube on a kilometre scale.

Direct interpretation gives the limiting depth parameter which is deduced from magnetic anomalies by making use of their property of decaying rapidly with distance from source. Magnetic anomalies caused by shallow structures are more dominated by short wavelength components than those resulting from deeper sources. Euler deconvolution determines the depth of magnetic anomalies. (Reeves C, 2005).

The equation is given as:

$$(x-x_o)\frac{\partial T}{\partial x} + (y-y_o)\frac{\partial T}{\partial y} + (z-z_o)\frac{\partial T}{\partial z} = \mathbf{N}(\mathbf{B}-\mathbf{T}) \quad \text{[33]}$$

Where (x_o, y_o, z_o) is the location of magnetic source whose total field magnetic anomaly at point (x, y, z) is **T** and **B** is the regional field. **N** is measure of rate of change of field with distance.

Indirect interpretation is when an attempt is made to match the observed anomaly with that calculated for a model by iterative adjustments to the model. Anomalies of regular shaped bodies can be calculated by building up the bodies from a series of dipoles parallel to the magnetisation direction. The poles are negative on the surface of the body where magnetisation vector enters the body and positive when it leaves body, hence a uniformly magnetised body can be represented by a set of magnetic poles distributed over the surface.

Conclusion

The methods used in this chapter and mathematical formulae shown in this and previous chapters have since been integrated in computer algorithms and programs which will make it very easier and efficient in processing magnetic data (informine, 2014). The software, however require the user to have a prior appreciation of the involved formulae for them to understand the concepts and language of data interpretation by such software and mapping programs. In the next chapter, oasis montaj and MAPINFO and other software are going to be employed in the various data correction and processing and anomaly mapping. All the involved steps shall be discussed as each step is taken.

CHAPTER 4: RESULTS AND DISCUSSIONS

Introduction

In this chapter, a comprehensive data reduction, correction, manipulation, map generation and interpretation together with the integration with geology will be discussed step by step in all the configurations necessary and applied for this project, as well as the employment of various mapping and processing software will be highlighted.

Data download

The magnetic field strength data that was recorded and stored by the GSM 19T proton precession magnetometer field roving machine was downloaded using the GEMlink 5.0 software. The output file is in text file (*.txt) format. The interface of GEMlink 5.0 connects the host computer (receiving computer) to the data logger software and allows data sync to take place swiftly. The sample text file for this project is pasted below (Fig 35). On the window, the name to which the text is saved (Masvingo 2.txt - Notepad) is displayed on the uppermost panel of the window. Within the body, the first line, written

"/Gem Systems GSM-19TW 7032249 v7.0 6 VI 2007 M t-ew3pl.v7ascm"

describes the instrument used, the serial number and software version installed on the data logger, and the second line,

"/ID 1 file 01survey.m 15 II 14"

describes the survey file ID and the date the survey was undertaken. On the third line, the X represents the x- coordinate, the Y represents the y-coordinate, nT is the magnetic field strength, and sq. stands for standard quality check, which has to read 99% accuracy to be considered. Cor-nT is a correlational nano tesla change, while the time represents the time when each reading was taken.

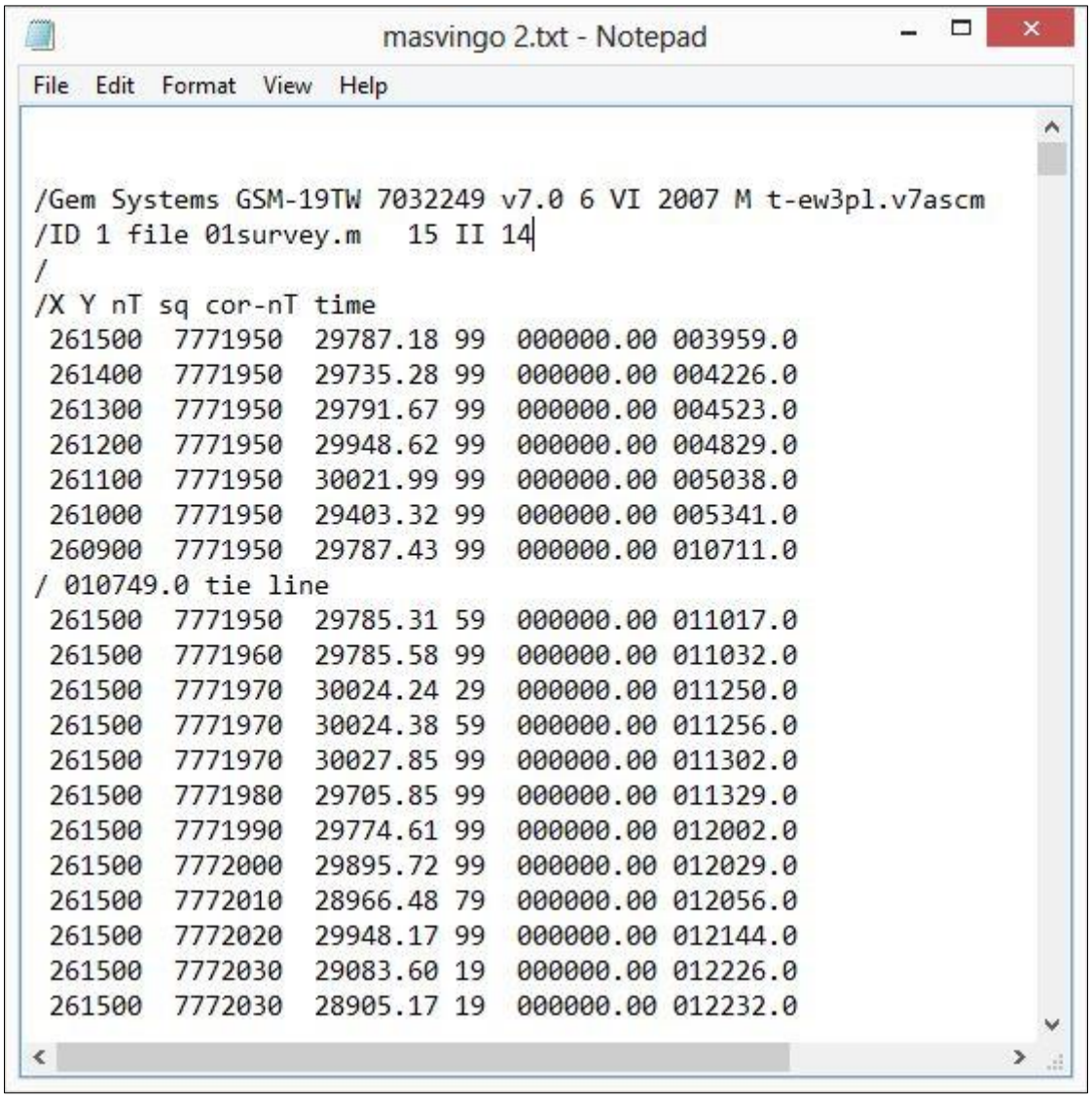

Fig 35 text file from the GEMlink 5.0 download for the project.

Data manipulation

Working with the magnetic data in the text file format is somewhat difficult since editing text files containing large volumes of numerical data may lead to confusion and many errors, hence the data was exported to Excel (*.xls) file format, which is easily compatible with mathematical formulae and equations necessary for data corrections and reductions. The Excel files are better guided and the data is grouped in relevant manageable columns and rows, and formulae can be applied to group data in great computer arithmetic speeds. Importing text files to Excel was made practically easy by employing the Open features provided by Microsoft Excel. Once the data was in Excel file format, the data reduction and correction was hence effected.

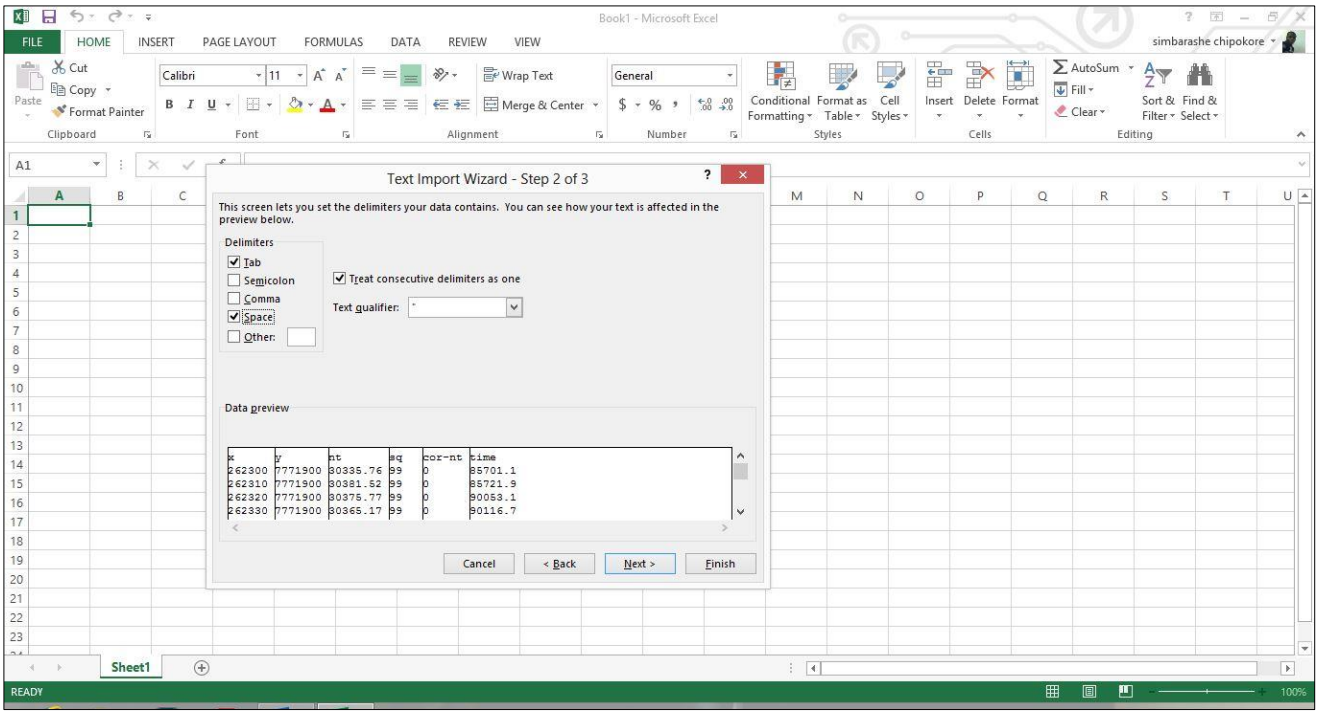

Fig 36 the text import wizard

Data reduction and correction

Data reduction was started by quality control check, where by each and every value which do not exhibit a 99% quality pass was removed (Grant, 1965). This was done by using the sort feature in Excel which sorts the sq. channel in ascending or descending order, hence grouping the less than 99% values together, which were then deleted from the file. Repeated values were also removed leaving only one value for each station. This eliminates conflicting magnetic values, and to get the best possible value, an average value between the two repeats was considered for the station.

The next step undertaken during data correction was the diurnal and drift corrections using the base correction method (QCtools, 2014). The bases used for the survey were rather tie-lines as explained prior in Chapter 3. Diurnal corrections for this survey were regarded also to cancel drift changes. To effect base, magnetic and diurnal corrections, the time when each reading was taken was inspected. Data collected in an interval of every hour needed to be corrected, hence after every hour, a difference of the readings from the first tie and the second or relative tie reading was calculated, and the difference was added to each reading collected within the respective hour. This, averaged becomes the corrected magnetic field value. Excel spreadsheet made it easier to work with the large volumes of data involved. Corrections for micro pulsations

was considered to have been effected together with diurnal corrections, since the survey did not use a base magnetometer but a tie line system.

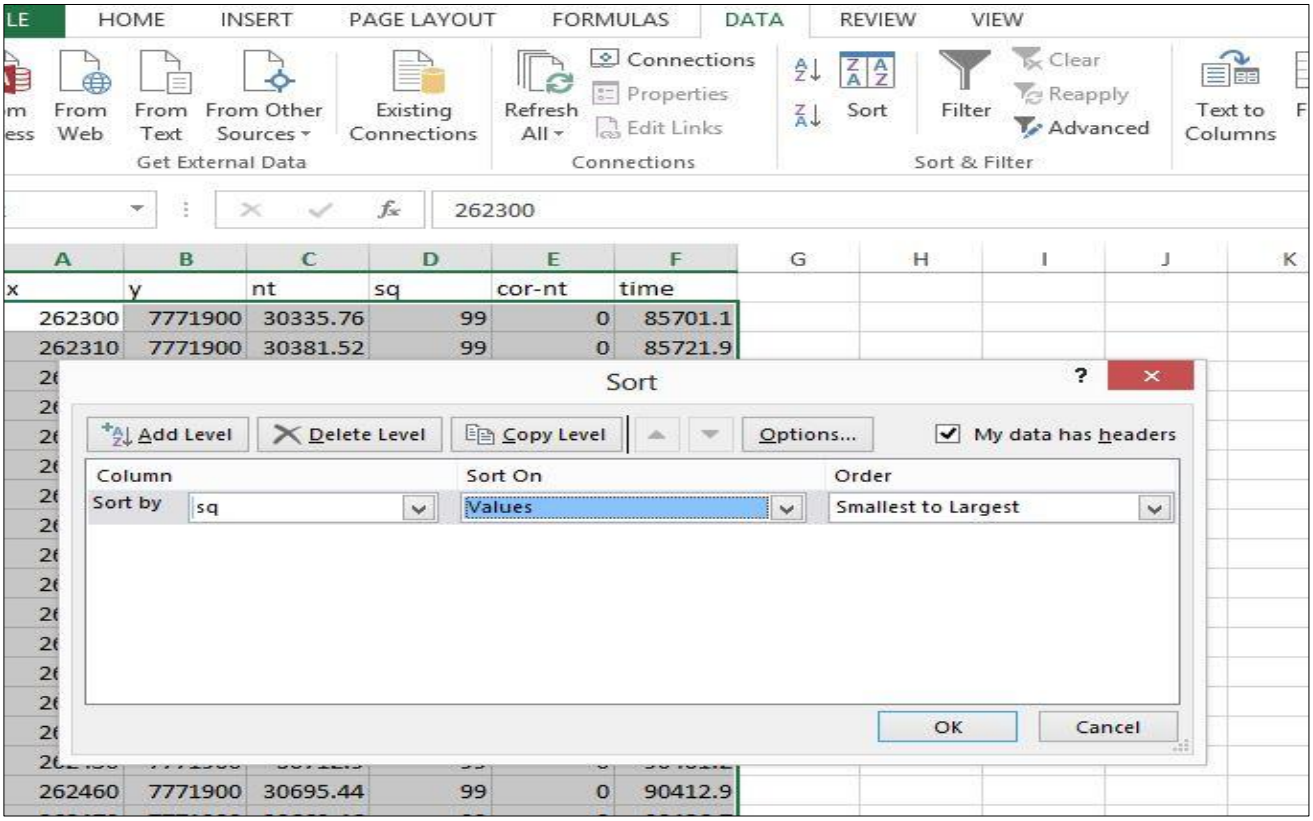

Fig 37 sorting data using MS Excel so as to perform data quality check.

No possible magnetic storms were recorded during the magnetic actual survey hence no magnetic storm corrections were made. The removal of temporal variations was done by applying the base station subtraction, which is basically the averaging of the first and last tie line values, and finding the difference between the averaged value and the mid tie line value. That difference, having been within the range of most diurnal variations readings, meant the data needed no further manipulation.

The magnetic declination for the Masvingo region is -11º2' west and the magnetic inclination is -58º18' (Ranganai, 1995). That is the same inclination and declination for the survey site in the Nyanda Mountains. The average magnetic value from known magnetic reference points around the area is 30103nT. These values helps to present magnetic anomaly information stripped of the dependence on the inclination of the earth's inducing field so that anomalies are positive and sit directly above their sources. This was achieved through reduction to the pole (Reeves C, 2005).

The elevation and terrain corrections were not applied as discussed prior in chapter 3.

During a survey, all possible sources of cultured noise, such as fence, power line, road, vehicles, buildings and human activity is recorded and kept within the data. Values for such cultured noise in this project were removed manually and noted down for further filtering during image production.

It is normal practice in the reduction of magnetic survey data to remove the appropriate IGRF once all other corrections to the data have been made (MacMillan, 2003). Since the xyz file has not been available, to remove the IGRF the grid was exported into the Oasis montaj database. The IGRF correction was made using Geosoft Geophysical Levelling system by calculating the IGRF channel for the specified survey date. A magnetic survey can be corrected for the IGRF by subtracting the IGRF model value at each point in the survey. Using Geosoft Geophysical Levelling system, the IGRF channel has been calculated and later subtracted from the magnetic channel. The following method was employed for the removal of earth magnetic field:

- Since there was no xyz file for the magnetic survey data, a database is created from the grid file. The z channel was not recorded during the survey hence the xyz file was incomplete.
- Using Oasis montaj projection & coordinate feature, the latitude and longitude of the xyz file was calculated.
- Using the IGRF GX Module the program calculated the IGRF model at the longitude, latitude points specified in the lat and lon channels. The field is calculated for February 2014. The IGRF strength (nT) was placed in the Total Field channel

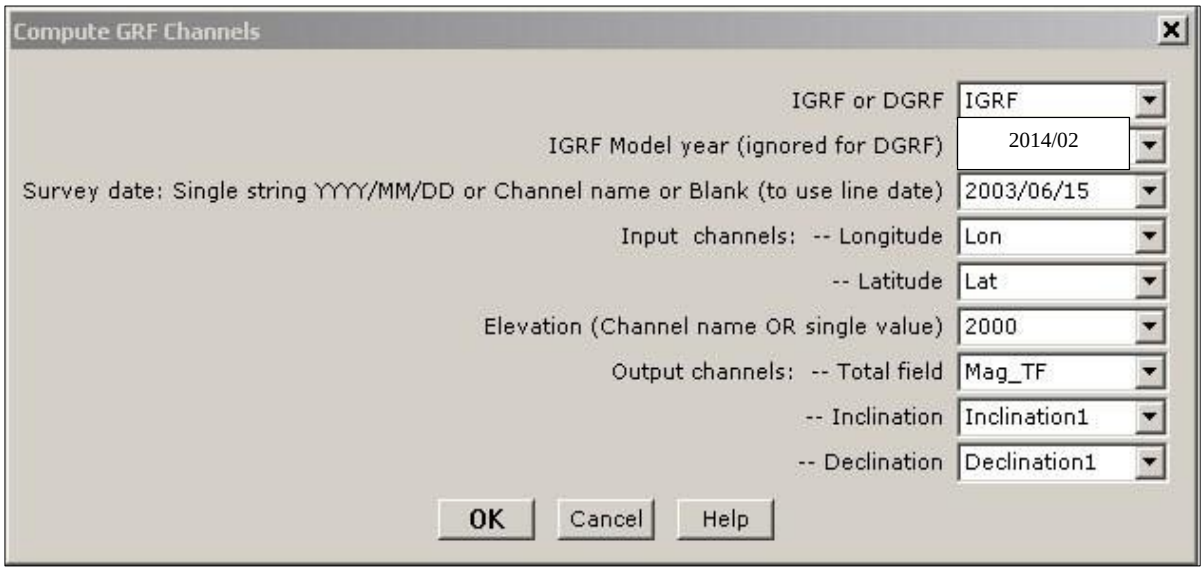

Fig 38 Oasis montaj IGRF calculator

- The Earth's normal magnetic field was removed from the magnetic channel by subtracting the calculated IGRF model.
- Finally the xyz file was re-gridded using the IGRF corrected column.

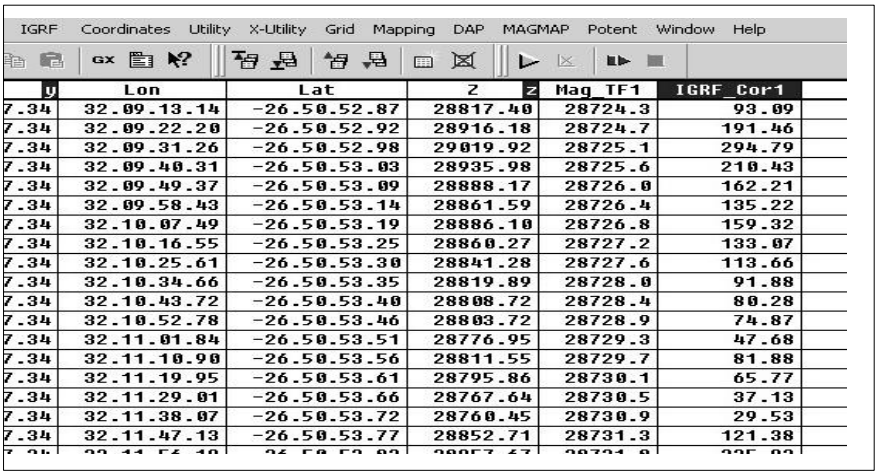

IGRF Coordinates Utility X-Utility Grid Mapping DAP MAGMAP Potent Window Help

y	Lon	Lat	Z	z	Mag_TF1	IGRF_Cor1
7.34	32.09.13.14	-26.50.52.87	28817.40		28724.3	93.09
7.34	32.09.22.20	-26.50.52.92	28916.18		28724.7	191.46
7.34	32.09.31.26	-26.50.52.98	29019.92		28725.1	294.79
7.34	32.09.40.31	-26.50.53.03	28935.98		28725.6	210.43
7.34	32.09.49.37	-26.50.53.09	28888.17		28726.0	162.21
7.34	32.09.58.43	-26.50.53.14	28861.59		28726.4	135.22
7.34	32.10.07.49	-26.50.53.19	28886.10		28726.8	159.32
7.34	32.10.16.55	-26.50.53.25	28860.27		28727.2	133.07
7.34	32.10.25.61	-26.50.53.30	28841.28		28727.6	113.66
7.34	32.10.34.66	-26.50.53.35	28819.89		28728.0	91.88
7.34	32.10.43.72	-26.50.53.40	28808.72		28728.4	80.28
7.34	32.10.52.78	-26.50.53.46	28803.72		28728.9	74.87
7.34	32.11.01.84	-26.50.53.51	28776.95		28729.3	47.68
7.34	32.11.10.90	-26.50.53.56	28811.55		28729.7	81.88
7.34	32.11.19.95	-26.50.53.61	28795.86		28730.1	65.77
7.34	32.11.29.01	-26.50.53.66	28767.64		28730.5	37.13
7.34	32.11.38.07	-26.50.53.72	28760.45		28730.9	29.53
7.34	32.11.47.13	-26.50.53.77	28852.71		28731.3	121.38

Fig 39 Overview of the IGRF correction process

Secular variations were also corrected together with the IGRF removals.

To review the data after all the corrections were made, data visualisations and enhancements were done. These included the profile plots and waveforms of the magnetic values and the sampling precision and frequency. The Excel function was used to create the profiles.

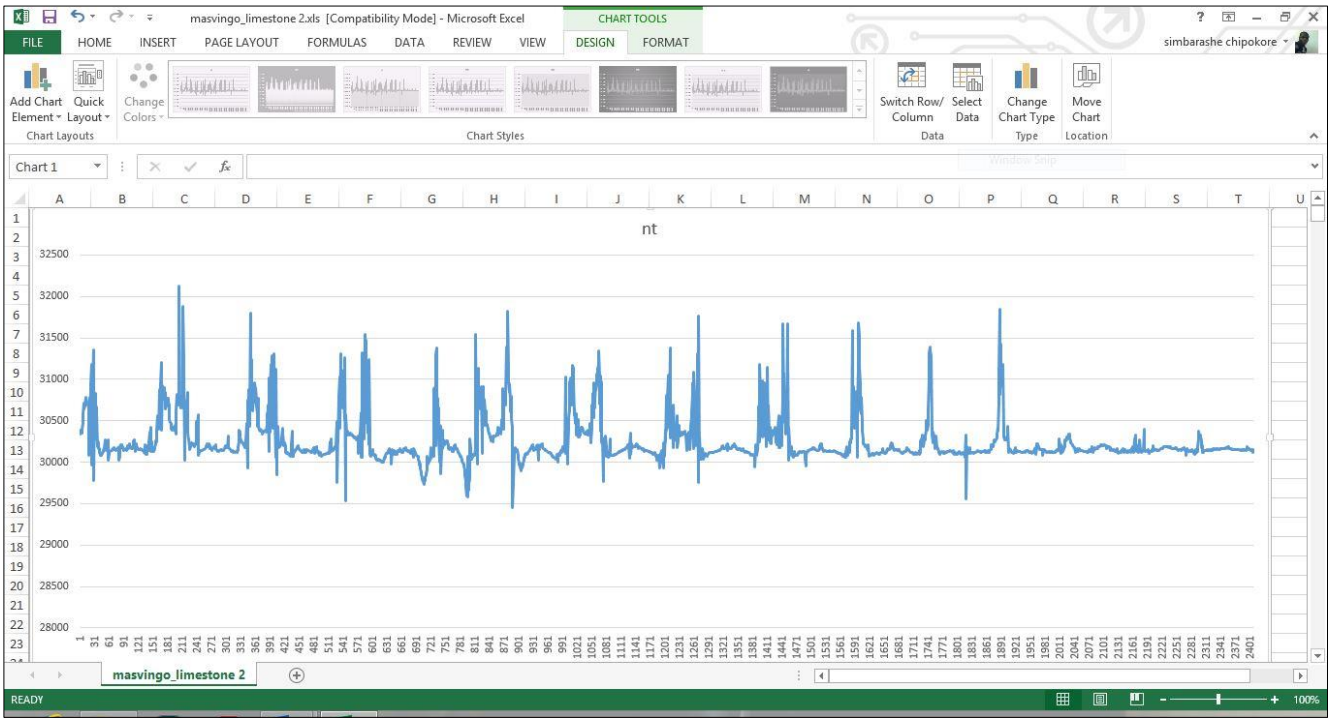

Fig 40 full window showing how excel was used to create profiles for the data

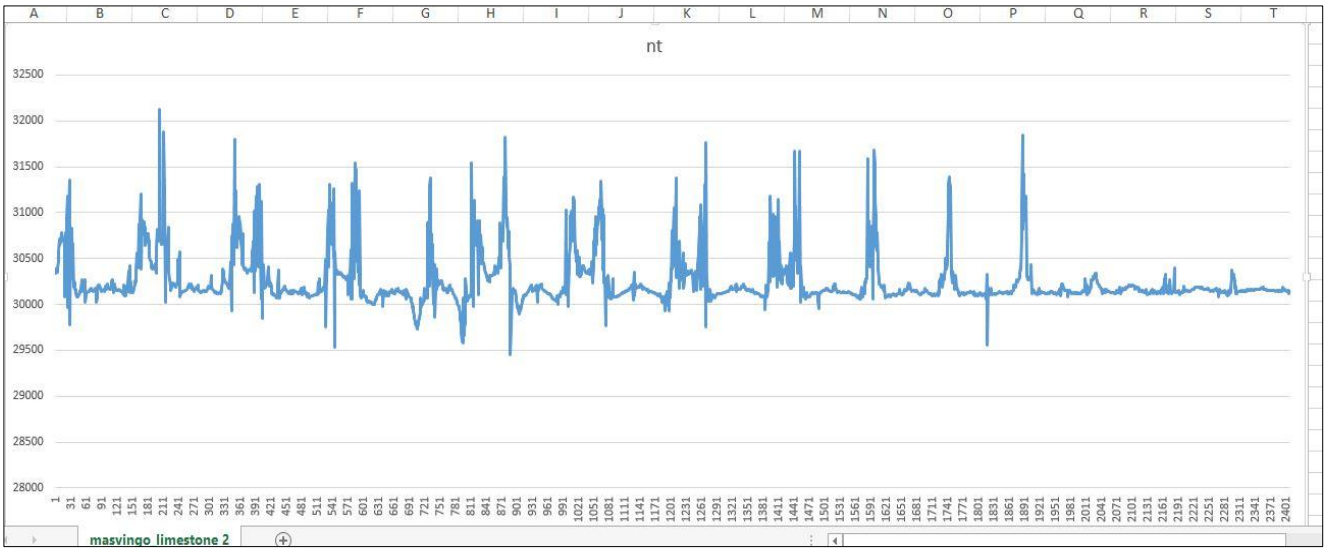

Fig 41 the profile plots for all the surveyed lines

Fig 42 profile plot for the first line of the survey

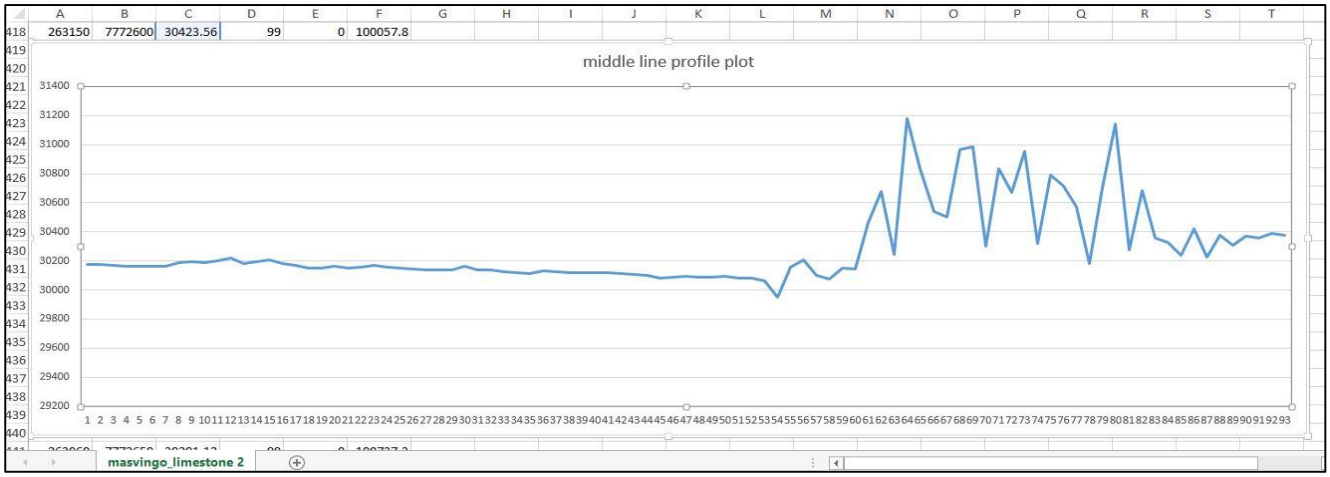

Fig 43 profile plot of the middle most surveyed line

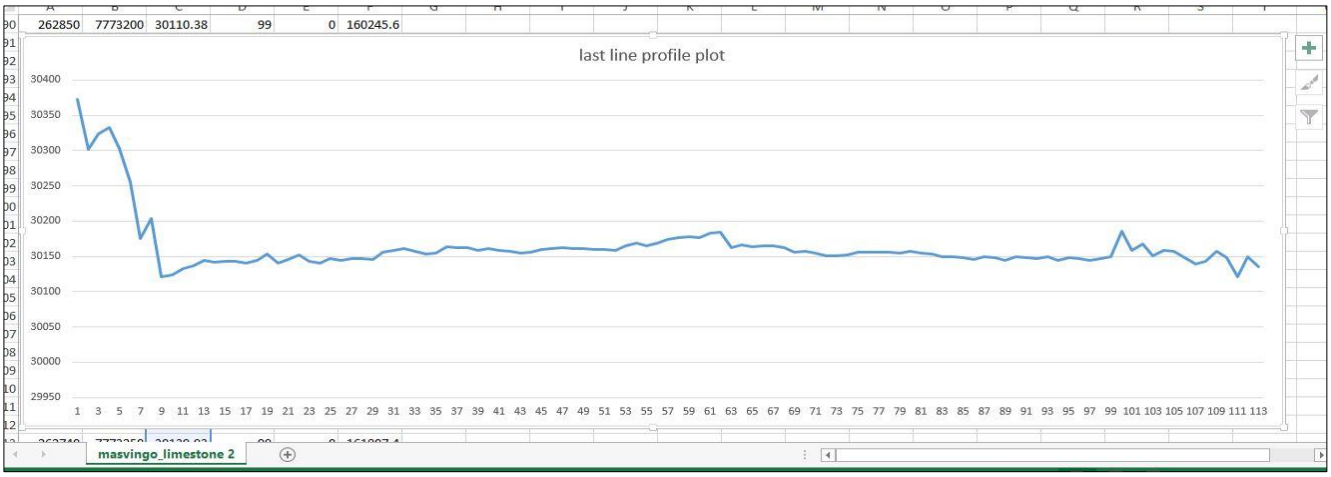

Fig 44 profile plot of the last surveyed line

It can be seen from the surveyed lines (Fig 41) that the area has places with high magnetic values but are few with respect to those with low values. Those with high values tend to reach peak values of 32000nT. Figs 42, 43 and 44 show trending variations for selected lines, with the first line having a considerable number of points with high magnetic values, the middle line is associated to a low profile and some high values while the last surveyed line has mostly a very low magnetic profile.

The sampling frequency for the survey data was taken as number of readings per line, and the average number of readings was taken to be 100 readings per line. This was so because the average line length for the surveyed lines was a kilometre and each station spaced at 10m intervals.

The sampling precision (dynamic range) was calculated as the ratio of largest amplitude (highest magnetic value reading) to the smallest amplitude (smallest magnetic value reading). The largest amplitude was 32130.07nT while the smallest extreme was 29457.62nT. Therefore, for the data for this survey,

$$\text{Sampling precision} = \frac{29457.62}{32130.07} = 0.916824. \quad \ldots\ldots\ldots\ldots\ldots\ldots\ldots\ldots\ldots\ldots\ldots\ldots\ldots\ldots \quad [34]$$

Image processing and discussions

The first step taken to process the data to produce magnetic anomaly images was to export the corrected and reduced data to Geosoft Oasis Montaj software. A database (*.GDB) file was created which hosted the main data for all the images and anomalies produced by the software. The Databases was organized in lines, channels and elements. All data "elements" of a particular type were stored in individual "channels" (or columns), and database "lines" being a

collection of related "channels". Each database "line" had a line number, version number, line type, and survey date and selection status. The column headings in the database are the same as those explained in the text file (Fig 35).

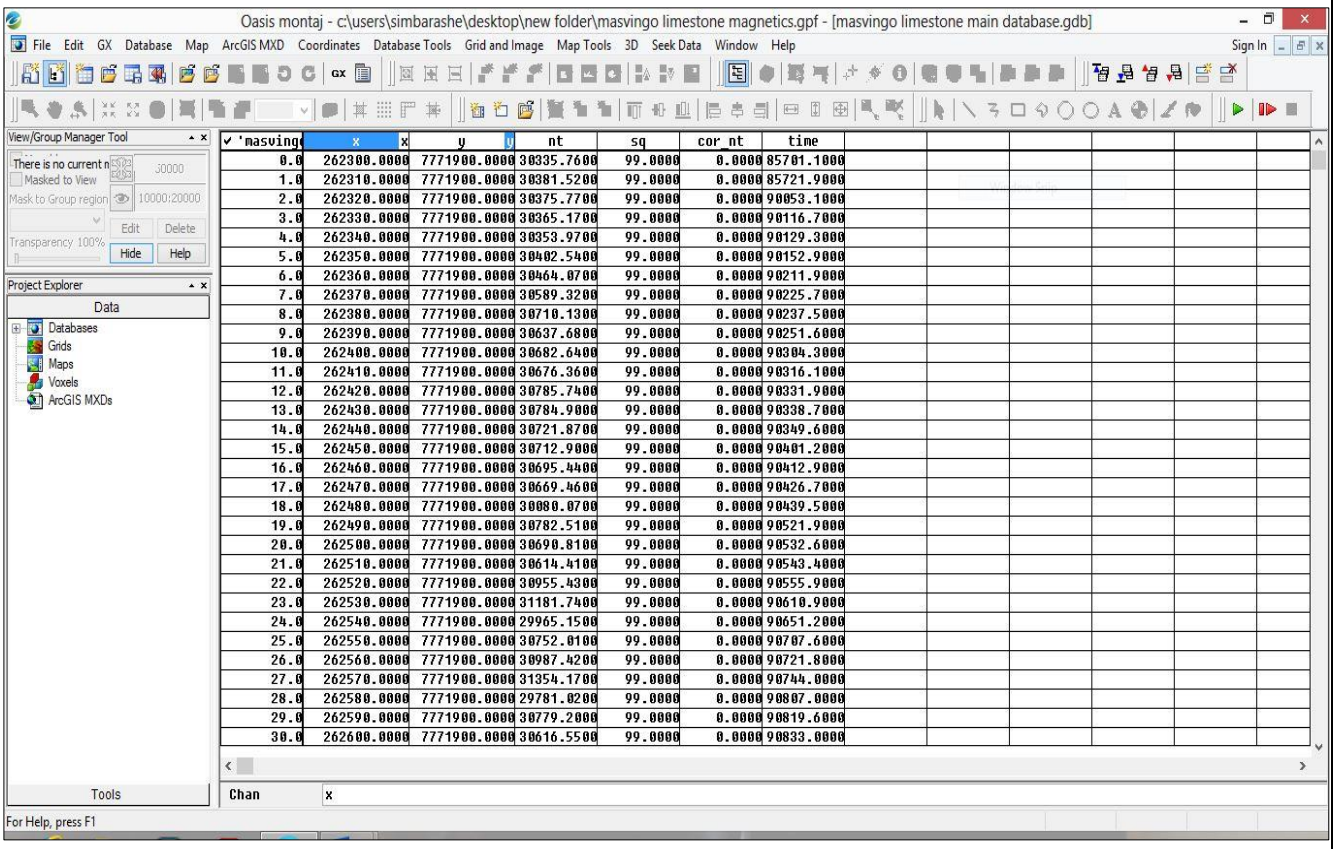

'masvingo	x	y	nt	sq	cor_nt	time
0.0	262300.0000	7771900.0000	30335.7600	99.0000	0.0000	85701.1000
1.0	262310.0000	7771900.0000	30381.5200	99.0000	0.0000	85721.9000
2.0	262320.0000	7771900.0000	30375.7700	99.0000	0.0000	90053.1000
3.0	262330.0000	7771900.0000	30365.1700	99.0000	0.0000	90116.7000
4.0	262340.0000	7771900.0000	30353.9700	99.0000	0.0000	90129.3000
5.0	262350.0000	7771900.0000	30402.5400	99.0000	0.0000	90152.9000
6.0	262360.0000	7771900.0000	30464.0700	99.0000	0.0000	90211.9000
7.0	262370.0000	7771900.0000	30589.3200	99.0000	0.0000	90225.7000
8.0	262380.0000	7771900.0000	30710.1300	99.0000	0.0000	90237.5000
9.0	262390.0000	7771900.0000	30637.6800	99.0000	0.0000	90251.6000
10.0	262400.0000	7771900.0000	30682.6400	99.0000	0.0000	90304.3000
11.0	262410.0000	7771900.0000	30676.3600	99.0000	0.0000	90316.1000
12.0	262420.0000	7771900.0000	30785.7400	99.0000	0.0000	90331.9000
13.0	262430.0000	7771900.0000	30784.9000	99.0000	0.0000	90338.7000
14.0	262440.0000	7771900.0000	30721.8700	99.0000	0.0000	90349.6000
15.0	262450.0000	7771900.0000	30712.9000	99.0000	0.0000	90401.2000
16.0	262460.0000	7771900.0000	30695.4400	99.0000	0.0000	90412.9000
17.0	262470.0000	7771900.0000	30669.4600	99.0000	0.0000	90426.7000
18.0	262480.0000	7771900.0000	30080.0700	99.0000	0.0000	90439.5000
19.0	262490.0000	7771900.0000	30782.5100	99.0000	0.0000	90521.9000
20.0	262500.0000	7771900.0000	30690.8100	99.0000	0.0000	90532.6000
21.0	262510.0000	7771900.0000	30614.4100	99.0000	0.0000	90543.4000
22.0	262520.0000	7771900.0000	30955.4300	99.0000	0.0000	90555.9000
23.0	262530.0000	7771900.0000	31181.7400	99.0000	0.0000	90610.9000
24.0	262540.0000	7771900.0000	29965.1500	99.0000	0.0000	90651.2000
25.0	262550.0000	7771900.0000	30752.0100	99.0000	0.0000	90707.6000
26.0	262560.0000	7771900.0000	30987.4200	99.0000	0.0000	90721.8000
27.0	262570.0000	7771900.0000	31354.1700	99.0000	0.0000	90744.0000
28.0	262580.0000	7771900.0000	29781.0200	99.0000	0.0000	90807.0000
29.0	262590.0000	7771900.0000	30779.2000	99.0000	0.0000	90819.6000
30.0	262600.0000	7771900.0000	30616.5500	99.0000	0.0000	90833.0000

Fig 45 Geosoft window showing the database for the magnetic data for this survey

The coordinate system was left in its local coordinates for easy reference during data processing. With the main and tie line databases in place, map generation and anomaly mapping was started. The line paths and location plots were plotted to verify the coordinate locations first. The two maps showing location plots and line paths are shown below (Fig 46). The lines can be seen to run from east to west and as we go towards the north east, the start points tend to move into the grid. This was due to accessibility to the proposed start point. The end points to the west were also changing due to accessibility as some points to the extremes of the lines could not be reached easily. The coordinates indicated in the maps are based on the local coordinates of the survey area with the north being the uppermost of each image and the scale used as indicated is 1:11725.29 metres.

Below are a series of maps and plates of the grids and filtered grids which resulted from the magnetic survey for limestone detection. These shall be described first then the interpretation will follow henceforth.

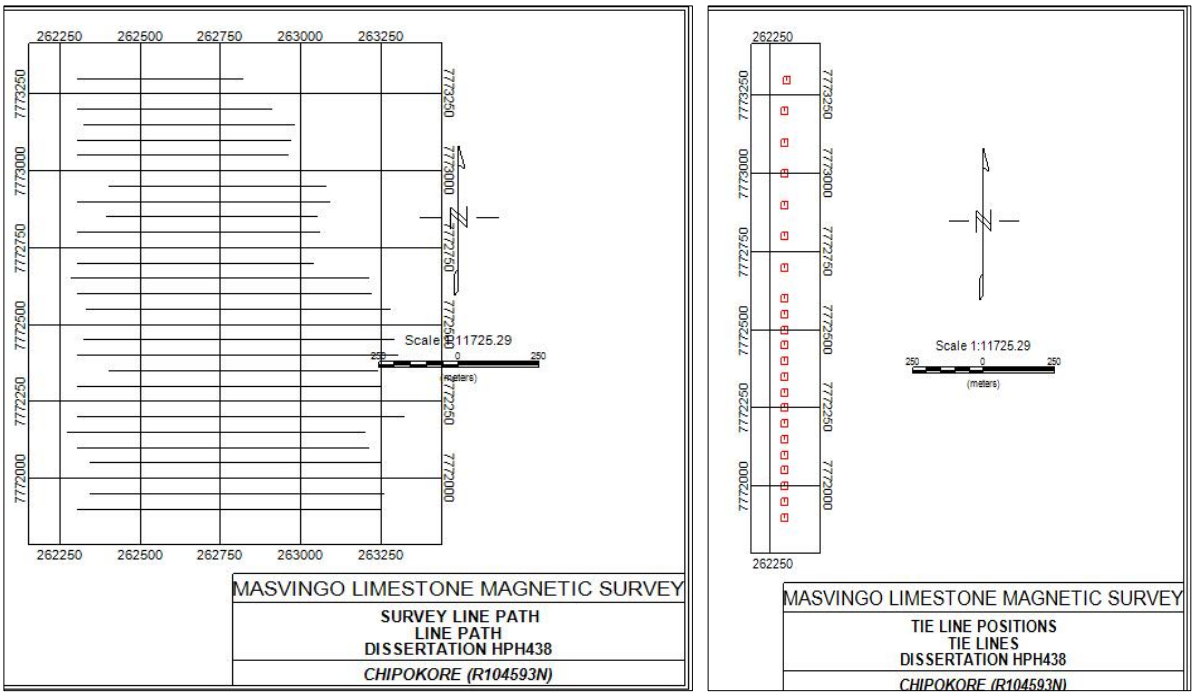

Fig 46 survey line path and tie line positions

The data did not contain any elevation recorded hence the 3D images were not generated. This implies that Euler images were not created also.

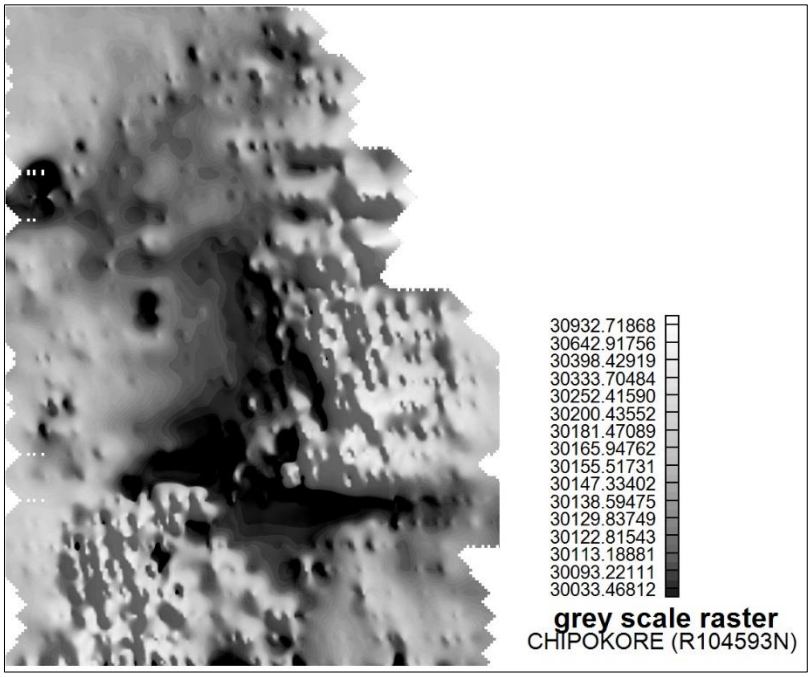

Fig 47 grey scale raster image from the magnetic survey data

Fig 47 is a grey scale raster image for the magnetic data as processed by Oasis Montaj. With reference to the scale, the darker regions are those with very low magnetic readings as compared to the regions with brighter shades.

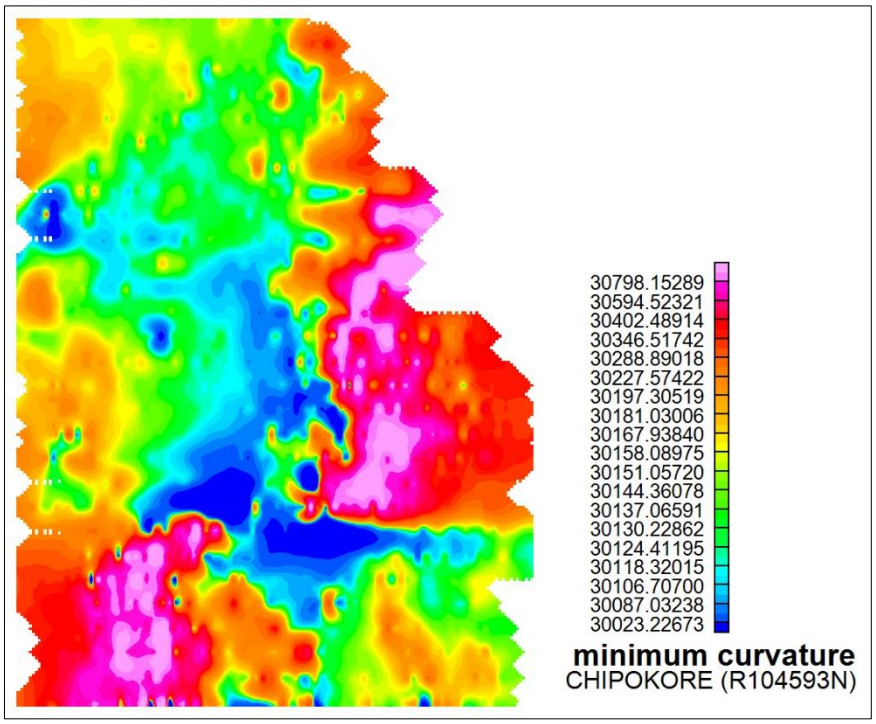

Fig 48 minimum curvature grid

The Minimum curvature gridding method (RANGRID GX) fits a minimum curvature surface to the data points using a method similar to that described by (Briggs, 1974). This minimum curvature surface is the smoothest possible surface that could fit the data values. Minimum curvature first estimates grid values at the nodes of a coarse grid (usually 8 times the final grid cell size). This estimate is based upon the inverse distance average of the actual data within a specified search radius. If there is no data within that radius, the average of all data points in the grid is used. By using the scale to the right of the grid, the deep blue regions are of the lowest magnetic values and the bright pink are of the highest magnetic field values recorded.

In a bid to map anomaly trends using the minimum curvature gridding method, different colour modes were used. These are the Normal Distribution colour mode (Fig 49a), Linear Distribution colour mode (Fig 49*b*), Log Linear Distribution colour mode (fig 50*a*) and Histogram Equalisation colour mode with the Wet Look shading effect (fig 50*b*). Scales signifying high magnetic values and low magnetic values are included on the plates. On all the 4 figures below, there is a prominent magnetic high region which lies mostly on the middle east of the grid and on the south west corner of the grid. The region is minimal in linear distribution (Fig 49b) and log linear distribution (Fig 50a) colouring methods which also show vast green shades which represent intermediate low magnetic readings. There is also a small

deep blue region representing deep low magnetic readings and it cuts the magnetic high region into two parts.

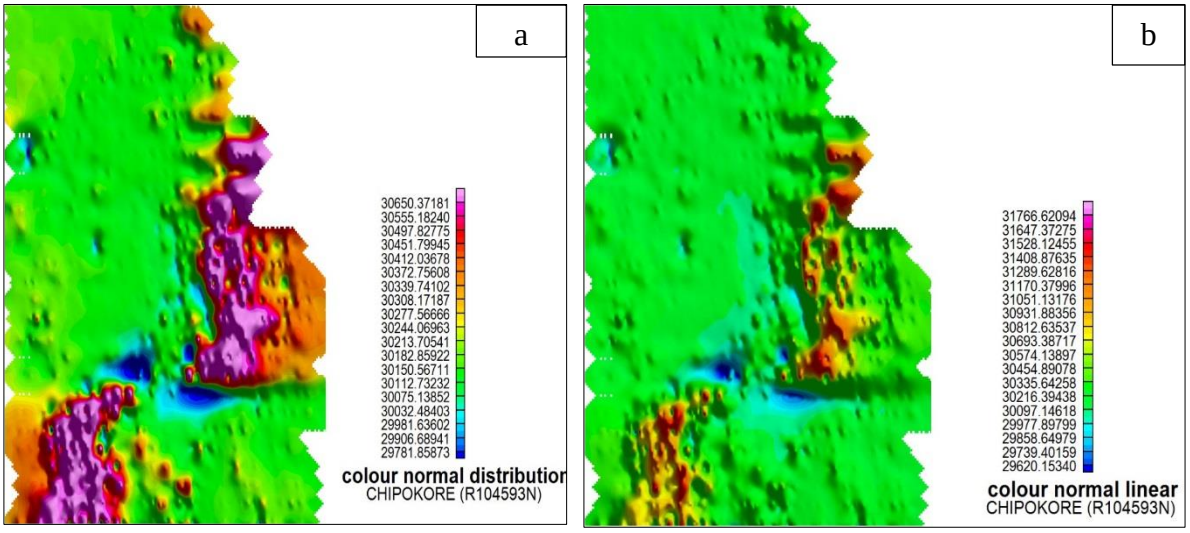

Fig 49 normal distribution colour (a) and linear distribution colour method (b)

The normal distribution colour method (Fig 49*a*) shows a grid similar to that of linear and log linear but it has enhanced deep blue (magnetic low) regions and magnetic high regions.

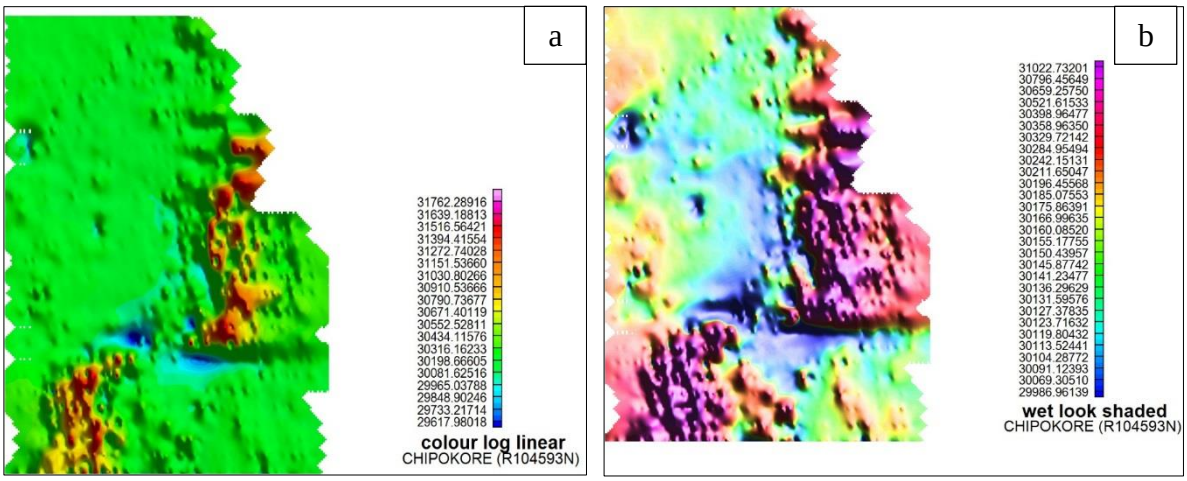

Fig 50 log linear colour method (a) and histogram equalisation colour method with wet look shading (b)

The wet look shading is showing the histogram equalisation colour method and a wider area shows some intermediate and deep blue regions of magnetic low values. Considerable high values are there too, but as in other grids, they are concentrated on the east and south west corners of the grid.

The data was gridded in four more gridding formats so as to try and study the magnetic anomalies before a full and comprehensive interpretation is made (Bhattacharyya, 1965). These

are bi-directional line gridding (Fig 51a), kriging gridding (Fig 51b), direct gridding (Fig 52a) and inverse distance weighted gridding (Fig 52b) methods.

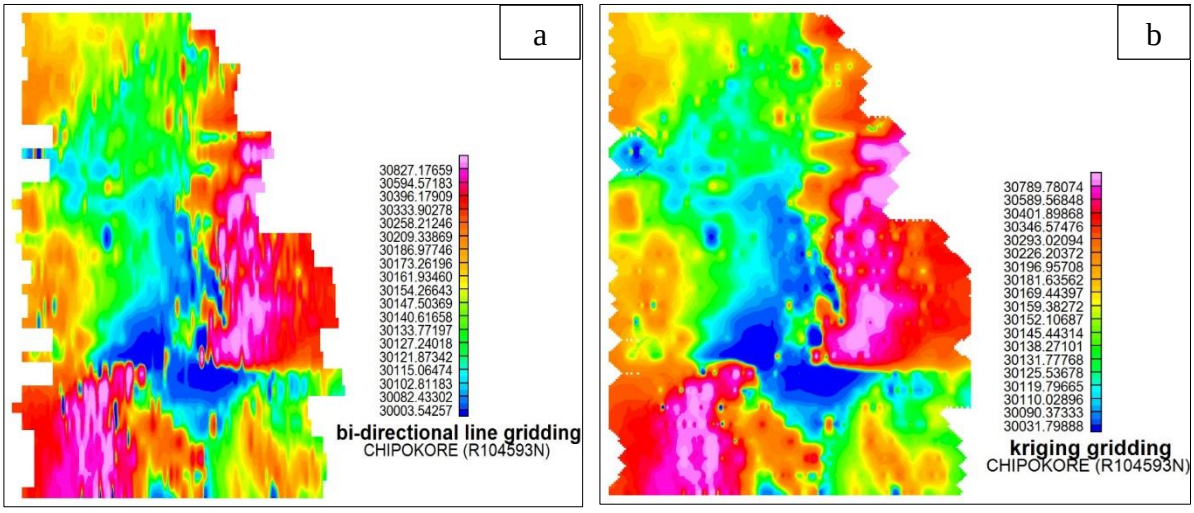

Fig 51 bi-directional line gridding (a) and kriging gridding (b)

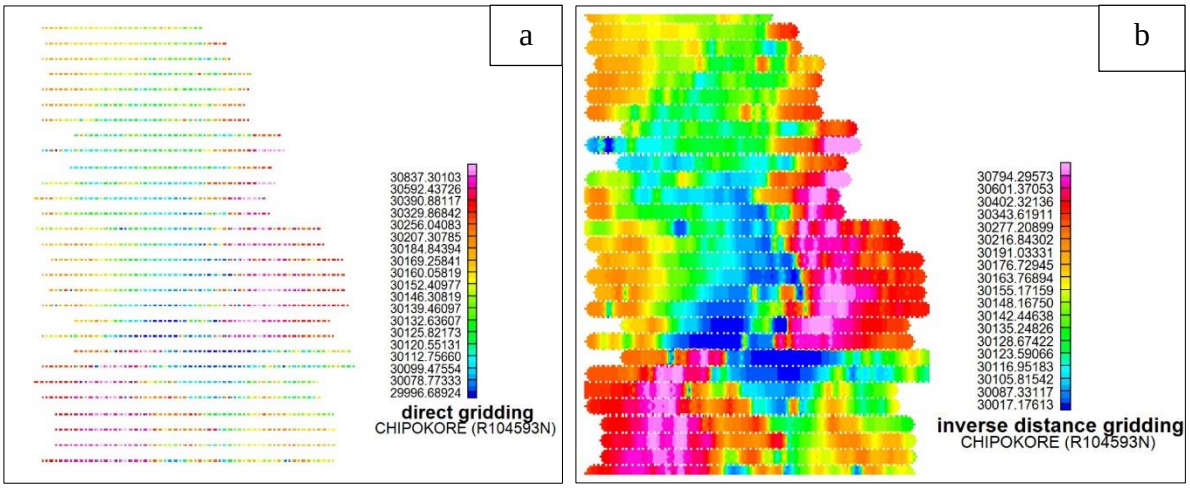

Fig 52 direct gridding (a) and inverse distance weighted gridding (b)

Bi-Directional line gridding method (BIGRID GX) is a numerical technique for parallel (or roughly parallel) survey lines such as the ones in this magnetic survey (Reeves C, 2005). The Bi-Directional gridding method is ideal for line oriented data because it inherently tends to strengthen trends perpendicular to the direction of the survey lines. In this way, Bi-Directional gridding can take advantage of the fundamental characteristics of line-based surveys. The gridding process was carried out in two steps. First, each line was interpolated along the original survey line to yield data values at the intersection of each required grid line with the observed line. The intersected points from each line were then interpolated in the across-line grid direction to produce a value at each required grid point. Geological trends in the data can

be emphasized by the appropriate orientation of the grid so that the second interpolation is in the direction of strike.

Looking at the grid (Fig 51*a*) it looks like a polished grid of the minimum curvature grid (Fig 48). The magnetic highs and lows are quite distinct and follow the usual trend such as that showing in all the previous shown maps.

Kriging gridding method is a statistical gridding technique for random data. The Kriging statistical gridding method determines a value at each grid node based on the XYZ data. Kriging first calculates a variogram of the data, which shows the correlation of the data as a function of distance. The kriging grid (Fig 51*a*) for this data (though not random) is somewhat similar to the minimum curvature grid (Fig 48), with slight variations and filtrations on the smaller data elements. This may be because the two methods are similar but simply differ in the randomness of the data being manipulated.

Direct gridding (Fig 52*a*) is usually for use with over sampled data (Grant, 1965). This method was used to provide a quick gridded view of the magnetic readings dataset. By looking, the blue areas and the hot pink areas as well as the green and red shades can be visualised. The colours can be interpreted using the scale bar to the right of the grid.

The Inverse Distance Weighting (IDW) algorithm is a moving-average interpolation algorithm that is usually applied to highly variable data. In this case it was not desirable to honour local data minima or maxima, but instead to look at a moving average of surrounding data points and estimate local trends. In IDW, a value for each grid node was calculated by examining surrounding data points that lie within a defined search radius. The node value was calculated by averaging the weighted sum of all the points, where the weighting inversely corresponded to distance from the grid node.

In Fig 52b, the boundaries between various magnetic level regions can be seen clearly and it shall make it easier to determine sheer zones and fault lines when used in interpretation and geological assessment. These grids are intended to be used collectively to get a single interpretation result of the magnetic anomalies in the surveyed area.

After gridding, several filters were applied to the minimum curvature grid so as to remove noise/errors, remove regional trends and/or enhance geological features (Bhattacharyya, 1965). The objective was to select a filter and parameters that did not introduce additional noise into

the data. 1D filters were applied to the nT channel in the database, while 2D filters were applied to gridded data used during image processing.

The filters applied to the data were the 3X3 convolution, 5X5 symmetric convolution, 9X9 symmetric convolution, a grid math application, analytic signal, automatic gain correction, horizontal gradient filters (Fig 53a), trend surface removal and vertical derivative convolution (Fig 53b).

The 3x3 convolution (Hanning) filter was passed to remove high frequency components of the data. The 5x5 symmetric convolution and the 9x9 symmetric convolution filters were passed to the grid respectively to further smooth the grid before contouring in order to improve the appearance of the contours. These were also used to remove regional data trends by producing a curvature grid. To do this, a 3x3 Convolution filter was passed once over the minimum curvature gridded dataset and the output curvature grid was then subtracted from the original grid. This created a residual gridded dataset. Here the residual is proportional to the curvature in the original grid, with zero values indicating inflection points. The curvature grid may also be subsequently filtered to smooth noise. The analytic signal filter was passed to the grid so as to remove the negative frequency components within the grid. Analytic signals are often shifted in frequency towards 0Hz, which creates non symmetrical negative frequency components. In this case, low pass filters with real coefficients were used to limit the bandwidth of the magnetic signal. In the automatic gain correction, the average peak output magnetic reading is used to adjust the gain of the grid values to a suitable level.

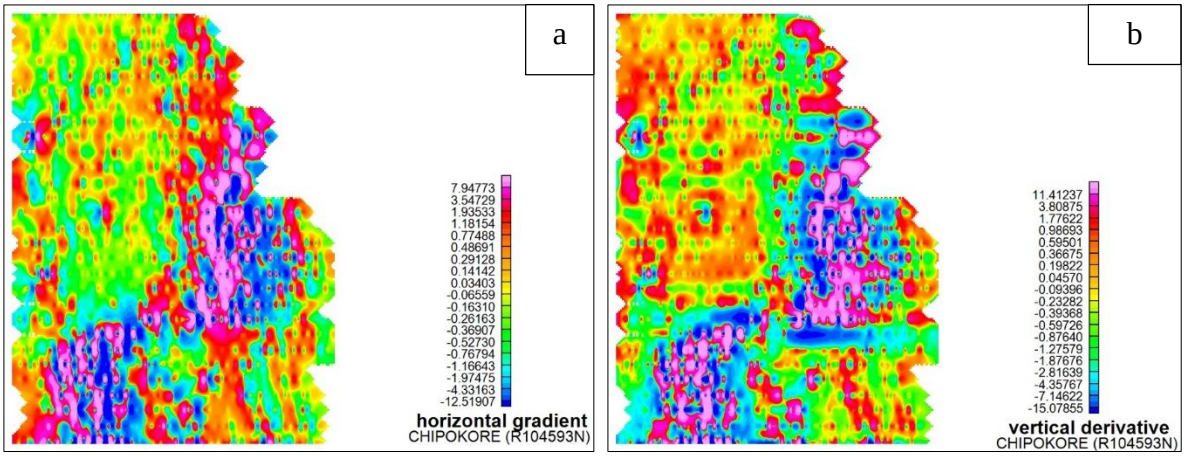

Fig 53 horizontal gradient filter (a) and vertical derivative filter (b)

The total magnetic field horizontal (Fig 53a) and vertical (Fig 53b) magnetic gradients were also used as filters to the magnetic anomaly grid.

The gradient applied was the change in grey level with direction. Horizontal gradient was formed by taking differences between nT column values.

After applying all the different gridding methods, the colour methods and the filtering methods, a final colour shaded grid (Fig 54a) was produced. This was the one placed on the fore during the magnetic data interpretation and the anomalies were mapped on this grid. All the other geological integrations such as sheer zones, faults, throw backs and cuts that were noted from the various grids and filters were also overlain on this grid during interpretation.

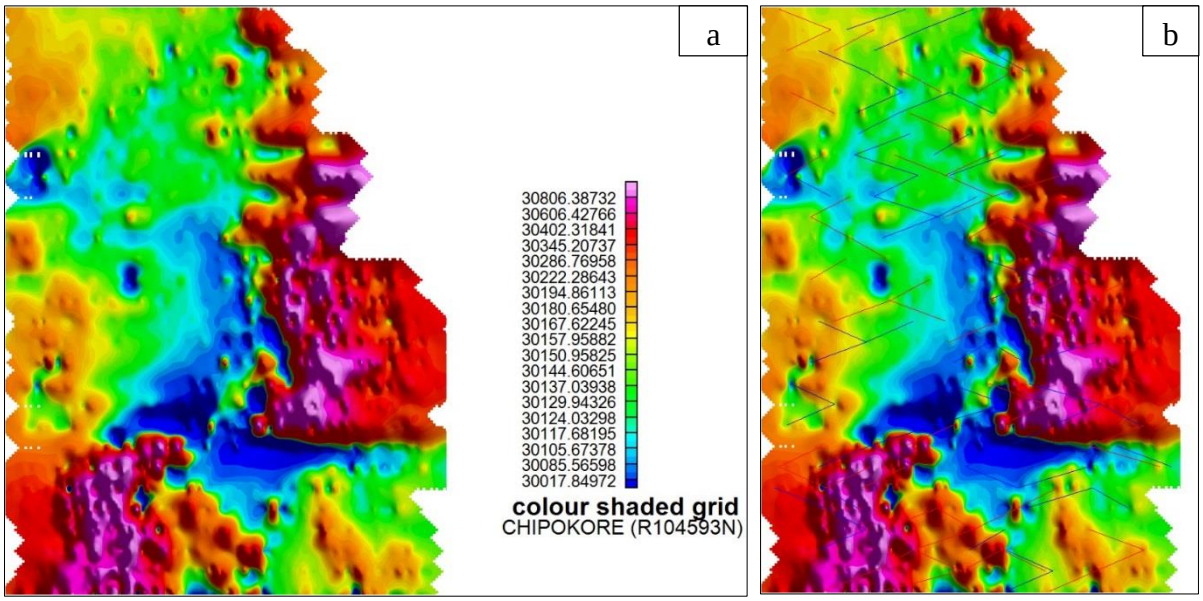

Fig 54 colour shaded grid (a) and showing trend lines removed (b)

Fig 54b shows the trends lines on the data, Fig 55a shows the contour lines on the magnetic data. These contours are not topographical contours but which maps the magnetic highs and lows on the area. Fig 55b is simply the survey line path overlain on the colour shaded grid.

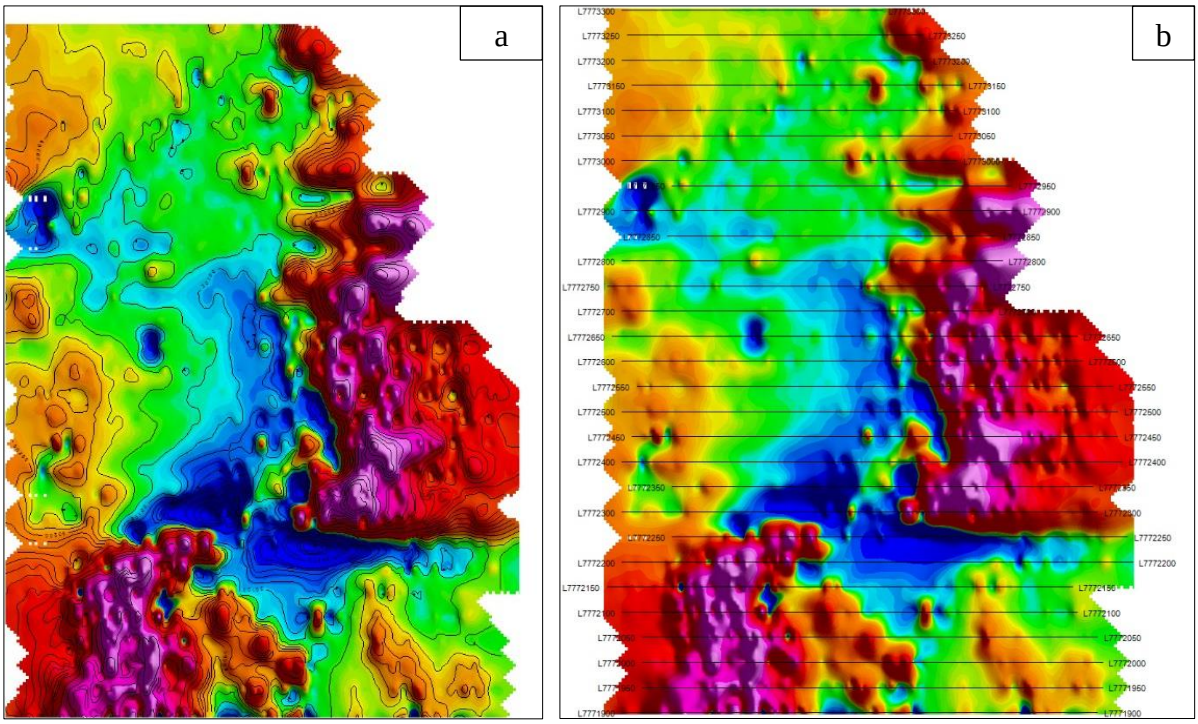

Fig 55 showing contour lines on the colour shaded grid (a) and showing the line path on the colour shaded grid (b)

Interpretations and geological integration

To begin with, it has to be noted that limestone is a sedimentary rock, hence is non-magnetic (Bakhtiar, 1986) (Parry, 1973). This magnetic survey hence was intended to map out areas with low, and preferably very low magnetic values with respect to the surrounding areas within the Nyanda mountains area, the survey site. So, during interpretation, the areas with low magnetic anomalies are of prime scrutiny, and these were considered to contain the limestone which was being explored for.

The maps and grids were all exported to MapInfo software for further comparisons which would aid interpretation.

Qualitative interpretation

All the maps, grids and plates discussed in sections above were scrutinised to come up with the qualitative interpretation.

Looking at Fig 49b, a prominent stretch of magnetic high values is noticeable running (winding) roughly from south west to north east. The stretch cuts a region of very low magnetic field strength in a manner of a geological fault. The same trend is seen in Fig 50*a*, where the area of the low magnetic field tends to decrease very slightly. In Fig 49*a*, the areas exhibiting

high magnetic values are enhanced and these surround the geological fault predicted in Fig 49*b*. High magnetic values are concentrated to the south westernmost and the middle to north eastern areas of the survey area. The two divided areas with very low magnetic readings are still visible and enhanced. Fig 52*a* predicts that the area with low magnetic readings is somewhat in the middle of the survey area and stretches roughly from the North West to the south east of the map. Fig 55a and Fig 55b clearly maps the area with very low and intermediate low magnetic values as being surrounded by those with high magnetic values. The area to the south east corner of the maps has high magnetic values and is broken from the high magnetic region by a strand of low values which cut at the northing 7772250N. The west, also, has a region of high values bounded between 262250E and 262500E, and is broken also between 7772750N and 7773000N by an area of very low magnetic values.

Fig 51*b* shows that areas with intermediate low magnetics values and are close/bounds to/with those with high magnetic values can be considered geologically ambiguous and hence need to be mapped out of the target areas which has low magnetic values. Looking at Fig 51*a* the areas with very low magnetic values can be seen to occupy mainly the middle most areas of the grid, bounded by northings 7772000N and 7772750N and eastings 262500E and 263000E. The low value anomaly is broken by a fault at 7772250N.

Fig 54a has minimal noise such that the low magnetic variations are clearly mapped and anomalies can be picked hence. Fig 50b and Fig 47 give the various views of the interpreted data and aids in picking up anomalies from the grid. Fig 48 and Fig 54*a* are the main final maps showing the low magnetic value sites which are likely to contain the limestone being looked for.

In Fig 56*a*, Fig 56*b* and fig 57, lines are added to grids to show anomaly demarcations. The fault line which is also the line with highest magnetic values is show over the fault and it cuts the magnetic low region which is bounded by the broken lines. The target site can be seen to fill the centre of the grid, while the areas with magnetic high values area edged out by the teeth lines. The words HIGH, VERY HIGH, LOW, and VERY LOW are embedded in the grid to indicate areas with high, very high, low and very low magnetic values respectively.

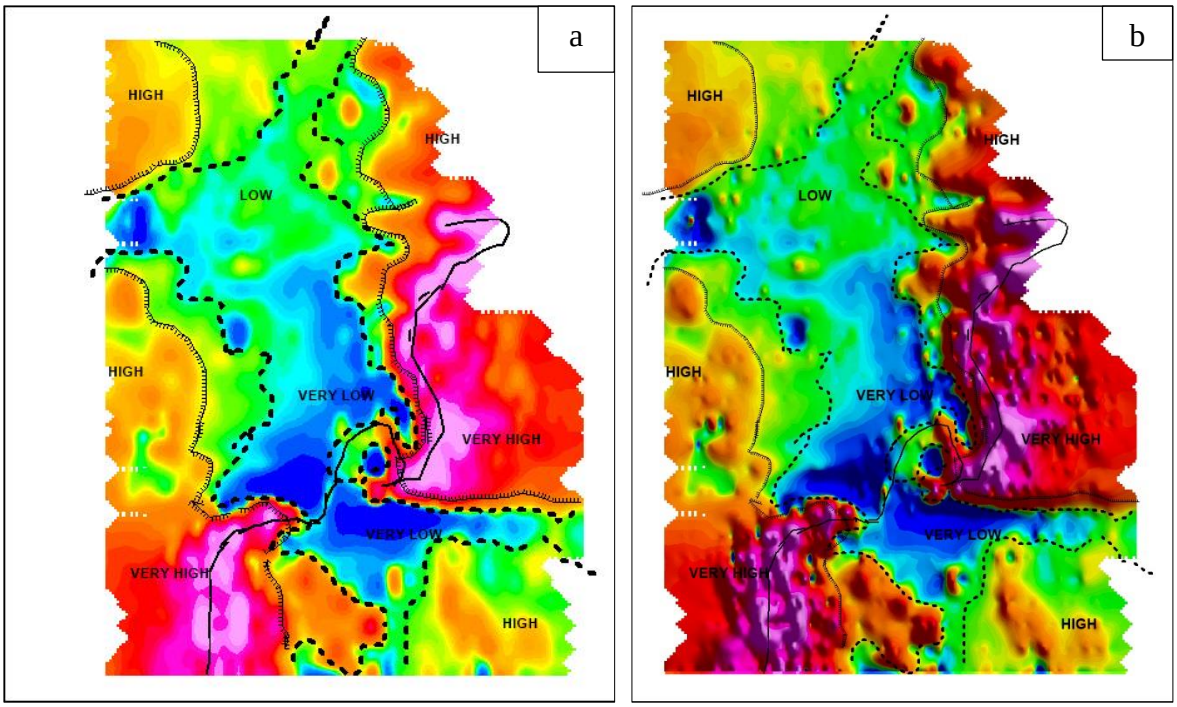

Fig 56 filtered grid showing the interpreted survey area (a) and showing interpreted colour shaded grid (b)

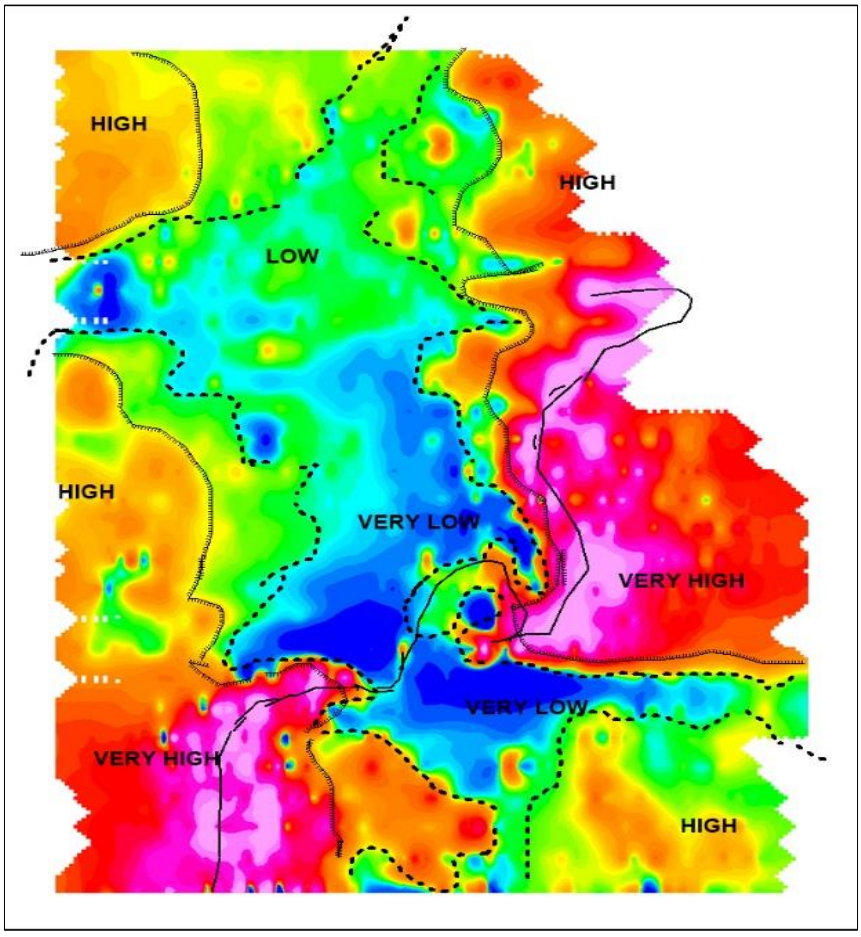

Fig 57 showing interpreted minimum curvature grid

Quantitative interpretation

The low magnetic anomaly shown in the map does cover a considerable large area with respect to the whole survey area, so limestone is expected to be concentrated in the deep blue regions and extending to the green intermediate low regions of the survey area. If the limestone is concentrated as shown, then the quantities are likely to be large such that extraction can initially be concentrated on the regions with very low magnetic readings, and eventually extend outwards to the low magnetic areas.

The principle of non-uniqueness

The data set used for this magnetic survey is two dimensional so it has been impossible to uniquely define three dimensional subsurface anomaly models for the survey area. There is an infinite number of possible physical models that could theoretically account for the low and very low magnetic anomalies shown. However, this does not mean that the interpretation exercise was pointless or endless, nor does it mean that all solutions were valid.

Economy of hypothesis - simplification of sources in modelling.

Geological bodies and structures are often very complex in nature and, as a first approximation in geophysical modelling, a simplification of the source was made which was also consistent with the principle of economy of hypothesis that requires that a minimum number of arbitrary assumptions be made. In other words, a more complex model is only invented when a simple model is found to be inadequate to explain all the available (geophysical and other) data.

A simple 2D model has been employed for the source modelling for the magnetic data (Milsom, 2002). The chosen model is invariable along strike and therefore is completely defined by one cross-section. This has been shown in Fig 58. The source body is illustrated as the blue limestone body as shown in the figure. Although this is clearly not perfectly true in nature, it is very often the case that errors due to the fact that the real source is of finite strike length are much less than those due to other causes.

The anomalies are seen to occur as local variations imposed upon other local variations, regional variations and noise. The regional variations may be defined as the value of the field which would exist if there were no local disturbance due to the limestone source which is being interpreted. The regional was actually unknown and hence becomes quite subjective. It could have been treated as an additional variable in an interpretation, but reasonable limits may were set from common sense provided by human intervention.

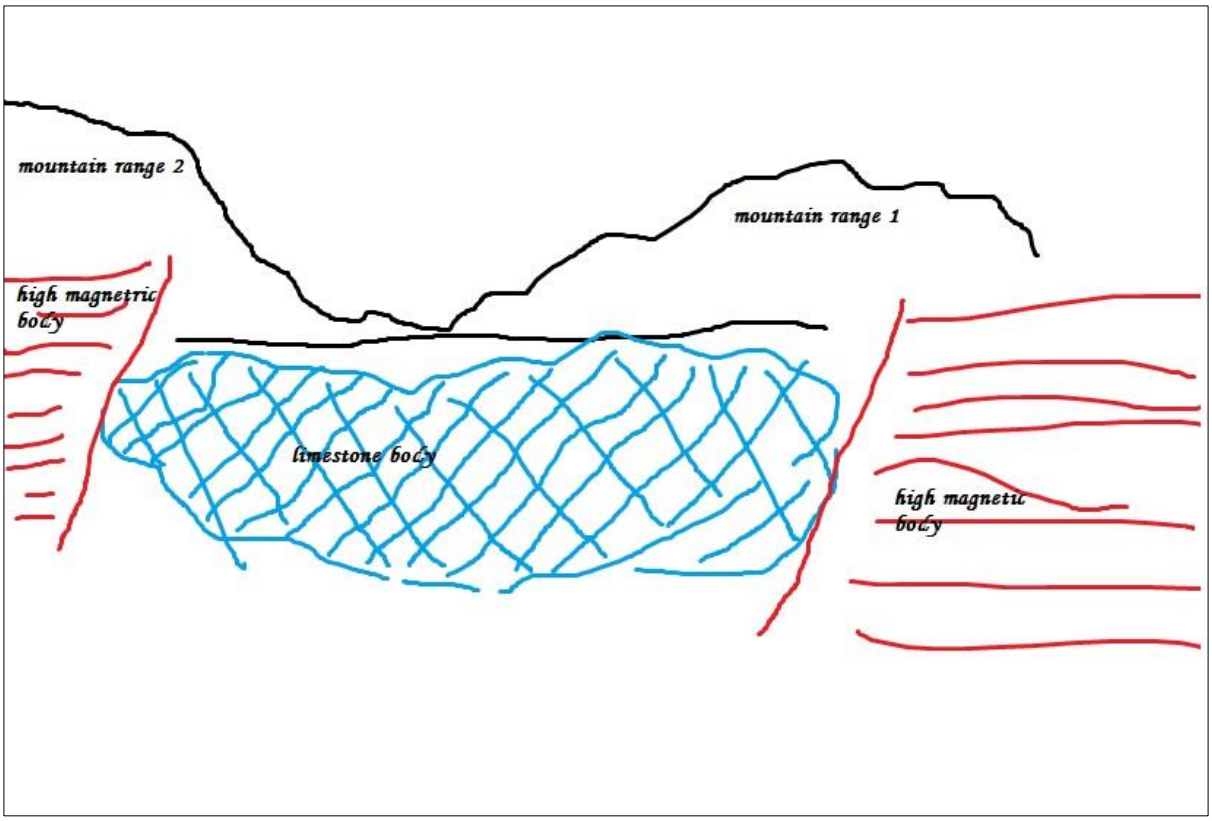

Fig 58 source modelling

Integration with the geology

Nyanda Mountains consist of two branches (Fig 6) and the survey area covered part of the mountain site, overlapping the eastern branch and reaching to the peak of the western branch. There is a valley between the two branches. From the interpreted magnetic data, the area with low magnetic values lies within the valley between the two branches and extend to the sides of the mountains. The areas with high magnetic values coincide with the peaks of the mountains while the fault which is cutting the low magnetic anomaly is a ridge connecting the two peaks through the valley.

The geological survey within the survey area showed vast karstic features underlying the valley and caves which littered the mountain sides. With this match, it can be stated that the geophysical zoning can be reconciled with geology sharply. The fault which is shown in fig 49b coincides well with the ridge (outcrop) which connects the two peaks.

For depth and strike modelling the strength of the anomalies was used to predict. The strike has been ignored since limestone is a sedimentary rock, it occurs in sediments. The areas with very deep low magnetic values have been predicted as being characterised by near surface limestone deposits (blue area in Fig 59) while intermediate low regions were due to limestone

deposits which were not so near the surface. Magnetic high values (red regions in Fig 59) were also predicted to be characterised the faulting body very near the surface.

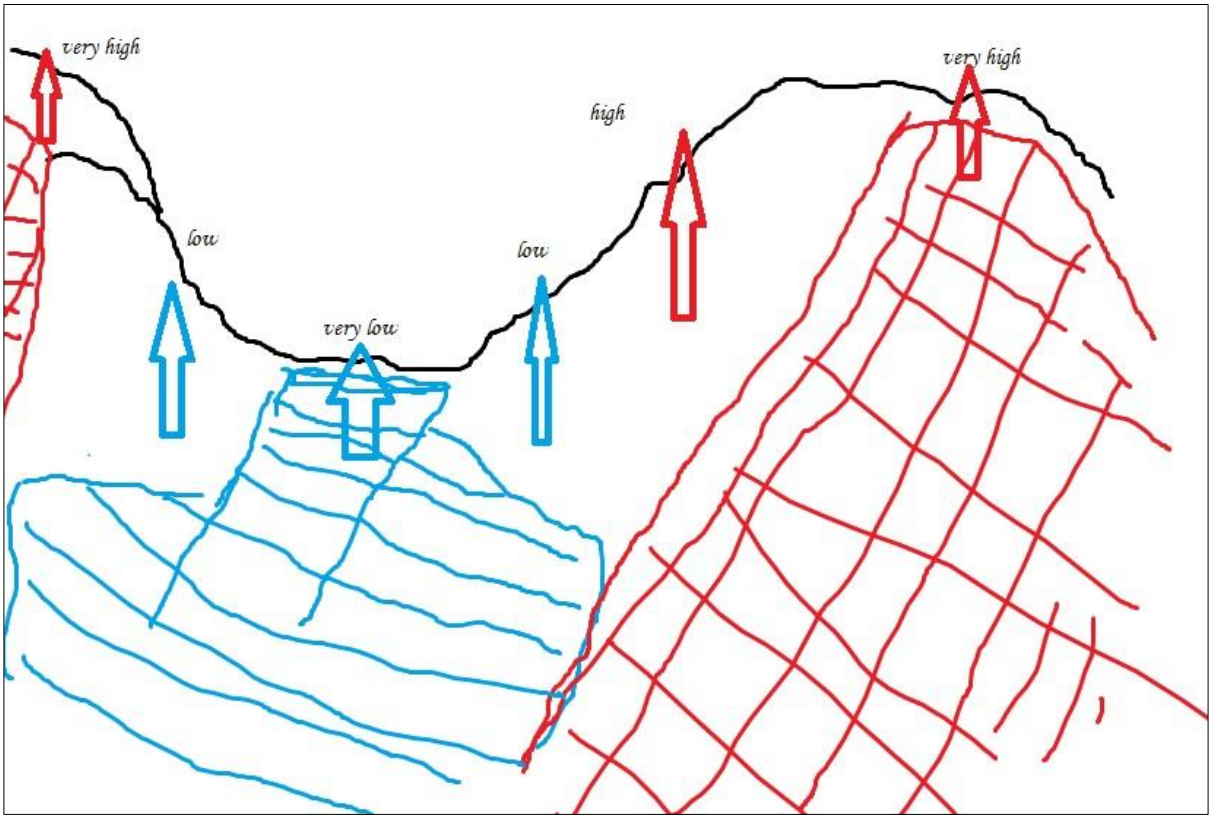

Fig 59 depth modelling

CHAPTER 5: CONCLUSIONS

The project was carried out successfully, and the main result was that the geophysical magnetic survey techniques employed were able to map out and detect limestone deposits in the Nyanda mountain range, Masvingo, Zimbabwe.

In response to the problem definition stated in the first chapter, magnetic lows on the regional magnetic data did imply the existence of limestone in the area, since areas which geophysics pointed to be low in magnetic values coincided with those which geology pointed to contain limestone deposits.

Ground magnetic measurements were employed during the survey, and the success of the survey has made it feasible to consider employment of ground magnetic surveys to detect limestone deposits in other areas since the survey is considerably cheaper, efficient and easier to carry out with respect to ground penetrating radar and resistivity surveys traditionally employed for the task. The take is to simply target areas with low magnetic values with respect to the survey region.

To meet the objective of the research as stated in the first chapter, the overburden layer covering the limestone deposit has been mapped. The layer has a greater depth in areas with intermediate low magnetic values and thin in areas with very low magnetic values. This is in correspondence to the depth evaluation of the low magnetic anomalous body.

The general objective of the survey was also reached and the interpretation of the magnetic survey data was done comprehensively. Limestone rich areas were delineated along the mountain range and valley. Filters and grid algorithms were applied successfully to the data to produce images with reduced noise and greater/sharper resolutions to anomalies.

To answer to the project research questions, the distribution of limestone deposits in the Nyanda Mountains have their distribution studied clearly and their relation to the low magnetic values was noted to be directly proportional in that areas with low magnetic values are rich in limestone.

The employment of GEOSOFT'S Oasis Montaj and MapInfo has shown that the combination of the software can be a criteria for creating user friendly mapping systems which can as well be integrated to match maps from previous works. A geodatabase has been designed which

contains all elements of the processed data and maps, grids and images/plates and which can be viewed and edited by other users.

The project however failed to map the prominent reflections of the voids in the caves and other underground carbonate features. The nature of the data (two dimensional) made it impossible to create third dimensional grids and anomaly maps hence the depth of body and strike was only assumed and mathematically determined.

Recommendations

The geodatabase can be further upgraded for the whole of the Nyanda Mountain area and other surrounding areas with a new magnetic survey to give a new set of magnetic data.

A new set of data with the *z* element (elevation) still need to be taken in a new survey so as to carry out the third dimension interpretation which maps out the ore body and show the dip and strike of the anomalous body (source modelling).

Much works is still needed to make complete the geodatabase by correlating the geophysical information with ground based geological observation and extracting the non-spatial information like rock type, age, etc.

REFERENCES

Ashwal, D., 1997. *Greenstone Belts, Oxford Monograph on Geology and Geophysics.* *O*xford: Clarendon Press.

Bakhtiar, 1986. Karst cavity detection in carbonate rocks by integration of high resolution geophysical methods. 3(1), p. 20.

Bhattacharyya, B., 1965. Two-dimensional harmonic analysis as a tool for magnetic interpretation. *Geophysics,* Volume 30, pp. 829-857.

Boyd, T., 1992. An annotated outline of GPS. *ASEG Preview*, pp. 15-26.

Briggs, I., 1974. Machine contouring using minimum curvature. *Geophysics,* Volume 39, pp. 39-48.

Clark, D. a. E. D., 1991. Notes on rock magnetisation in applied geophysical studies. *Exploration Geophysics,* 22(4), pp. 547-555.

CSIR, r., 1975. Geomagnetic secular variation observations in southern Africa. *CSIR report MAG.C6,* p. 19.

GEOMAGMODELS, 2014. *GEOMAGMODELS.* [Online] Available at: http://www.ngdc.noaa.gov/geomagmodels/IGRFWMM.jsp [Accessed 18 APRIL 2014].

googlemaps, 2014. *googlemaps.* [Online] Available at: www.google.maps/ [Accessed 26 april 2014].

Grant, F. a. W. G., 1965. *Interpretation theory in applied geophysics.* New York: McGraw-Hill.

Hadipandoyo, S., 1986. A comparison of several methods of gridding and contouring geophysical anomaly field. *MSc thesis*, p. 133.

Hoover, D. H. W. a. H. P., 1992. The Geophysical Expression of Selected Mineral Deposit Models. *Geological Survey Open File Report for United States Department of the Interior,* 92(557), p. 128.

Hruska, J. H. F., 2000. Landslides investigation and monitoring by a high performance and cavities in limestone. *Proceedings of the 8th International Conference on Ground-penetrating Radar* .

informine, 2014. *informine.* [Online] Available at: http://www.infomine.com/index/pr/Pa032168.PDF [Accessed 18 april 2014].

Jelsma, P. H. G. M. D. a. H. A., 1998. Silicic Layer-Parallel Shear Zones in a Zimbabwean Greenstone Sequence: Horizontal Accretion Preceding Doming. *Gondwana Research.*

Kearey, P. a. B. V., 1984. *Introduction to Geophysical Exploration.* 1st ed. s.l.:blackwell science.

Kearey, P. B. M. a. H. I., 2002. *An Introduction to Geophysical Exploration.* 3rd ed. Oxford: blackwell science.

Kearey & Vine, 1996. *global geophysics.* 2nd ed. oxford: blackwell science.

MacMillan, S. e. a., 2003. list the coefficients for the current IGRF. *EOS,* 84(46).

Mafirakureva, 2012. geological & geophysical survey report for lady a mine. *Report Number: gl01/12.*

maphill, 2014. *maphill.* [Online] Available at: www.maphill.com/masvingo-zimbabwe [Accessed 28 april 2014].

Maponga, g., 2011. *the herald.* [Online] Available at: www.thehearld.co.zw/cement-plant-for-masvingo [Accessed 28 march 2014].

McCann, 1997. *magnetics for engineering.* 1st ed. new york: new york university press.

McElhinny, M. a. M. P., 2000. *Paleomagnetism – continents and oceans.* s.l.:Academic Press.

Milsom, J., 2002. *field geophysics.* 3rd ed. london: university college london.

Mussett, A. a. K. M., 2000. *Looking into the Earth: An Introduction to Geological Geophysics.* Cambridge: Cambridge University Press.

Parasnis, D., 1996. *Principles of Applied Geophysics.* 5th ed. london: chapman and hall.

Parry, L. G., 1973. Superparamagnetic and single-domain threshold sizes in magnetite. *Geophys,* 7(78), p. 1780.

QCtools, 2014. *qc-tools.* [Online] Available at: http://www.qc-tool.com/en/download/manuals/QCTool_Diurnal_Correction.pdf [Accessed 14 april 2014].

Ranganai, O. G. a. R. T., 2009. O. GThe Geology and Structure of the Masvingo Greenstone Belt and Adjacent Granite Plutons from Geophysical Data, Zimbabwe Craton. *South African Journal of Geology,* 112(3-4), pp. 227-290.

Ranganai, R. T., 1995. *Geophysical Investigations of the Granite-Greenstone Terrain in the South-Central Zimbabwe Archaean Craton.* Leeds: University of Leeds.

Reeves C, 2005. *Aeromagnetic Surveys Principles, Practice & Interpretation.* 1st ed. Canada: Geosoft.

SEG, 2014. *SOCIETY OF EXPLORATION GEOPHYSICISTS.* [Online] Available at: http://www.seg.org/ [Accessed 14 APRIL 2014].

T. G. Blenkinsop, e. a., 1992. The Zimbabwe Craton. *M. J. de Wit* .

Telford, W. e. a., 1990. *Applied Geophysics.* 2nd ed. Cambridge: Cambridge University.

USGS, 2014. *usgs.gov.* [Online] Available at: http://minerals.usgs.gov/minerals/pubs/country/2000/zimyb00 [Accessed 3 may 2014].

Van Blaricom, R., 1992. *Practical Geophysics II.* 1st ed. Spokane: Northwest Mining Association.

Vogelsang, 1995. *geophysics in structural foundations.* 3rd ed. chicago: university press.

wikipedia, 2014. *wikipedia.* [Online] Available at: www.wikipedia.com/ [Accessed 23 april 2014].

William J., e. a., 2013. *Exercises Overview for Gravity and Magnetic Exploration: principles, Practices, and Applications.* Cambridge: Cambridge University Press.